Non-invasive time-resolved techniques for the quantification of human brain functions

MEG & EEG

Virginie van Wassenhove, PhD

Exec Dir MEG center
CEA/I²BM/DSV/ NeuroSpin
Cognitive Neuroimaging Unit (INSERM U992)

agenda

1. Overview euroimaging techniques

2. MEG, EEG, MEEG

   Techniques
   Origins of the recorded signals
   Recording techniques
   Experimental design
   Data processing

3. In practice

   Clinical MEG
   Neurosciences
   Cognitive neurosciences

overview

neuroimaging techniques

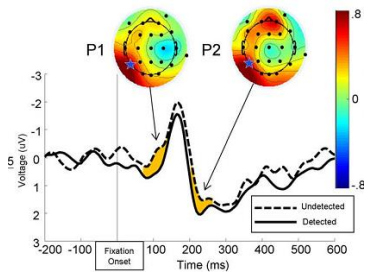

Matthewson et al JNeuro 2009

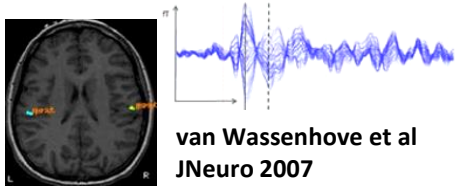

van Wassenhove et al JNeuro 2007

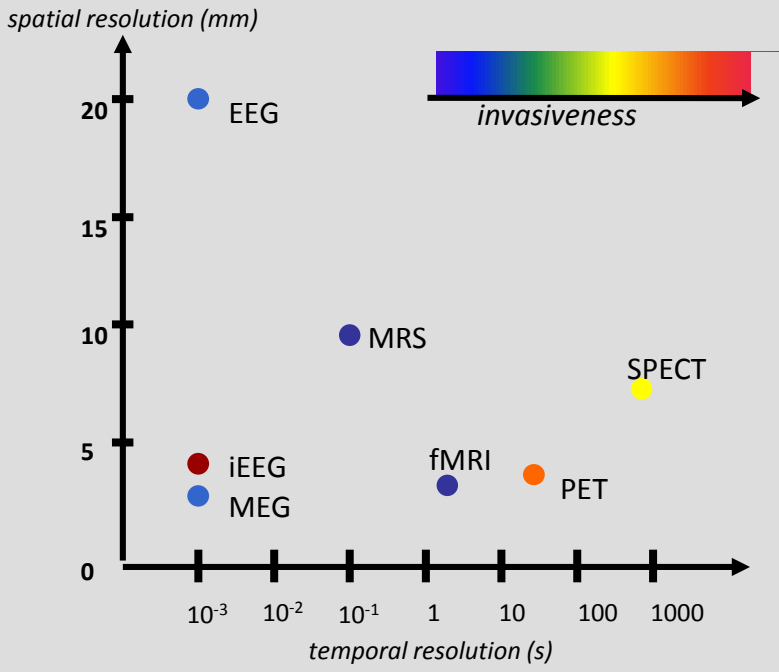

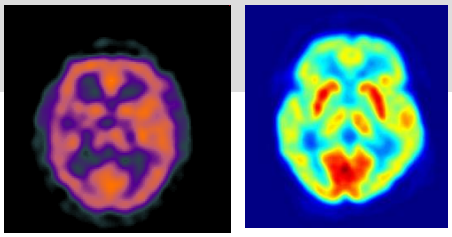

PET SPECT

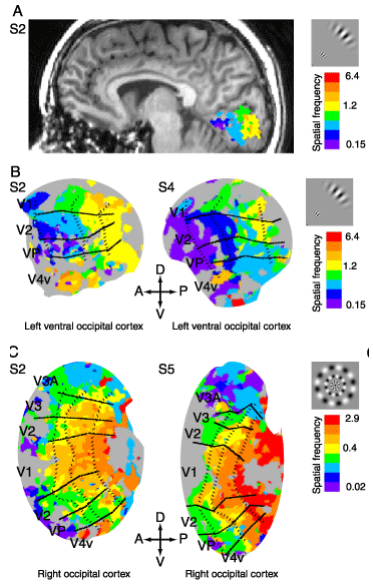

Erikson et al JOV 2008 (fMRI)

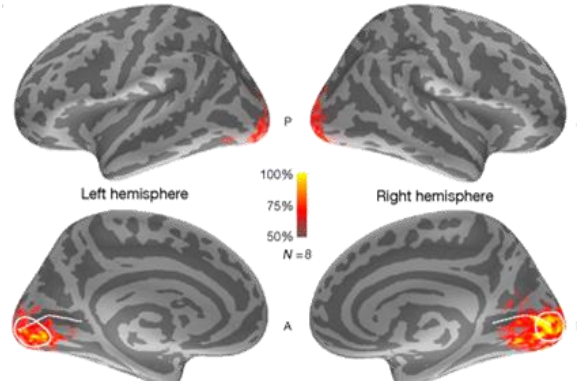

Parkkonen et al PNAS 2009

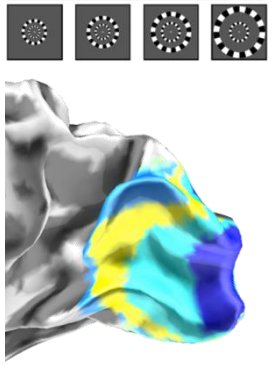

Gramfort 2009

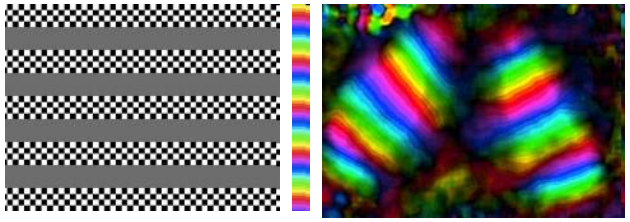

Near InfraRed Spectroscopy (NIRS)

spatiotemporal sensitivity

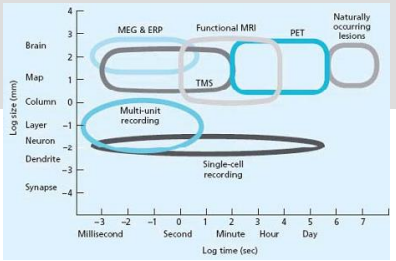

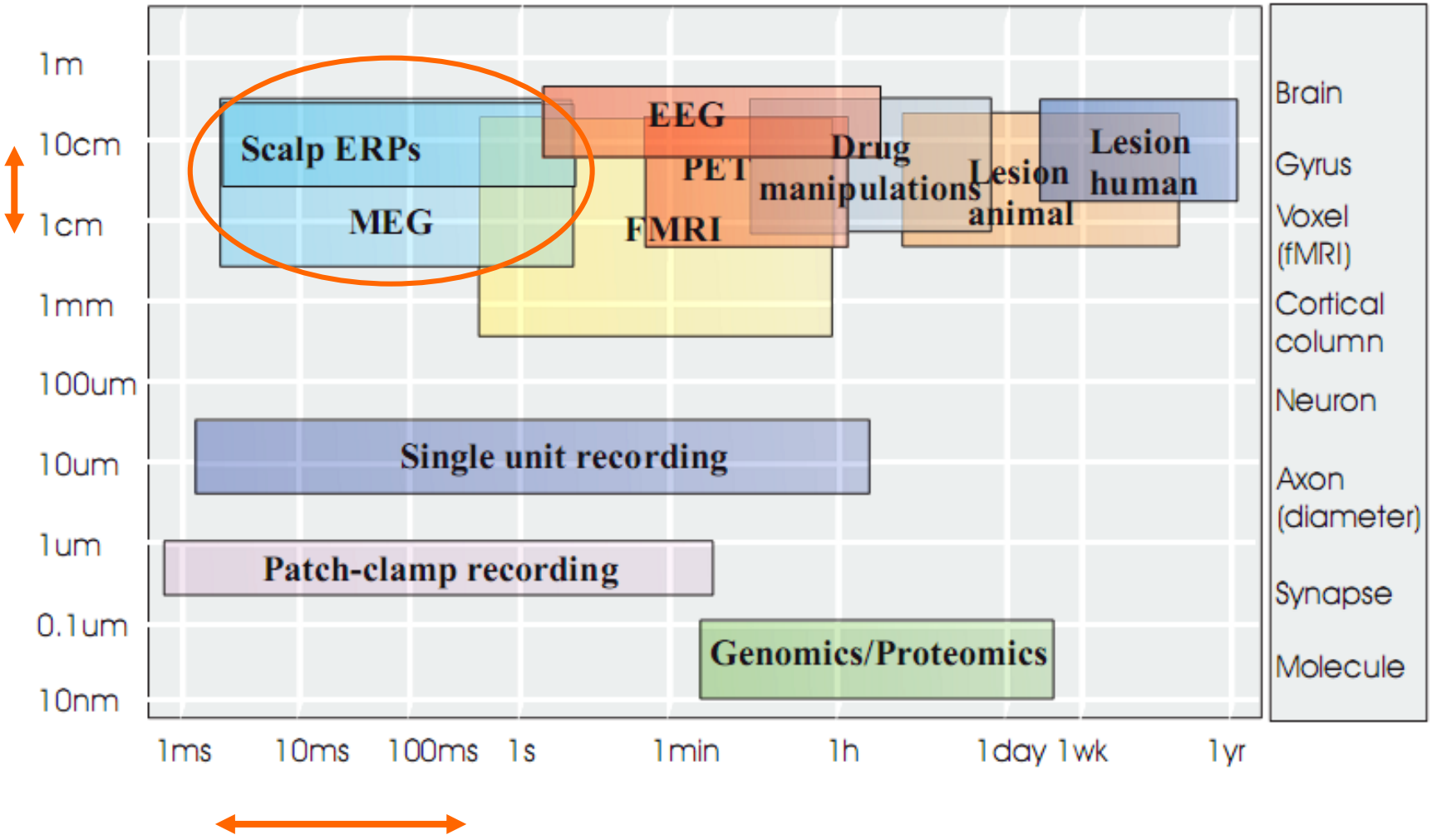

adapted from Bezerianos & Moraru (2008) Nonlinear Phenomena in Complex Systems 11(2) pp164-170

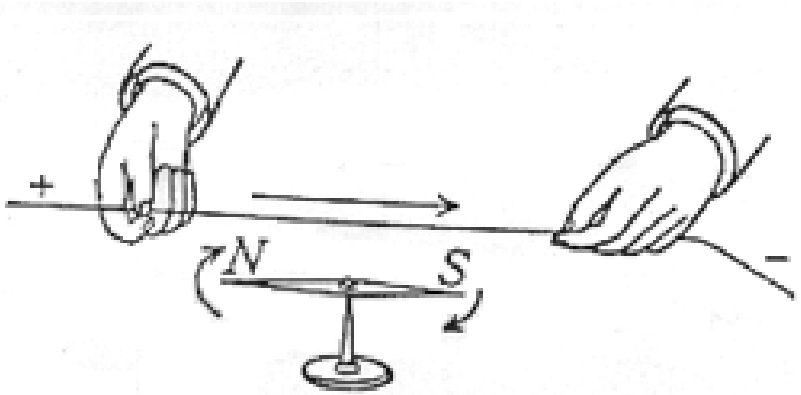

electric currents
ALWAYS
generate a
magnetic field

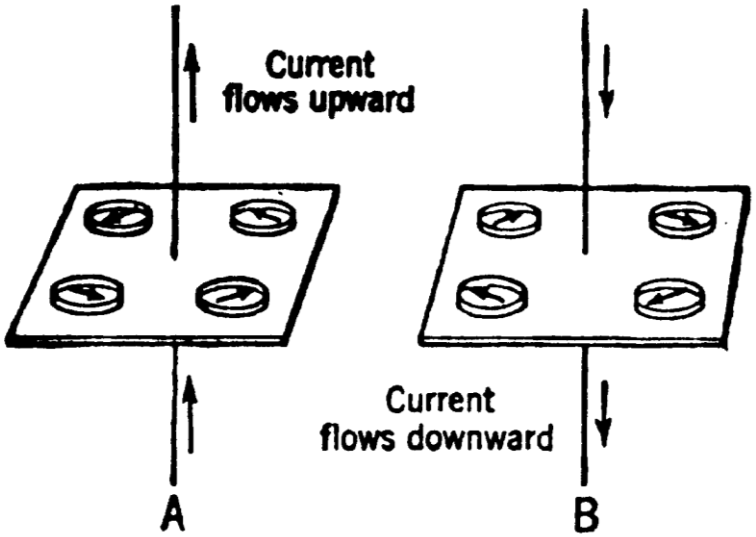

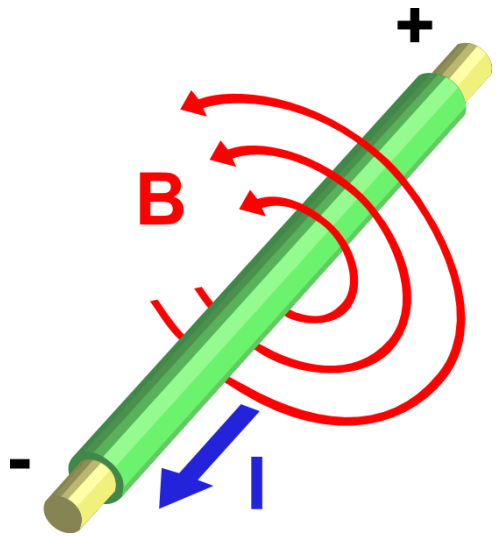

courtesy of Lauri Parkkonen

environmental magnetic fields

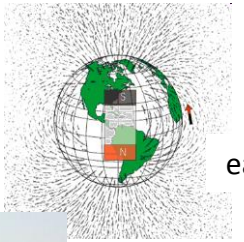

earth magnetic field

lignes haute tension

car 50 m away

screwdriver 5 m away

transistor 2 m away

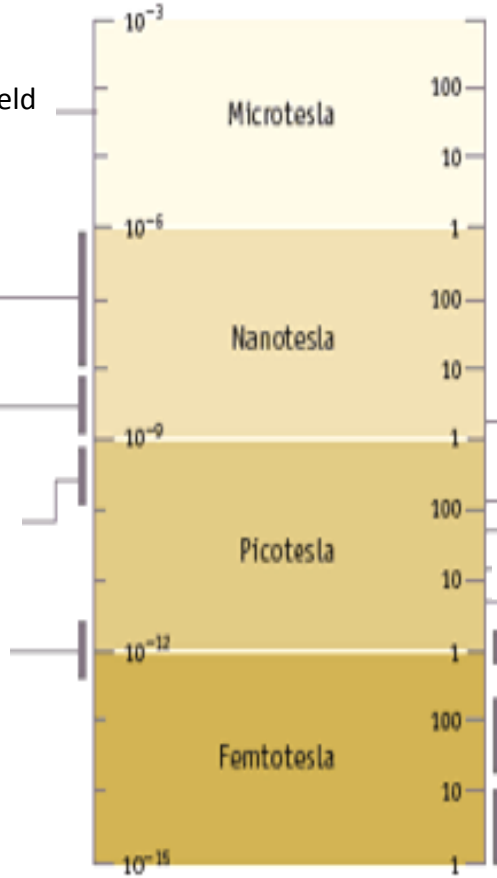

lungs

heart

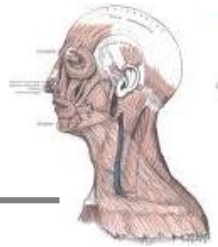

muscles

eyes

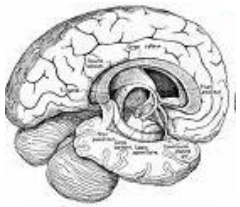

human brain

noise level of a SQUID

signals of interest = 10^{-12} to 10^{-13} Teslas
1picoT to femtoT

MagnetoEncephaloGraphy MEG

MagnetoEncephaloGraphy = brain imaging technique recording tiny magnetic fields produced by neural activity in the brain.

pioneered by David Cohen (1968, 1971)

Fig. 3. General features of the measured B-vector distribution around the head due to alpha-rhythm currents, inion-trigger averaging being used.

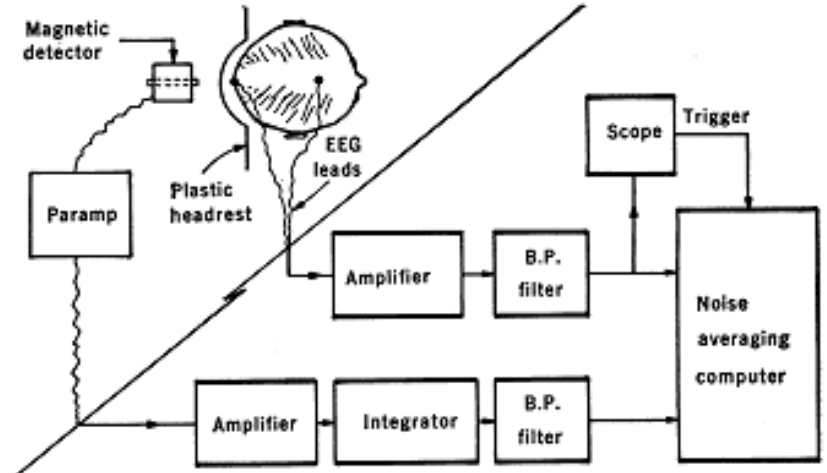

Fig. 1. Arrangement for magnetic alpha-rhythm detection. Subject and detector are inside the shielded enclosure, seen from the top; electronics are at an external station. The ferrite rod on the axis of the electrostatically shielded coil is in line with the subject's inion; this particular orientation detects the magnetic component normal to the scalp at the back of the head.

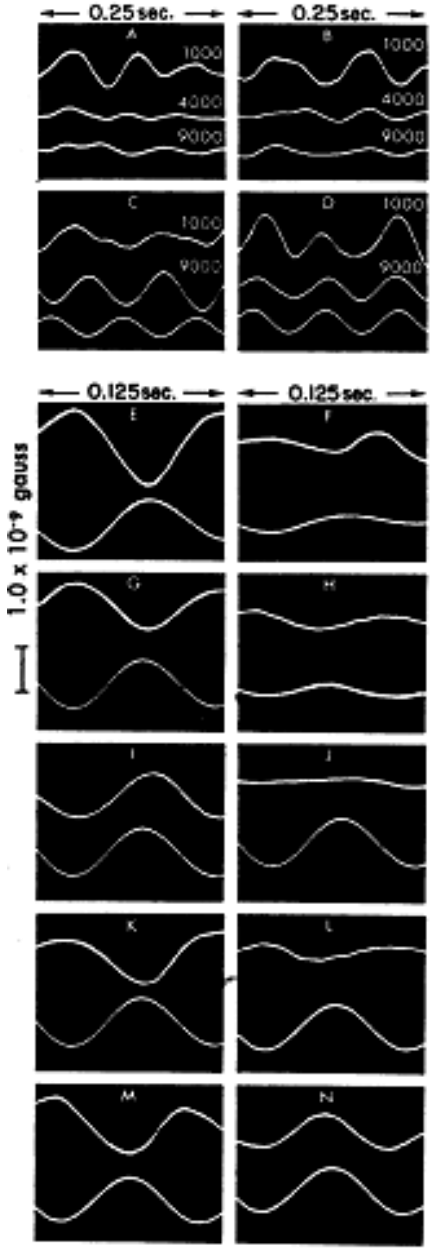

MEG

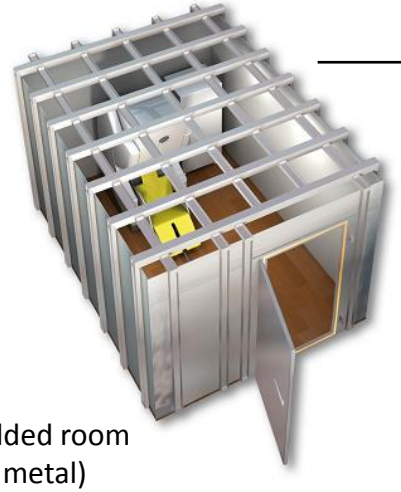

shielded room
(mu metal)

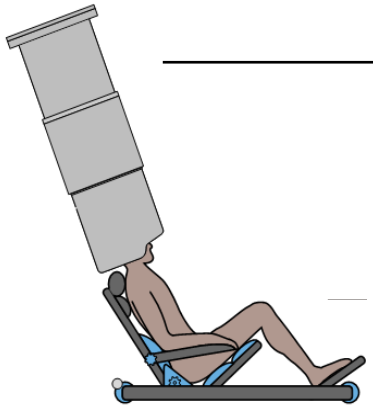

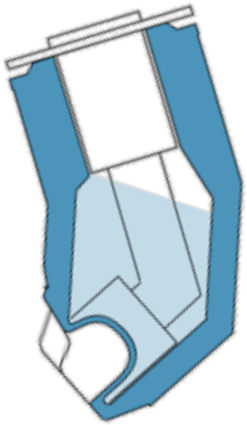

liquid He
(4K / -269°C)

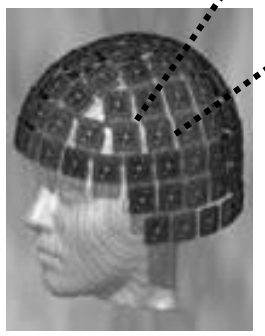

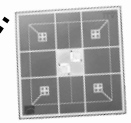

At the temperature of liquid Helium (*4K or -269°C*) SQUIDs conduct current without resistance.

SQUIDS are bathed in the MEG dewar at that temperature.

SQUIDs measure the changes in magnetic flux in their superconductive loop via quantum-mechanic interferences.

The MEG (Elekta system) @ NeuroSpin uses 306 sensors covering the entire head.

SQUID = Super-QUantum Interference Device

NeuroSpin setup

MEG dewar
(~80 liters of liquid He)

Projection screen (visual stimuli display; instructions for the task)

chair or bed
can be used

ElectroEncephaloGraphy EEG

pioneered by Hans Berger (1940's)

signals of interest = a few microvolts

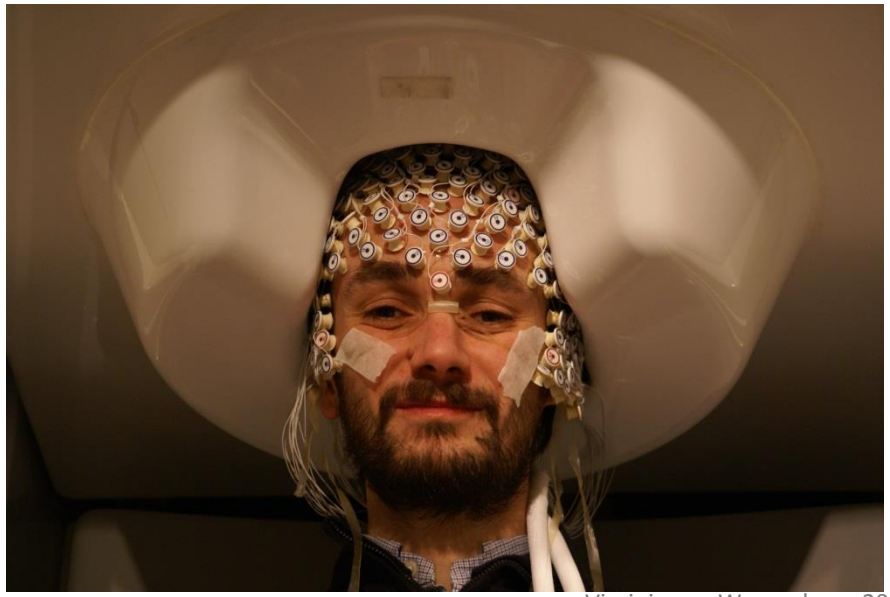

origins of the recorded signals

brain scales

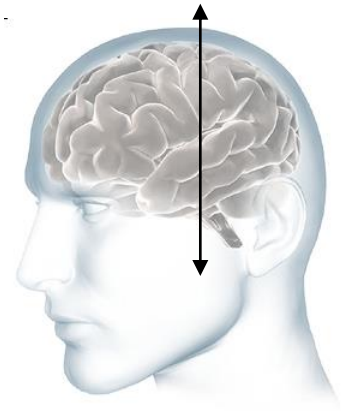

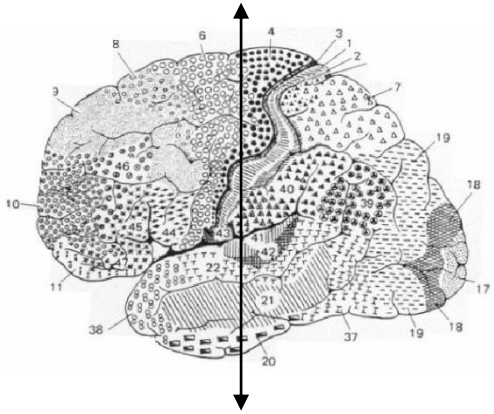

Brodmann areas
(cytoarchitectonically defined)

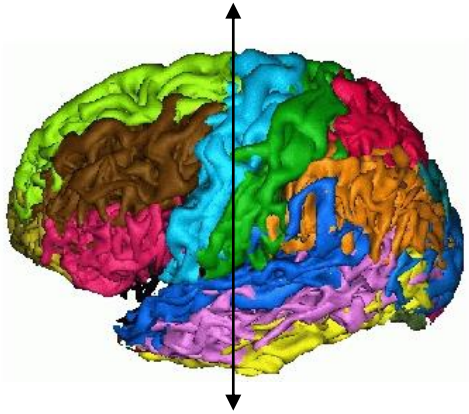

Brodmann areas
(MRI defined)

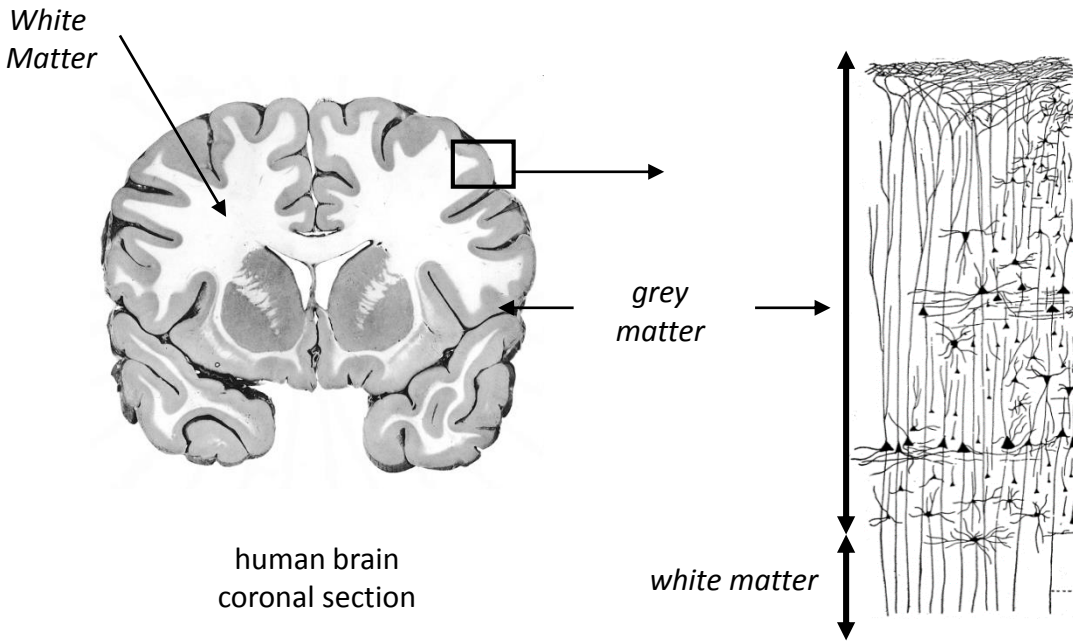

human brain
coronal section

pyramidal neuron

Ramon y Cajal (Nobel / 1906 with Golgi) silver impregnation

pyramidal cells

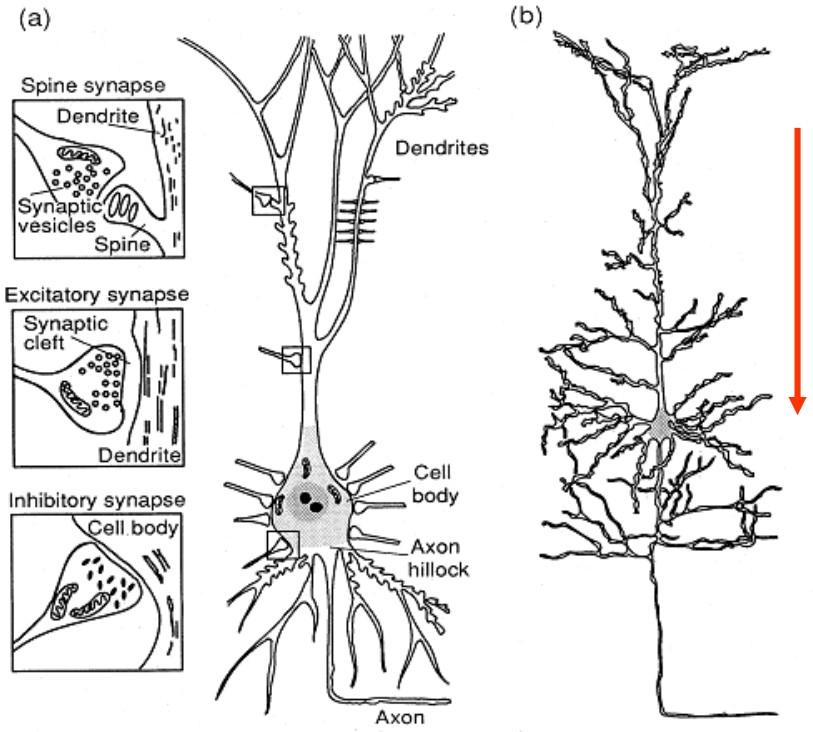

FIG. 15. Cortical neuron. (a) Schematic illustration of a pyramidal neuron and three magnified synapses (modified from Iversen, 1979); (b) pyramidal neuron, redrawn from Ramón y Cajal.

adapted from Iversen (1979)

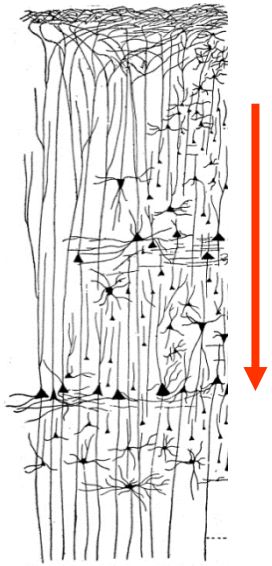

cortical column 10^5- 10^6 neurons

currents in axons and dendrites

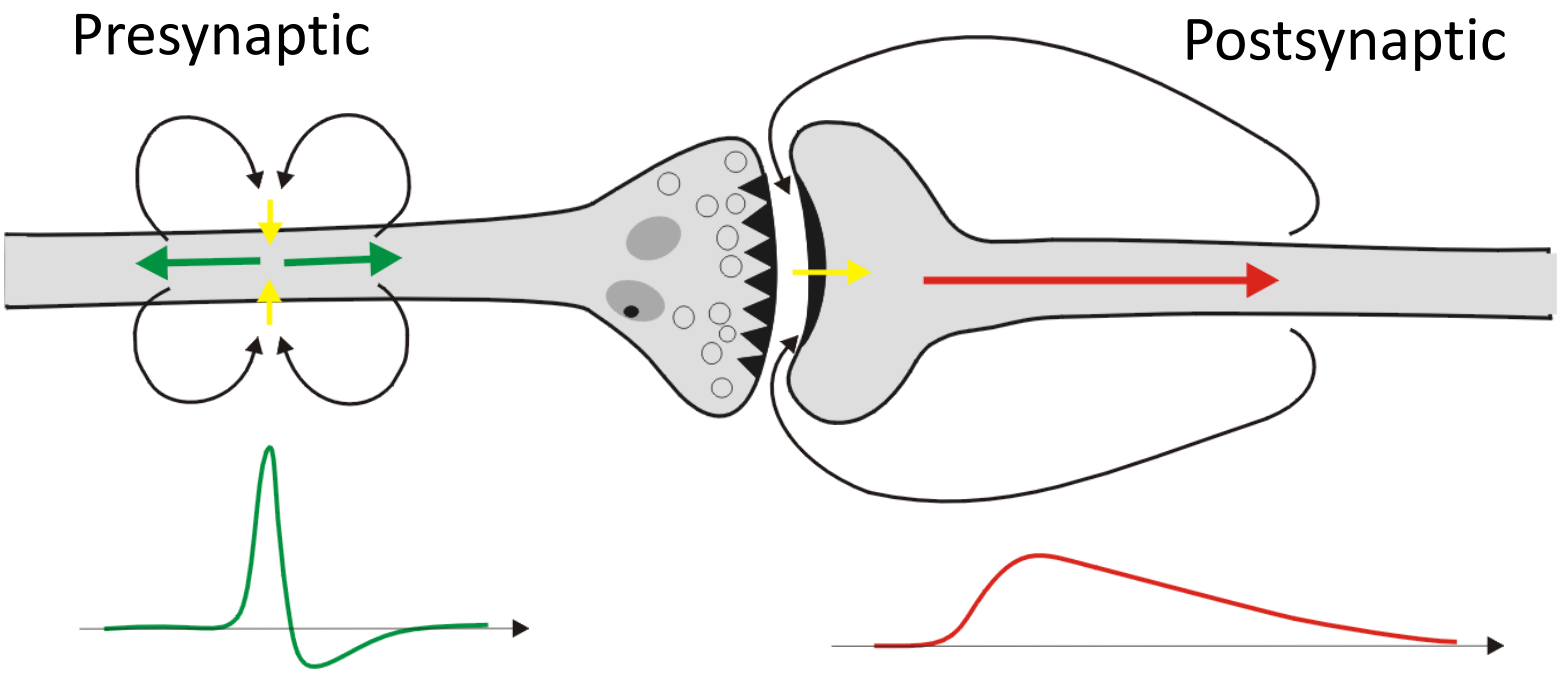

- Action potentials:
  - Fast: no/little temporal summation
  - Cancellation: fields diminish rapidly

- Postsynaptic currents:
  - Slow: temporal summation
  - dipolar currents
  - **the main source of MEG&EEG!**

courtesy of Lauri Parkkonen

neural currents

- **Impressed currents $\mathbf{J}_i(\boldsymbol{r})$**

  are due to electrochemical gradients and open ion channels across the cell membrane

- **Primary currents $\mathbf{J}_p(\boldsymbol{r})$**

  are due to impressed currents

  ⇔ currents inside dendrites and axons

  decay with distance from the synapse

  (leaky cell membrane and resistive conductor)

- **Volume currents $\mathbf{J}_v(\boldsymbol{r})$**

  –due to primary currents

  –**passive, ohmic current flow**

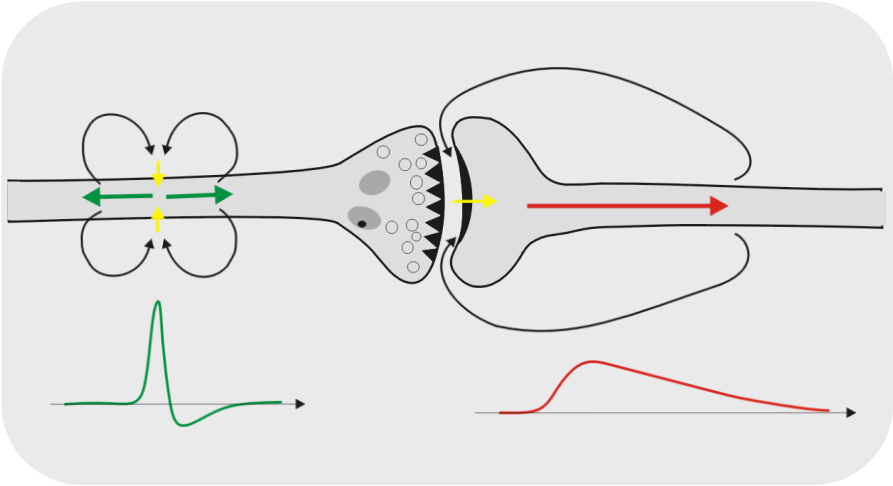

courtesy of Lauri Parkkonen

EEG electrical brain activity

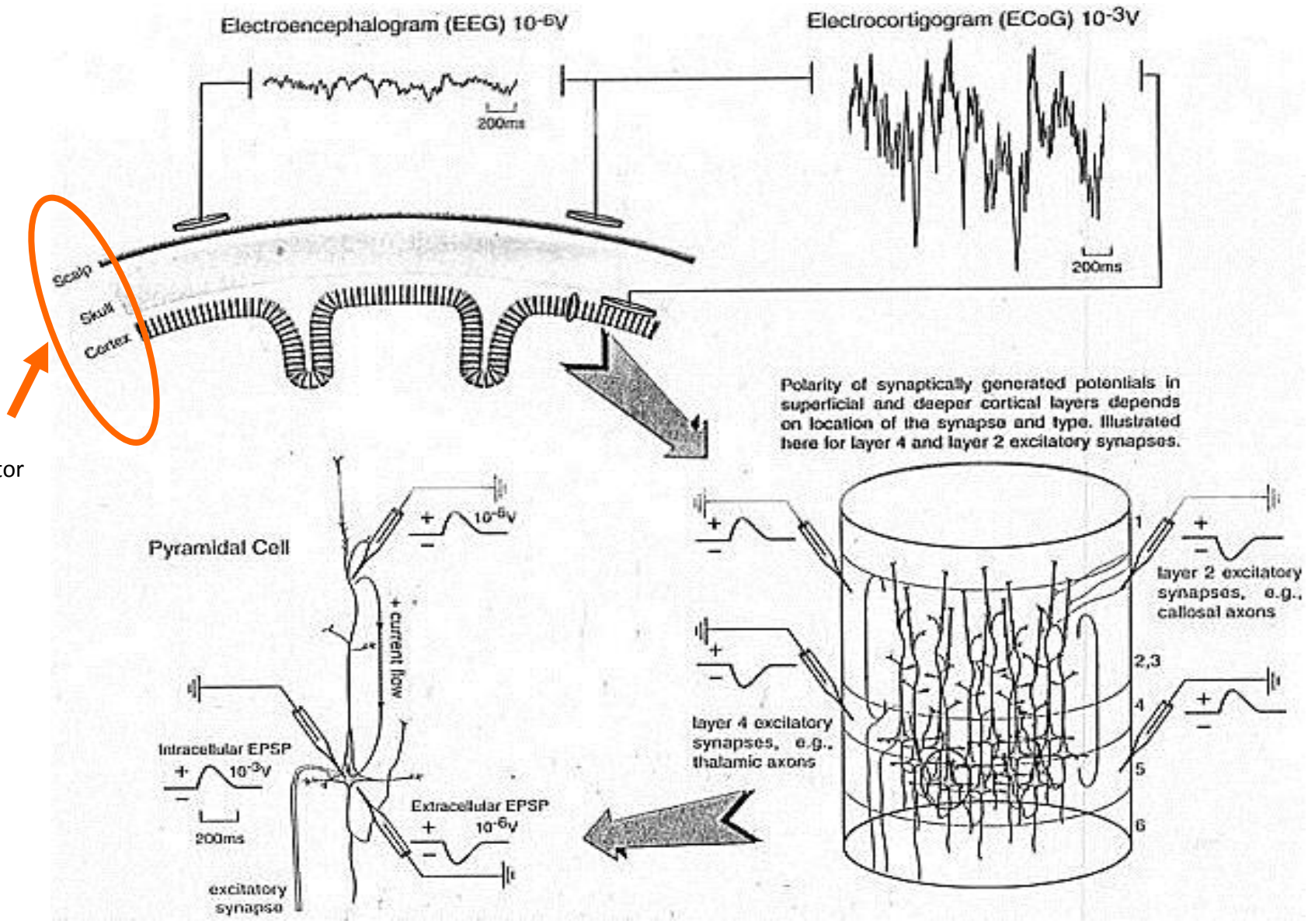

resistance
low conductor

EEG

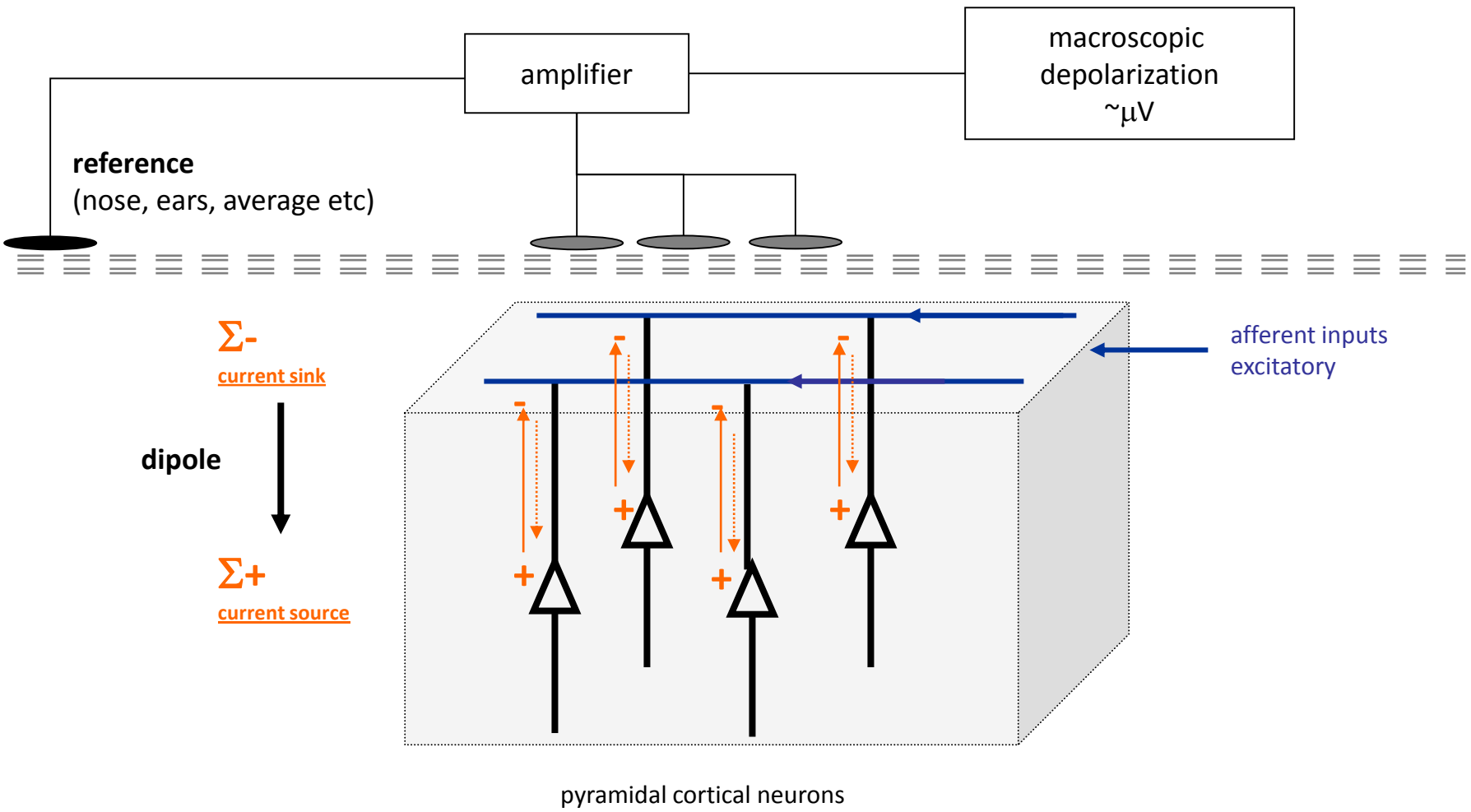
amplifier
macroscopic
depolarization
~μV
reference
(nose, ears, average etc)
Σ-
current sink
dipole
Σ+
current source
afferent inputs
excitatory
pyramidal cortical neurons

EEG

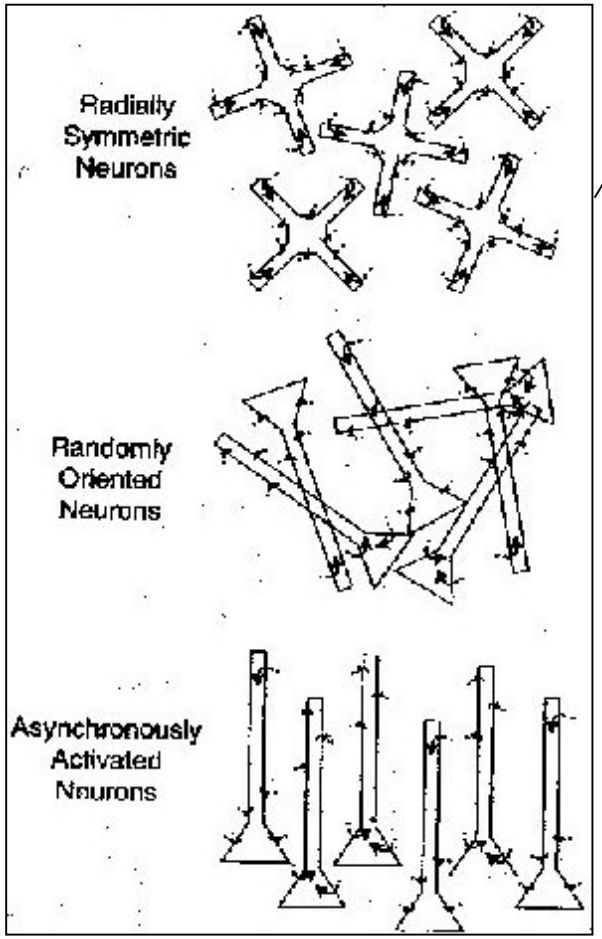

CLOSED fields
cancellation

OPEN fields

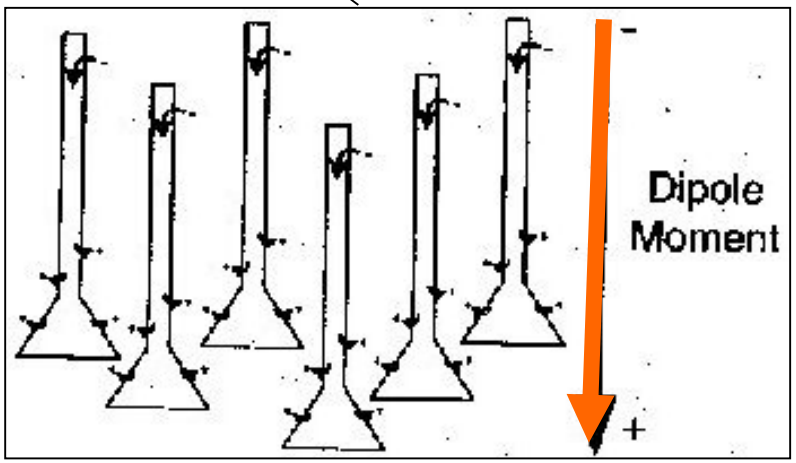

synchronized neural populations ⇔ transmembrane currents of pyramidal neurons apical dendrites

Why not action potentials?

spike vs. dendritic currents	::	synchronization issue
dendritic electrical dipoles vs. AP propagation	::	cancellation issue
spike rate vs. dendritic time constant	::	duration issue

EEG - MEG

By ***population of synchronized neurons***, we mean the following statistics:

BRAIN	≈ 10^{11} neurons
CORTEX	≈ 10^{10} neurons
PYRAMIDAL cells (excitatory)	≈ 85% (8.5^{10})
SYNAPSES	≈ 10^4 to 10^5
	(5% of connections from subcortical structures)
	=> <u>mostly cortico-cortical connections</u>
CORTICAL SURFACE	≈ 3000cm^2

=> temporal resolution **1 ms (fs dependent)**

=> spatial resolution **at best 1 cm^2 (at worst 100cm^2) for EEG**
at best 0.5 cm^2 for MEG, MEG-EEG

=> sensitivity **10^7 to 10^9 neurons**
down to 50 000 neurons for 10 nAm (Hämäläinen, 1993)

~1% of neurons fire synchronously for a given stimulus within a cortical patch yet contribute to > 80% of the signal

MEG *vs* EEG - orthogonality & complementarity

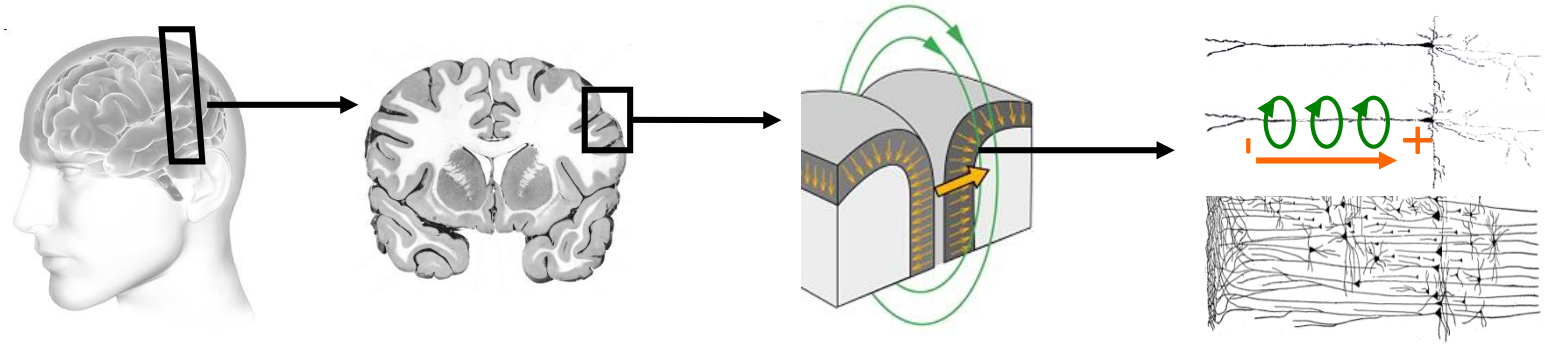

MEG benefit:

whereas the electrical brain signals are distorted and attenuated by the skull, scalp etc, the magnetic field is NOT.

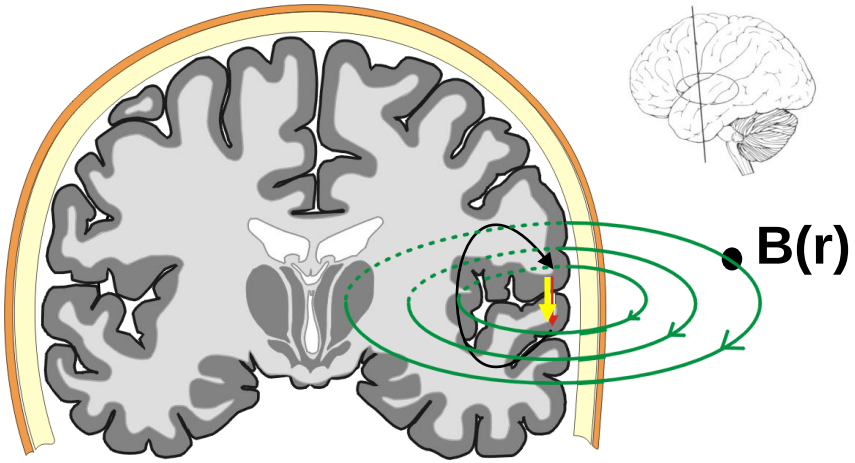

courtesy of Lauri Parkkonen

MEG vs EEG - orthogonality & complementarity

EEG sensitive to combinations of tangential (sulci) & orthogonal sources (top of gyri & radial sources)

MEG sensitive to tangential sources (sulci)

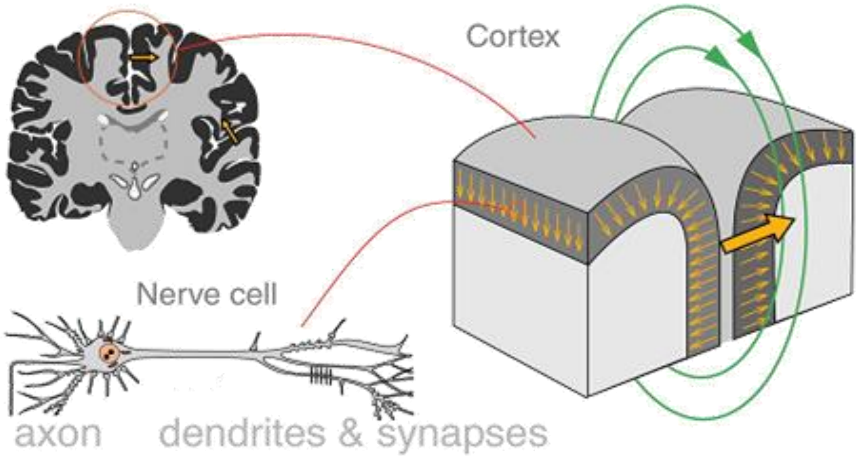

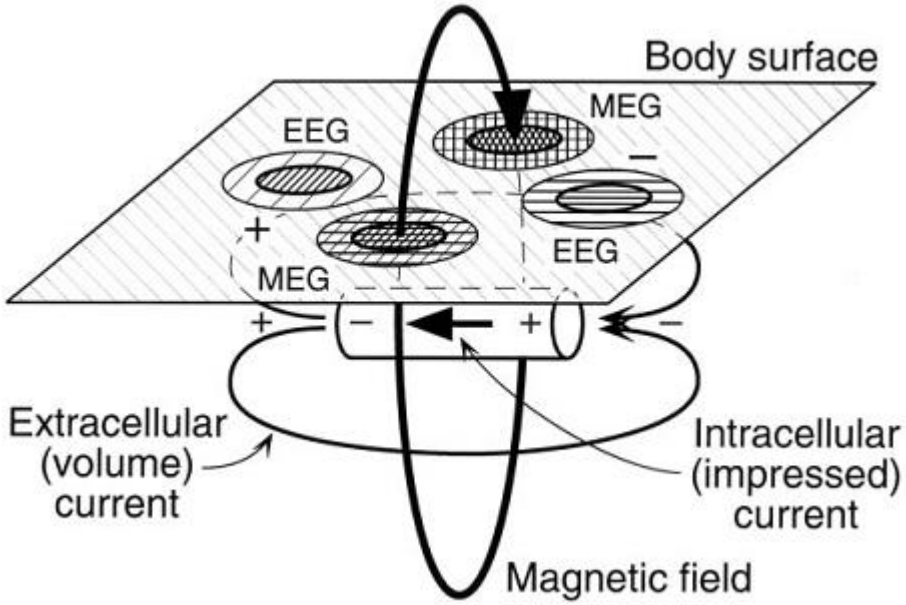

adapted from Vrba & Robinson (2001) Methods

MEEG

MEG & EEG are complementary methods which can be used simultaneously
(204 grad sites + 102 magneto sites + 256 EEG sites)

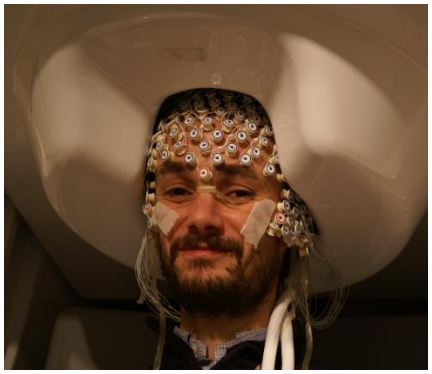

MEG @ NeuroSpin (courtesy Lauri Parkkonen)

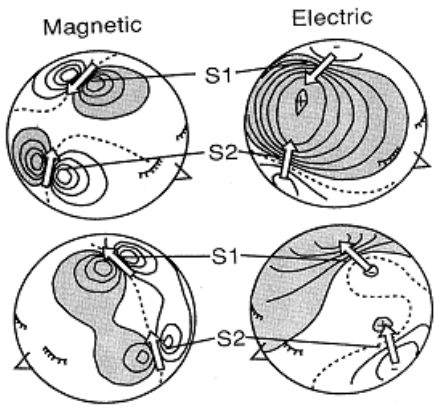

adapted from Hämäläinen et al (1993) Rev. Mod. Physics

MEG+EEG data fusion for improved source localization

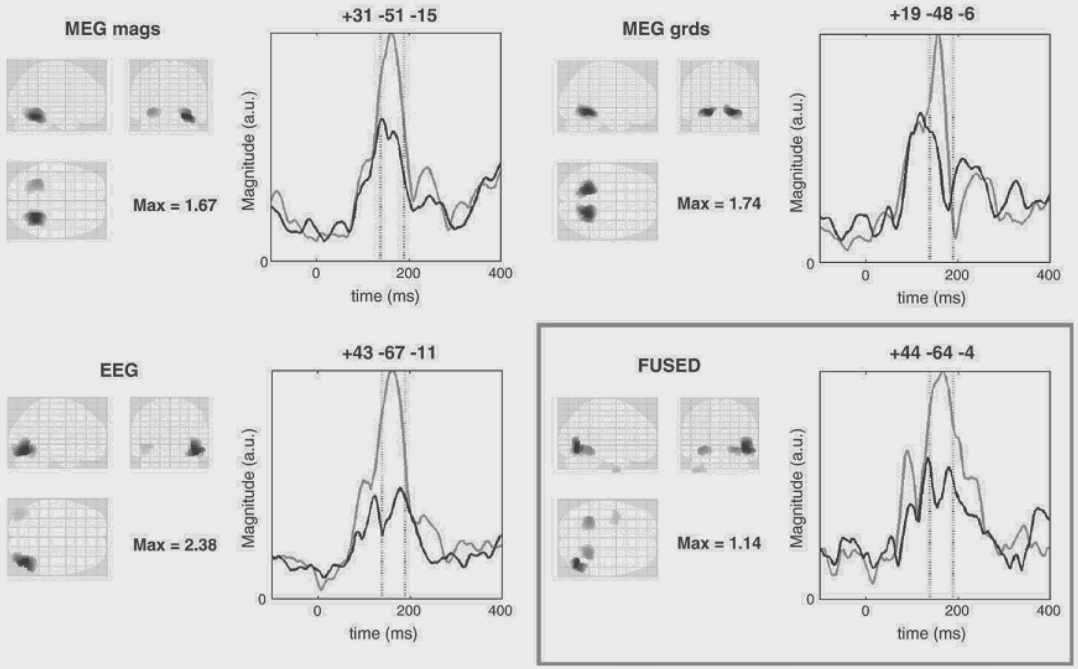

adapted from Henson, Mouchlianitis, Friston (2009) NIMG

depth

the deeper the primary current, the more attenuation

no magnetic signal from the center of a conducting sphere

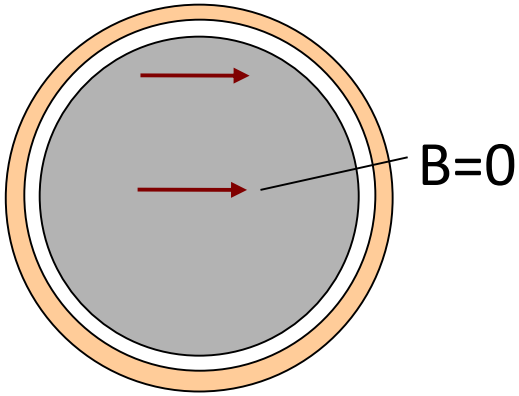

cancellation

close-by areas with simultaneous, opposing current flow

decrease the signal

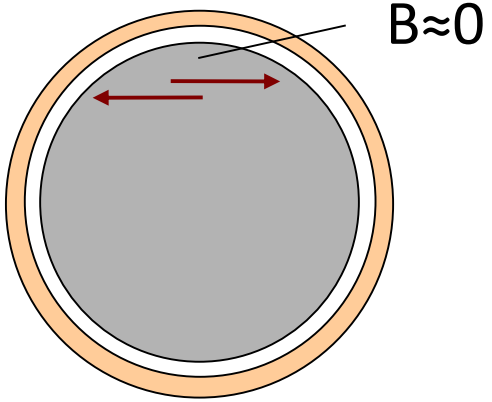

courtesy of Lauri Parkkonen

magnetic vs electric fields patterns on the scalp

out of the head

in the head

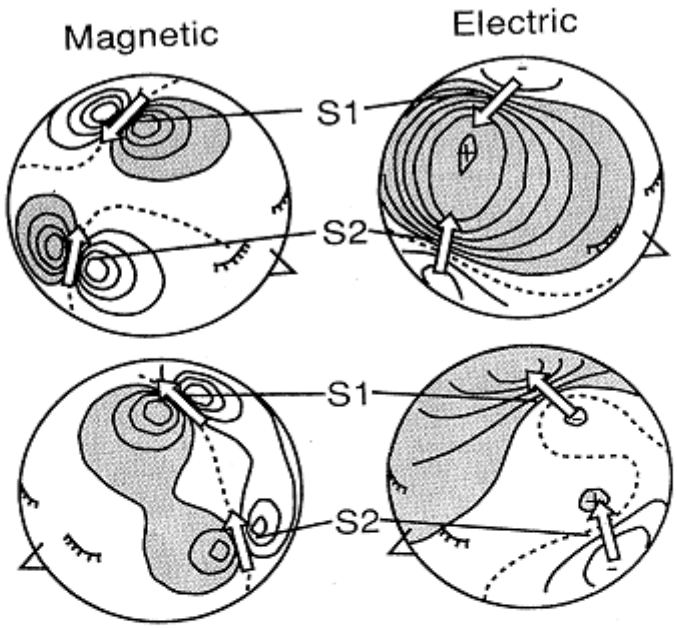

FIG. 54. Schematic illustration of electric and magnetic patterns due to activity in the first and second somatosensory cortices S1 and S2. In the simulations, the head was assumed to be a spherical conductor with four layers of different conductivities, corresponding to the brain, the cerebrospinal fluid, the skull, and the scalp. The situation corresponds to that observed after left-sided peroneal nerve stimulation at the ankle, with simultaneous activity at S1 in the inner central wall of the right hemisphere and at both S2 areas. The dipole strengths were assumed equal at S1 and at the right S2, and $\frac{1}{3}$ smaller at the left S2. The shadowed areas indicate magnetic flux out of the head and positive electric potential. Modified from Kaukoranta, Hari, *et al.* (1986).

adapted from Hämäläinen et al (2003) Phys Rev

MEG sensors

adapted from Hämäläinen et al (2003) Phys Rev

Super QUantum Interference Device

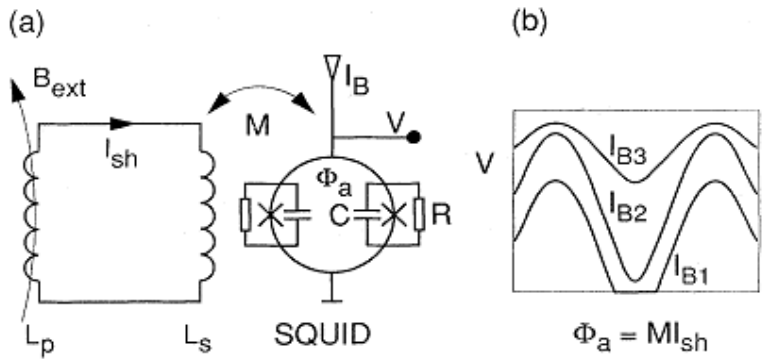

FIG. 28. SQUID basics. (a) Schematic diagram of a dc SQUID magnetometer. The external field B_{ext} is connected via a superconducting flux transformer (L_p,L_s) to the SQUID. In a gradiometer, there is an additional compensation coil in series with L_p. (b) The average voltage V across the SQUID depends on the dc bias current I_B and is a periodic function of the flux Φ_a coupled to the SQUID ring.

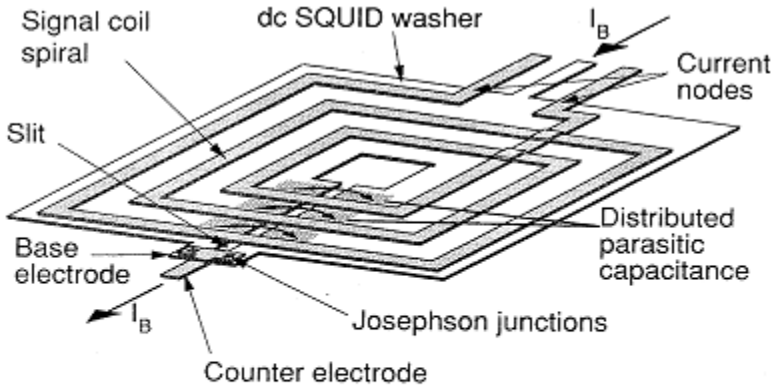

FIG. 29. Simplified structure of a planar thin-film dc SQUID with an input coil. The distributed parasitic capacitances across the SQUID washer and the locations of the current nodes for the microstrip resonance are indicated.

adapted from Hämäläinen et al (2003) Phys Rev

flux transformers

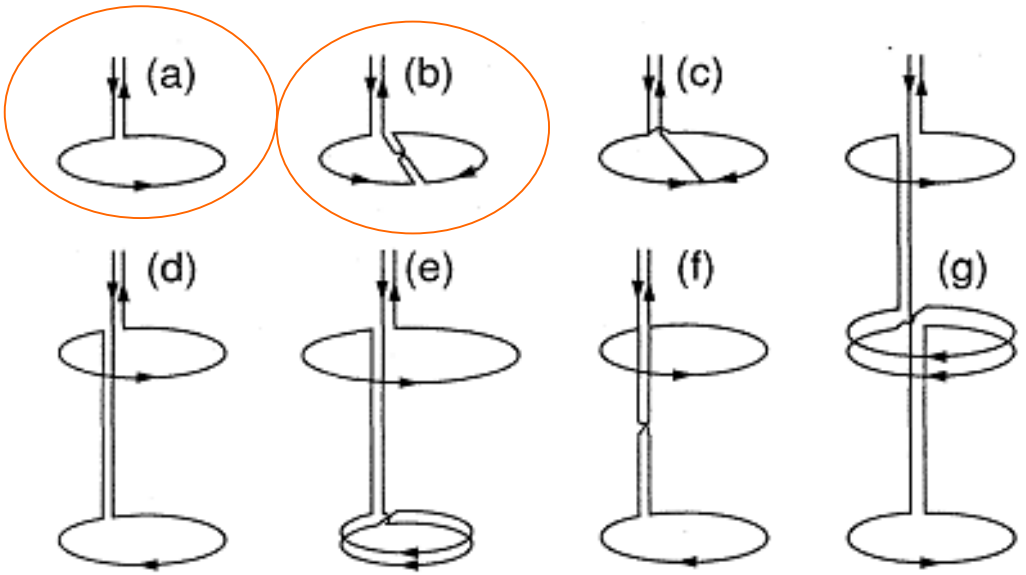

FIG. 26. Various types of flux transformers: (a) magnetometer; (b) series planar gradiometer; (c) parallel planar gradiometer; (d) symmetric series axial gradiometer; (e) asymmetric series axial gradiometer; (f) symmetric parallel axial gradiometer; and (g) second-order series axial gradiometer.

flux transformers =
measure the magnetic flux over a given surface

adapted from Hämäläinen et al (2003) Phys Rev

sensor arrays

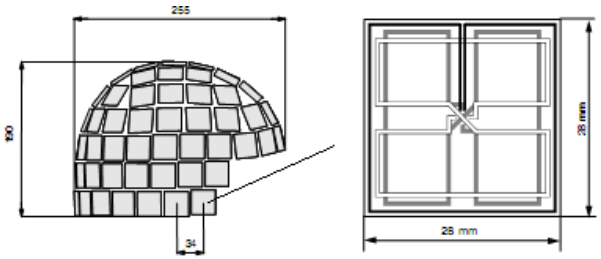

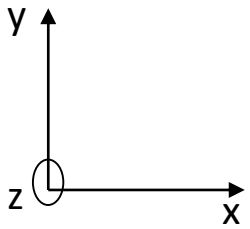

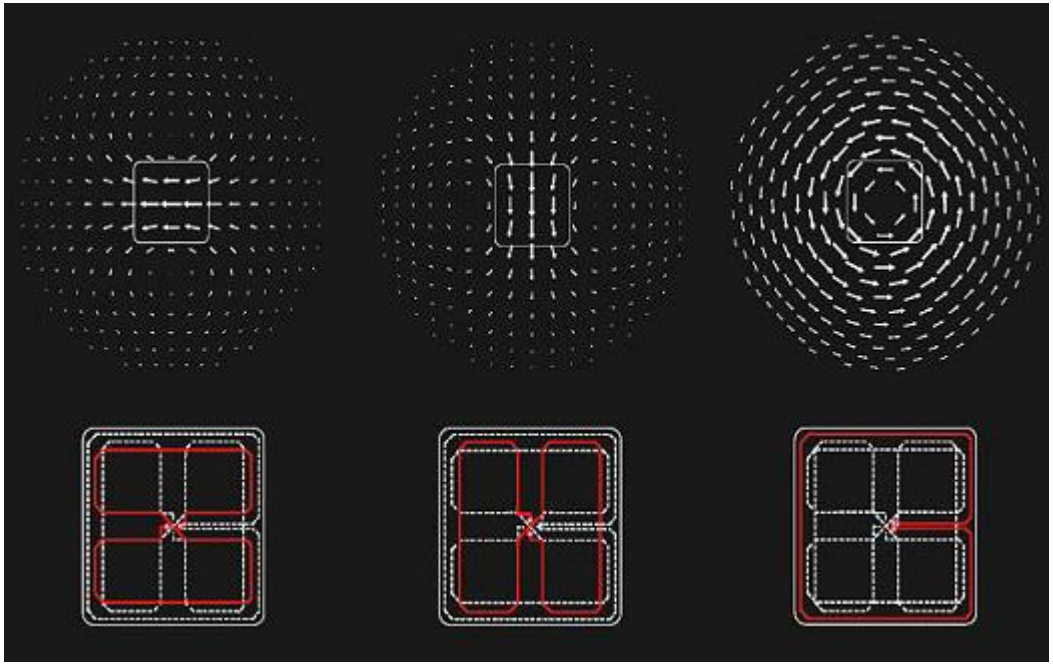

gradio (dB_z/dy)

gradio (dB_z/dx)

magneto (B_z)
axial gradiometer (dB_z/dz)

at each recording site (306 total): 2 gradiometers + 1 magnetometer ⇔ 510 pick-up coils

204 planar gradiometers with **focal sensitivity, spatial gradient**
(102 B' along longitude/polar, 102 B' along latitude/azimuthal)
+
102 magnetometers (**widespread sensitivity**, field component B)

neuromag system convention

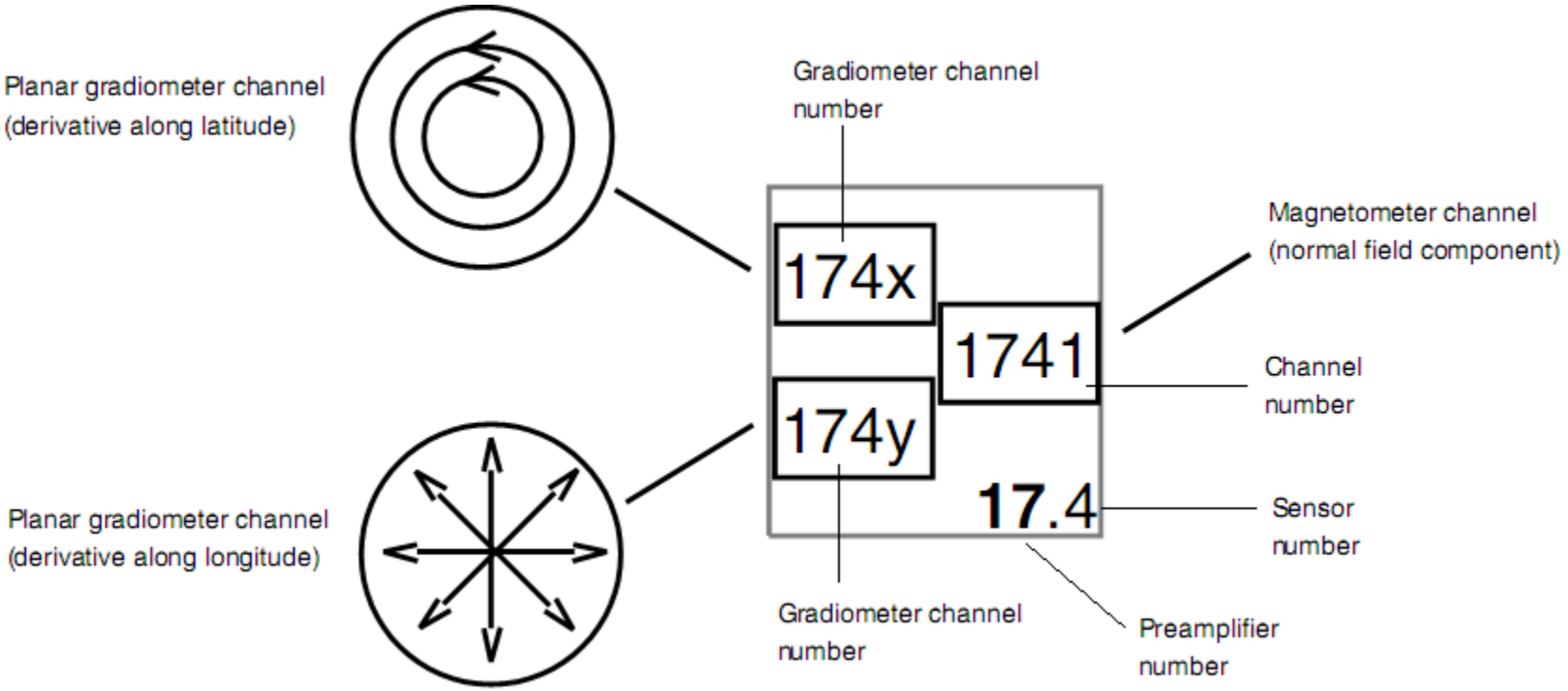

1 recording site gives 3 quantitative descriptions

example . tibial nerve

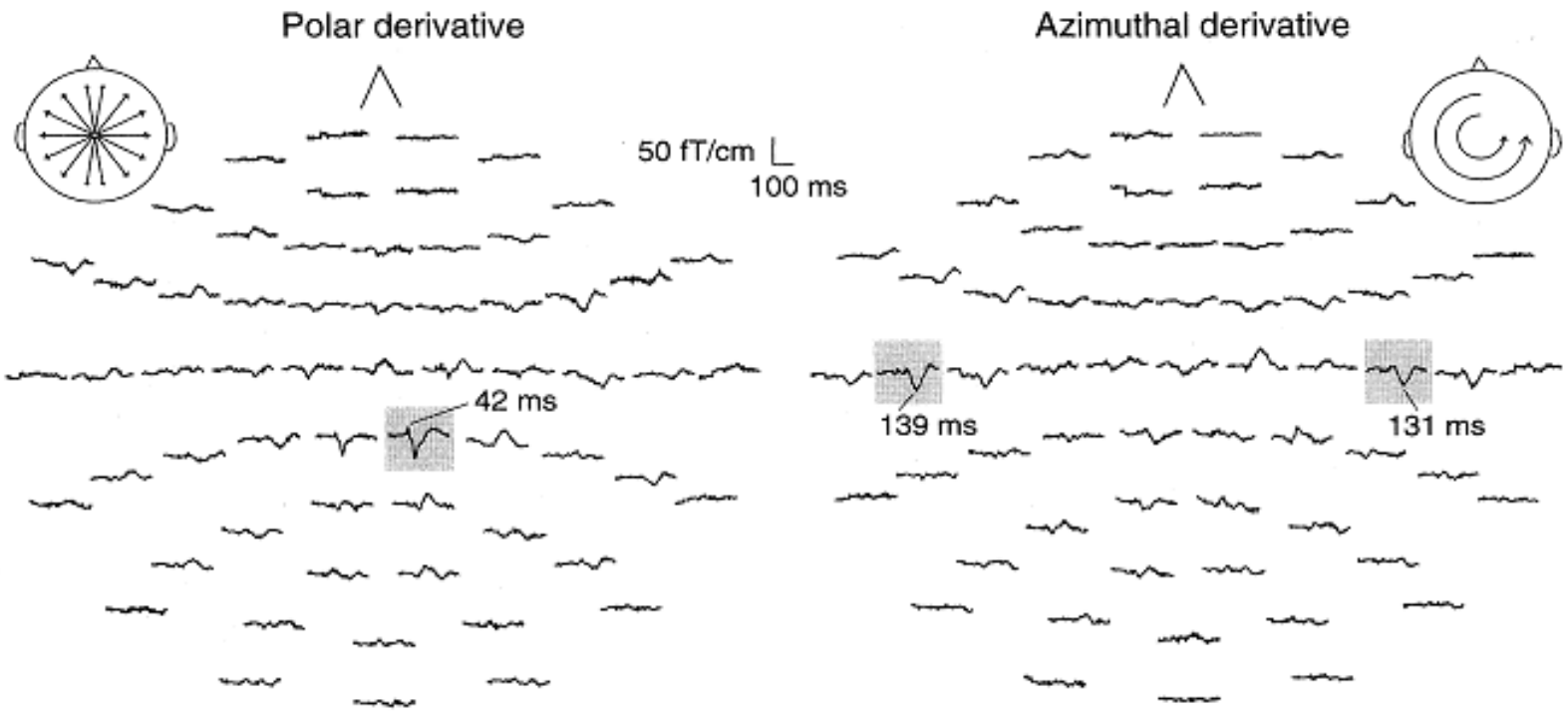

FIG. 56. Responses to stimulation of the left tibial nerve at the ankle. The recording was made with the whole-head 122-SQUID magnetometer (see Figs. 41 and 42). The ISI was 2 s, the recording passband 0.05–180 Hz, and about 150 single responses were averaged. The traces were digitally low-pass filtered at 140 Hz. The field gradients are shown separately in the polar direction (left) and in the azimuthal direction (right). From Hari *et al.* (1993).

example. auditory cortical response

polar derivative (grad)

azimuthal derivative (grad)

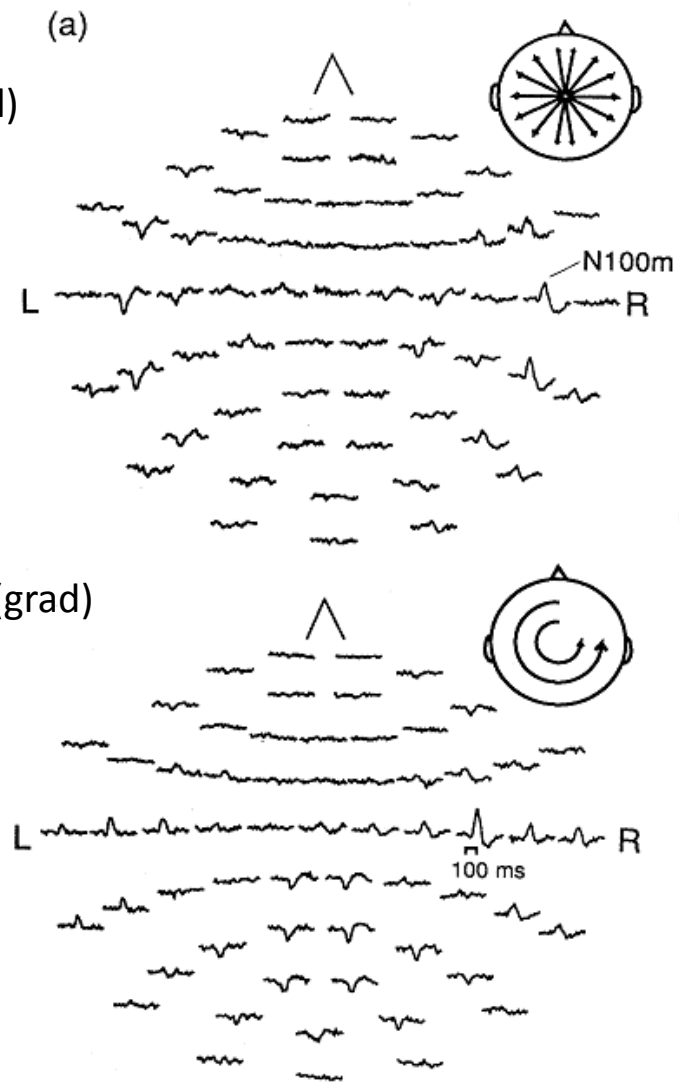

sensitivity

EEG vs MEG sensitivity

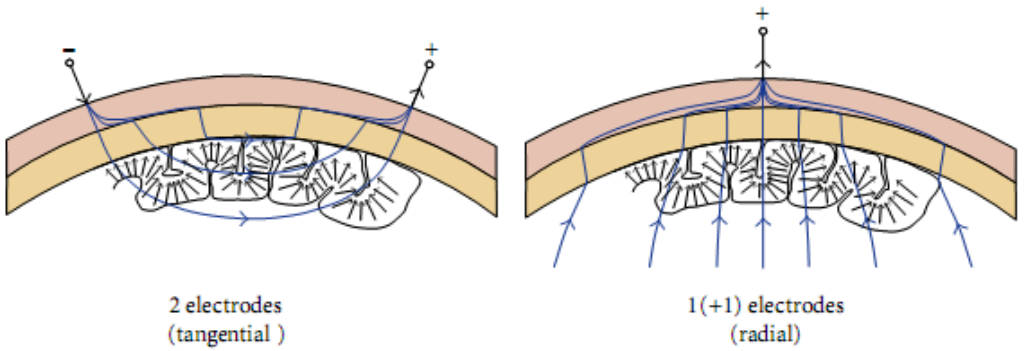

FIGURE 2: The Sensitivity Distributions of EEG. (Left) An EEG setup measuring the tangential components of neuroelectrical activity, where each bipolar lead is located relatively close to each other. (Right) An EEG setup measuring the radial components of neuroelectric activity, where the measuring electrode is located far from the reference electrode. The arrows in both figures represent macrocolumns of cellular architecture not dipolar sources.

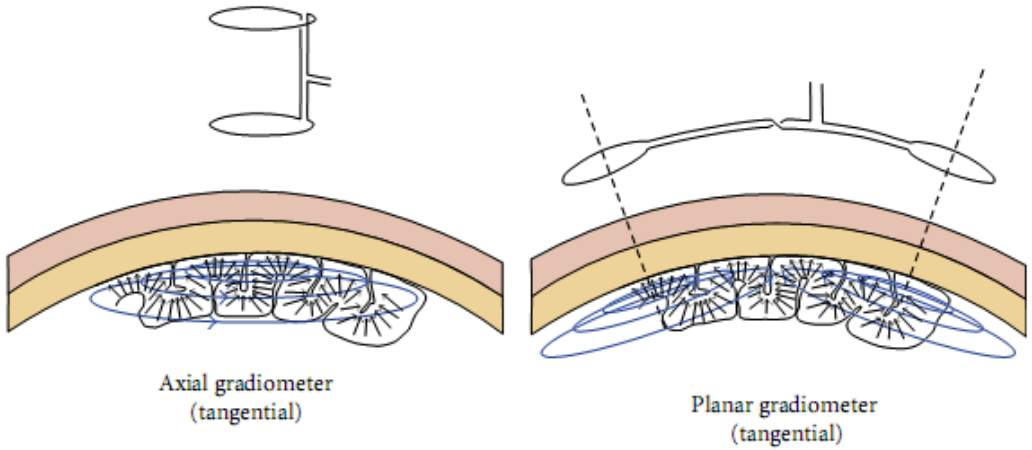

FIGURE 3: The Sensitivity Distributions of MEG. (Left) An MEG setup measuring the tangential components of neuroelectrical activity, using an axial gradiometer. (Right) An MEG setup measuring the tangential components of neuroelectric activity, using a planar gradiometer. The arrows in both figures represent macrocolumns of cellular architecture not dipolar sources.

adapted from Wendel et al (2009) Comp Int Neuro

EEG/MEG

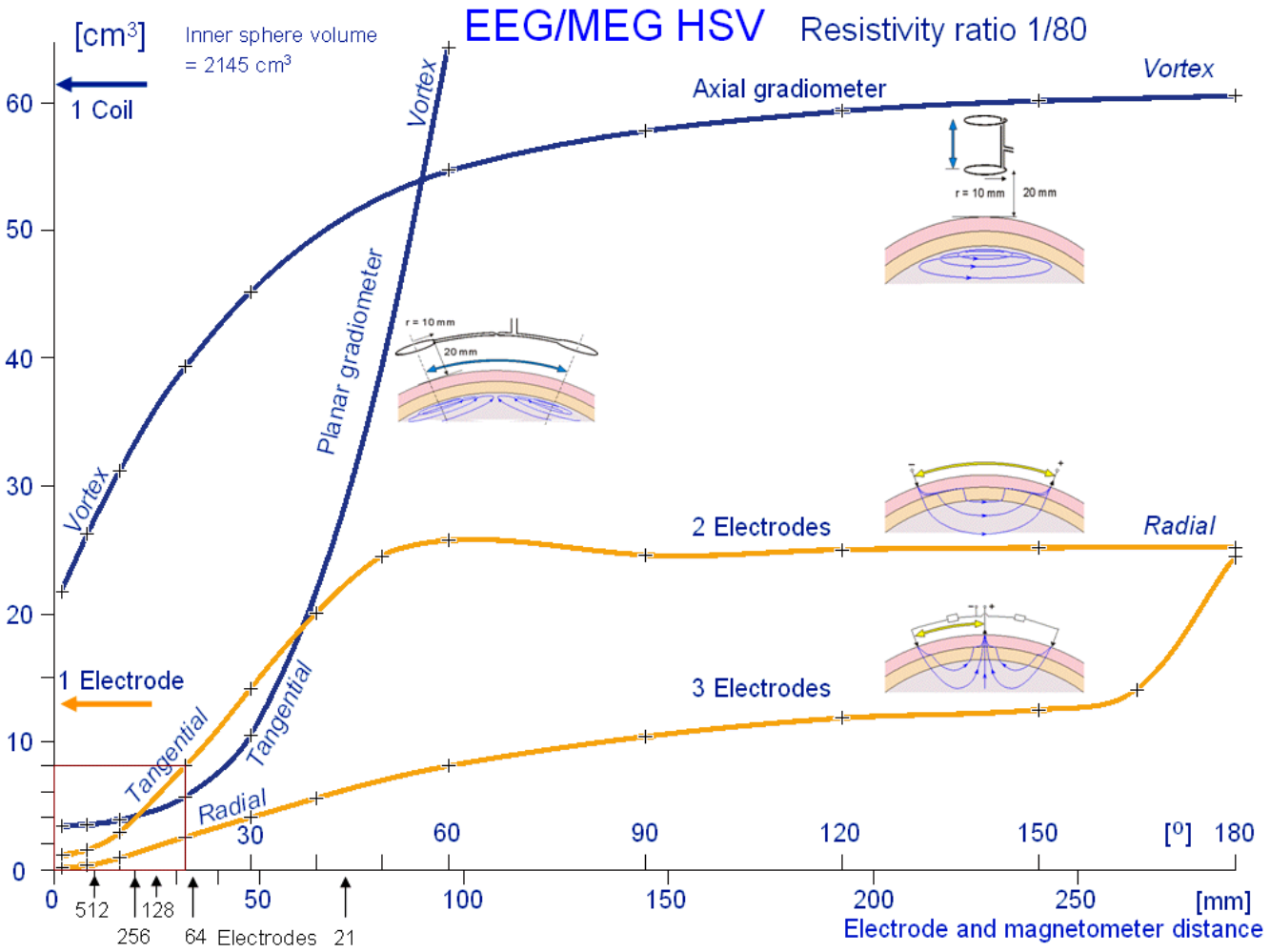

adapted from Wendel et al (2009) Comp Int Neuro

Magnetometers

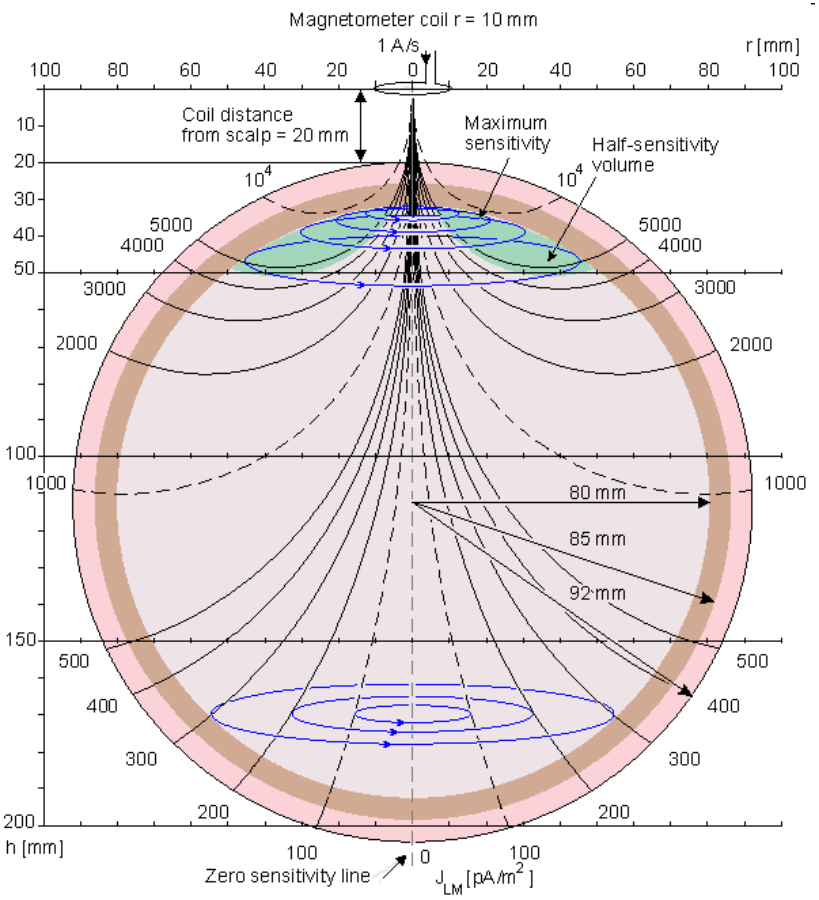

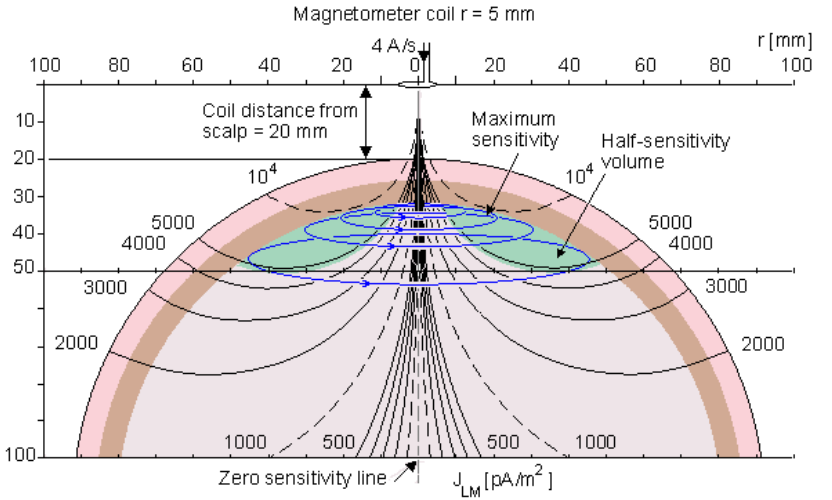

adapted from Wendel et al (2009) Comp Int Neuro

Planar Gradiometers

Sensitivity profiles

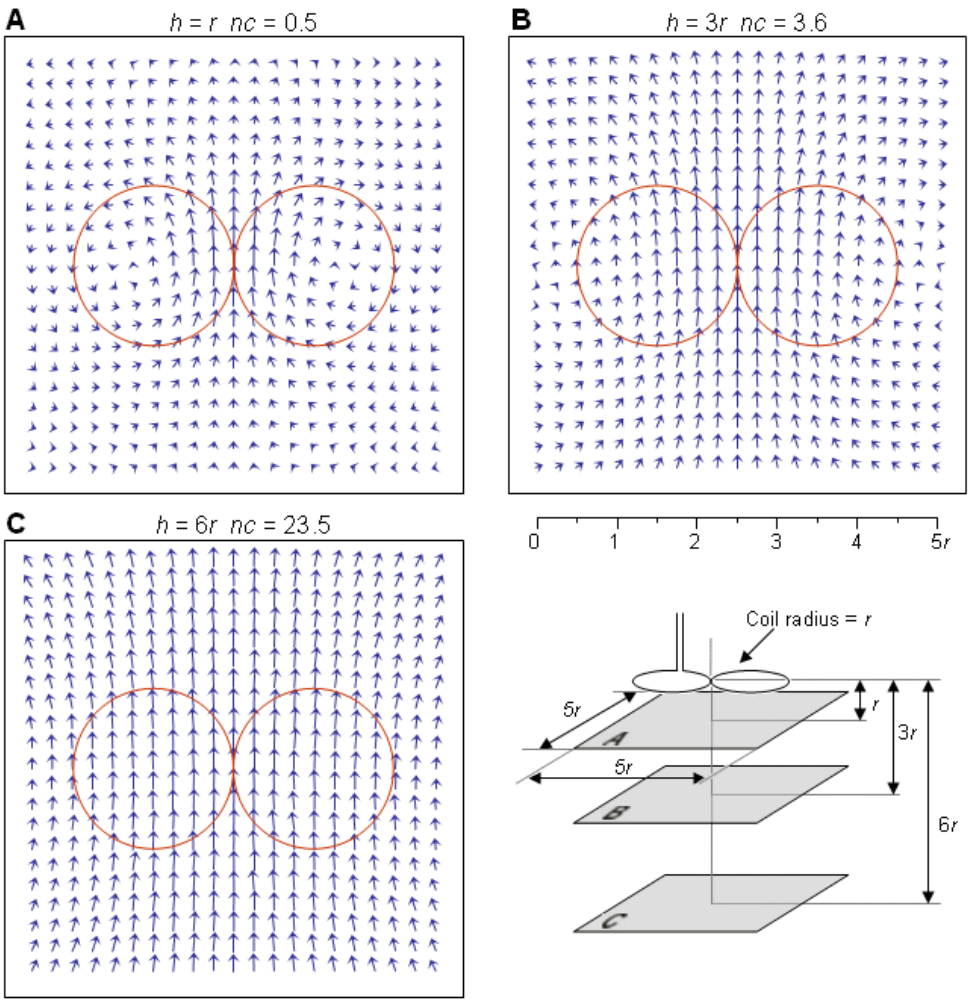

adapted from Wendel et al (2009) Comp Int Neuro

Planar Gradiometers

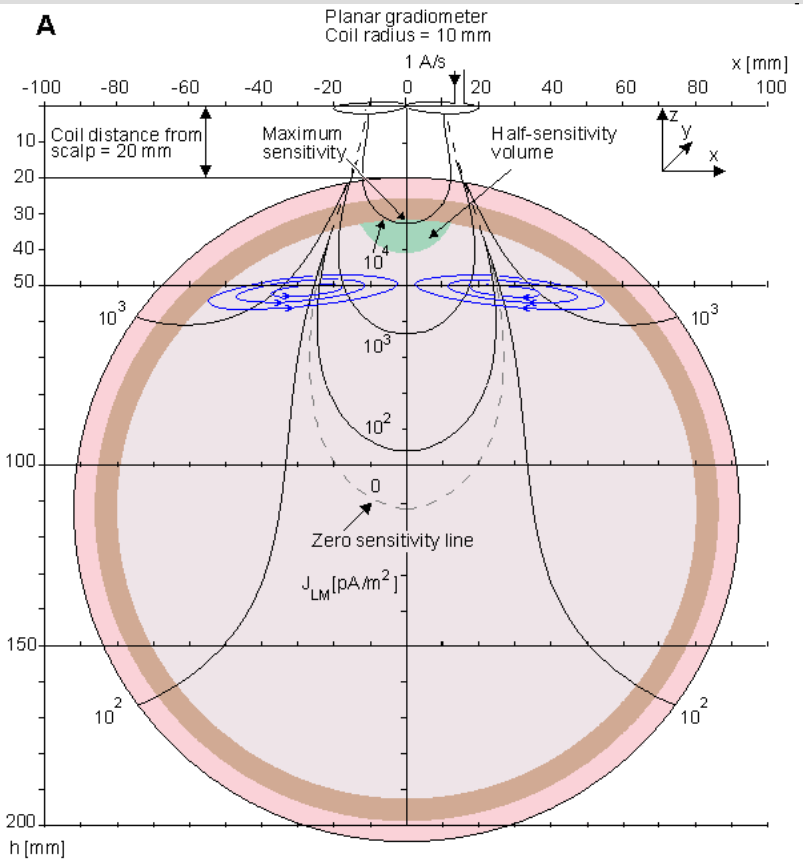

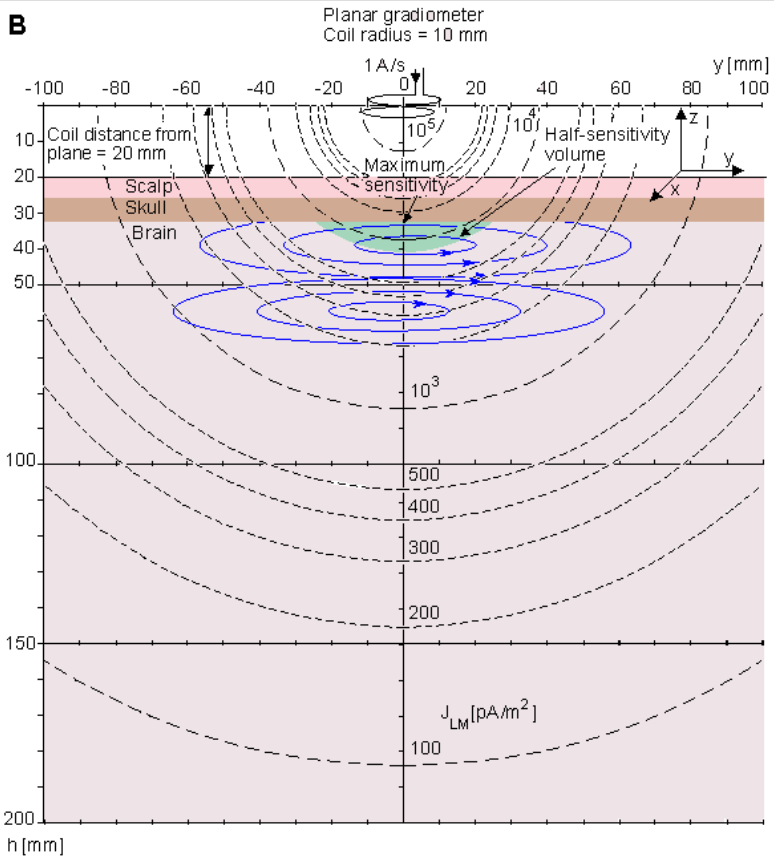

Isosensitivity lines (dashed lines) and half-sensitivity volume for a planar gradiometer calculated for a conducting half-space. Lead field current flow lines are drawn with thin solid lines. They are not accurate solutions.

A) In the *xz*-plane the zero sensitivity line approaches asymptotically the line which makes a 35.27° angle with respect to the z-axis.

B) In the *yz*-plane the isosensitivity lines approach concentric circles at long distances concentric circles

adapted from Wendel et al (2009) Comp Int Neuro

Leadfield

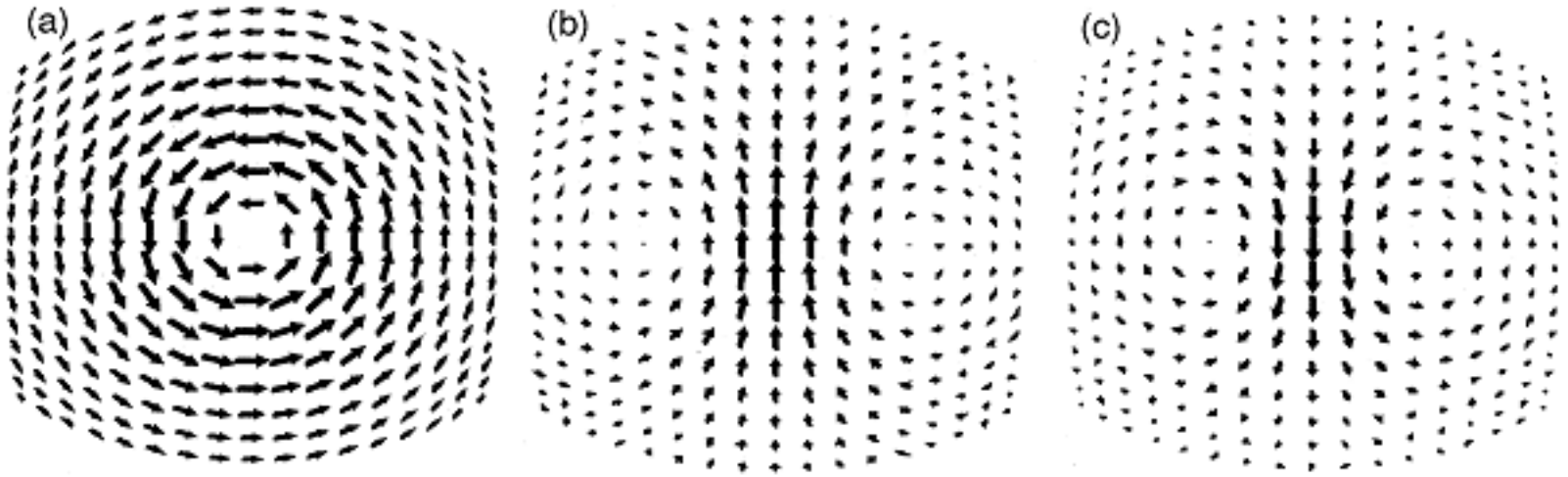

FIG. 19. Two-dimensional projections of the lead field $\mathcal{L}(\mathbf{r})$ of point magnetometers measuring (a) B_z, (b) B_x, and (c) of a gradiometer measuring $\partial B_z/\partial x$, sampled on a surface whose radius is 90 mm. Each signal coil is located at $x = y = 0$, $z = 125$ mm.

adapted from Hämäläinen et al (2003) Phys Rev

experimental design in MEEG

general MEG pipeline

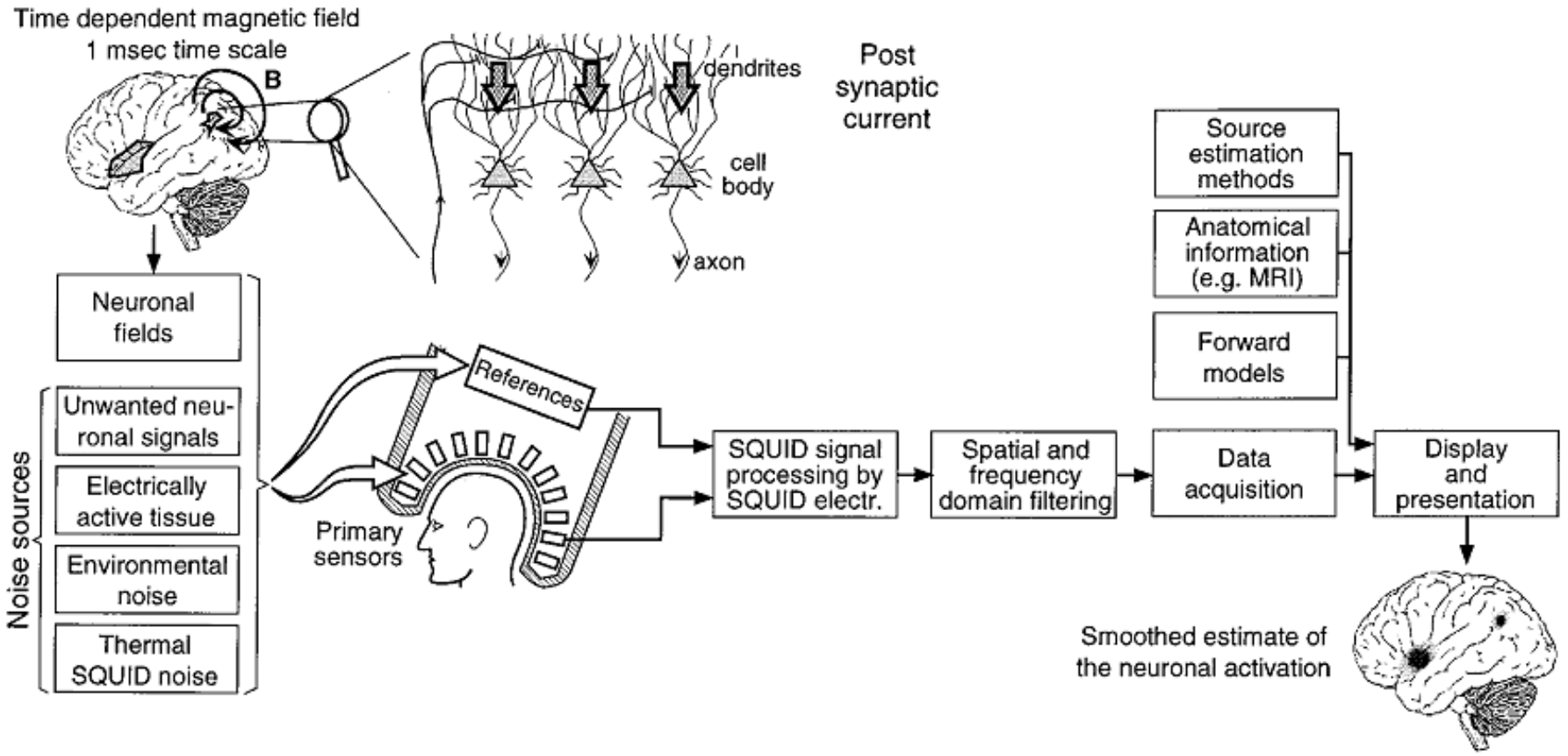

adapted from Vrba & Robinson (2001) Methods

experimental design

before anything: what are you interested in & what is your question?

- Spontaneous activity ("resting-state")?

  > continuous recording, clinical observation and/or temporal and/or spectral and/or coherence etc

- Evoked or phase-locked responses?

  typically within 1 s of stimulus onset

  transient ON/OFF responses

  > time-domain averaging

- Modulation of cortical rhythms or induced responses?

  non-phased locked

  longer time frame

  > spectral type analysis (frequency, time-frequency analysis)

- Changes in interareal synchronization / functional dynamic network ?

  from transient to long-lasting effects

  > coherence, phase-synchronization

EEG. spontaneous activity

- **Hans Berger** (1929) - first electroencephalogram

  Scalp potential changes were recorded with string galvanometer.

- **Jasper** (1941): EEG profiling of different states of the consciousness.

  The following states: 'excited', 'relaxed', 'drowsy', 'asleep', 'deep sleep' and 'coma' then defined are still being used for clinical purposes. Traces are characteristic enough to be observed online.

- **G.D. Dawson**: signal averaging technique.

  The principle is to repeat a stimulus condition many times and average the recordings together. This method allows to remove most of random noise or more specifically signals non causally related to the stimulus.

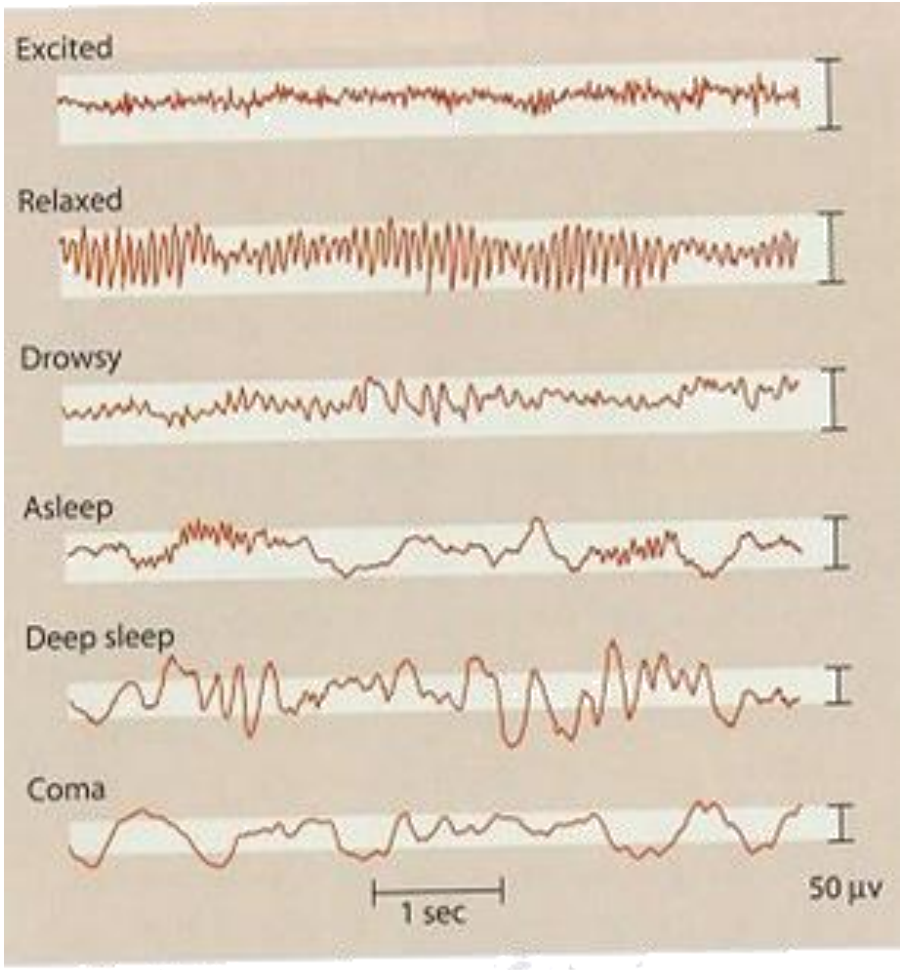

igure 4.24 EEG profiles obtained during various states of onsciousness. From Kolb and Whishaw (1986) after Penfield nd Jasper (1954).

MEG. spontaneous activity (tau rhythm)

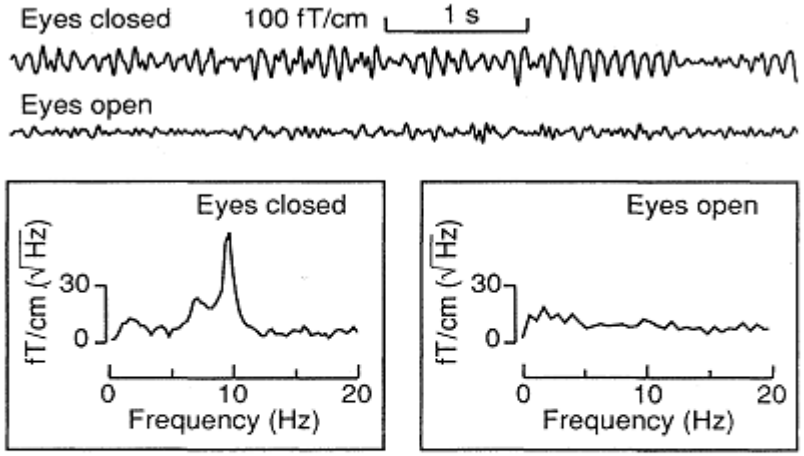

FIG. 58. Alpha rhythm on one gradiometer channel from the occipital area when the subject had his eyes closed or open. The frequency spectra were calculated from 20-s time sequences.

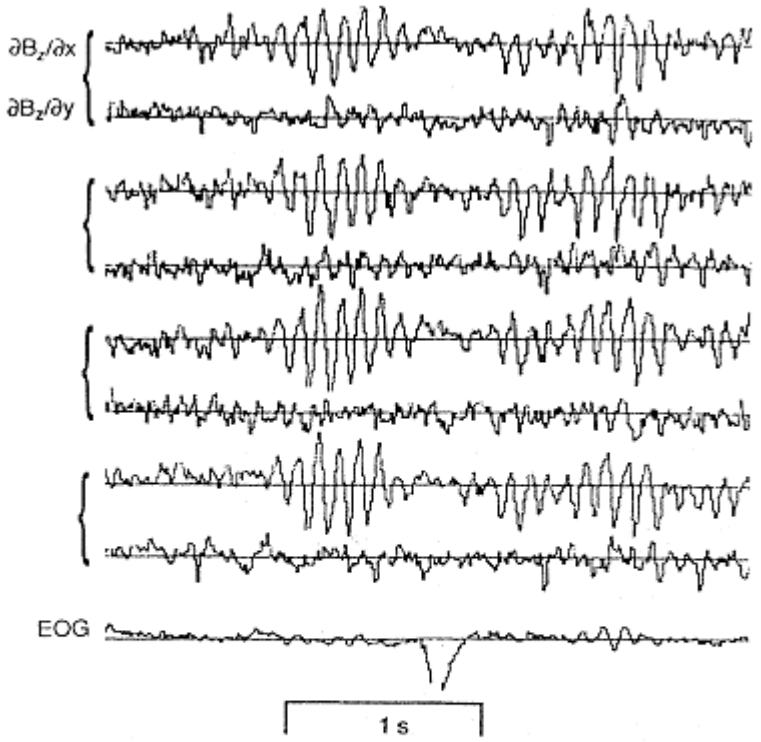

FIG. 59. Spontaneous magnetic activity recorded by eight MEG channels ($\partial B_z/\partial x$ above and $\partial B_z/\partial y$ below for each pair) over the right temporal area from a subject who had his eyes open. EOG refers to electro-oculogram. The signals were low-pass filtered at 40 Hz. Prominent τ oscillations can be seen. Modified from Hari (1993).

adapted from Hämäläinen et al (2003) Phys Rev

MEG. spontaneous activity (tau rhythm)

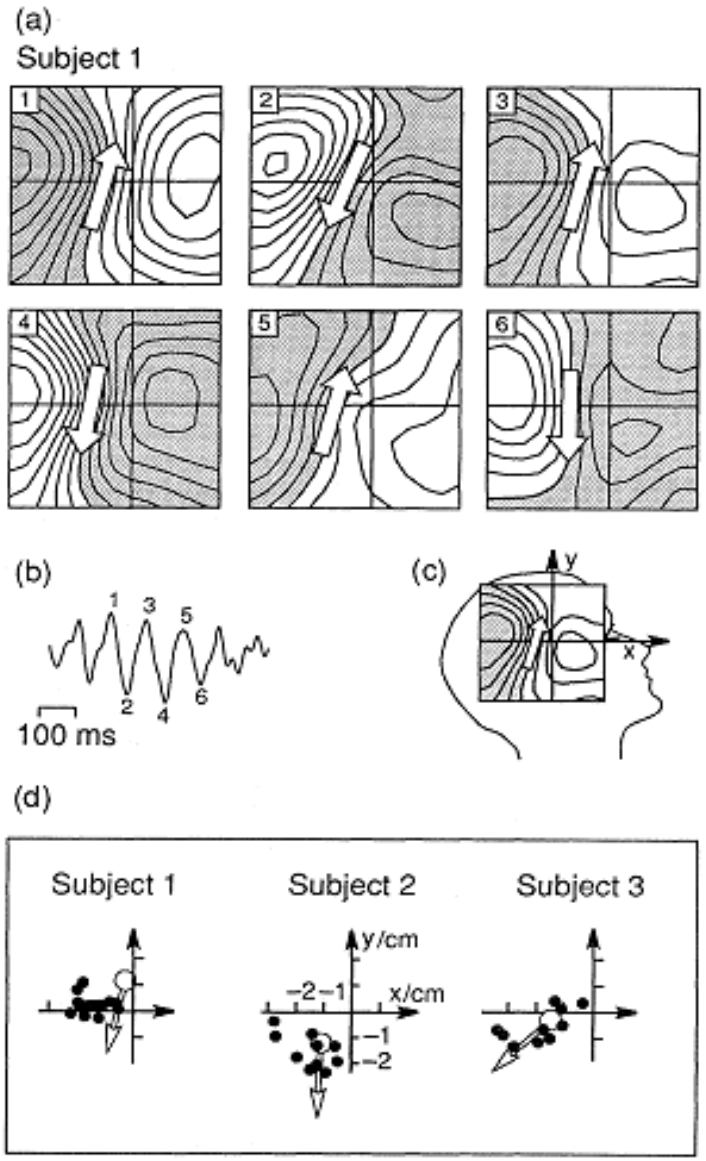

FIG. 60. Source locations of the τ rhythm. Maps in (a) show the magnetic-field component perpendicular to the head during the six successive peaks 1–6 in a representative section of the τ rhythm shown in (b). The inset (c) depicts the measurement region with respect to the subject's head. The shadowed areas indicate magnetic flux out of, and the white areas flux into, the head. The isocontours are separated by 100 fT. The white arrows in (a) show the locations and orientations of the equivalent current dipoles. For the coordinate system, see Fig. 47. Shown in (d) are the locations of the equivalent dipoles (solid circles) for ten peak deflections of the spontaneous 8–10-Hz oscillation for three subjects. The open circles and the white arrows show the dipole locations and orientations for the 100-ms auditory response. Modified from Tiihonen *et al.* (1991).

adapted from Hämäläinen et al (2003) Phys Rev

event-related potentials (EEG.ERP) or fields (MEG. ERF)

rule of thumb : SNR decreases w/ sqrt(2)

repeat stimuli ~100 x / no real benefit above 150 trials, SNR loss below 100 trials

+

plan for ~20% **artifact rejection** due to blinks, muscle artifacts etc / **120 trials**

+

artifact correction may be necessary if insufficient SNR (e.g. pca, ica) / independent recording of typical sources of artifact EOG (eye blinks, movements, etc) and ECG (heart beat)

random presentation preferred unless specific adaptation design (e.g. MMN)

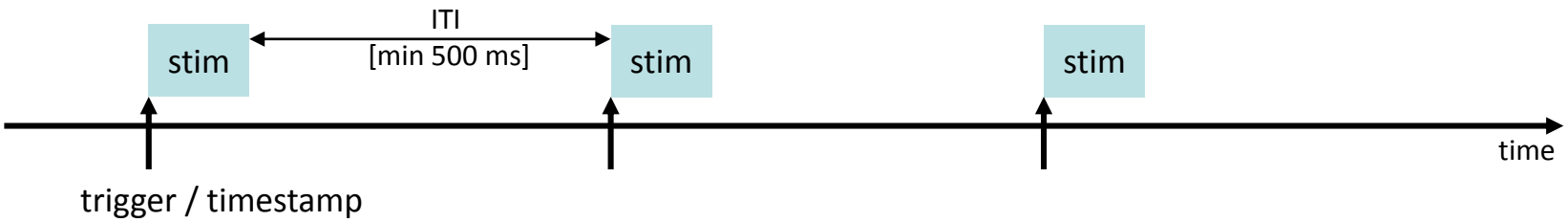

example of cardiac artifact

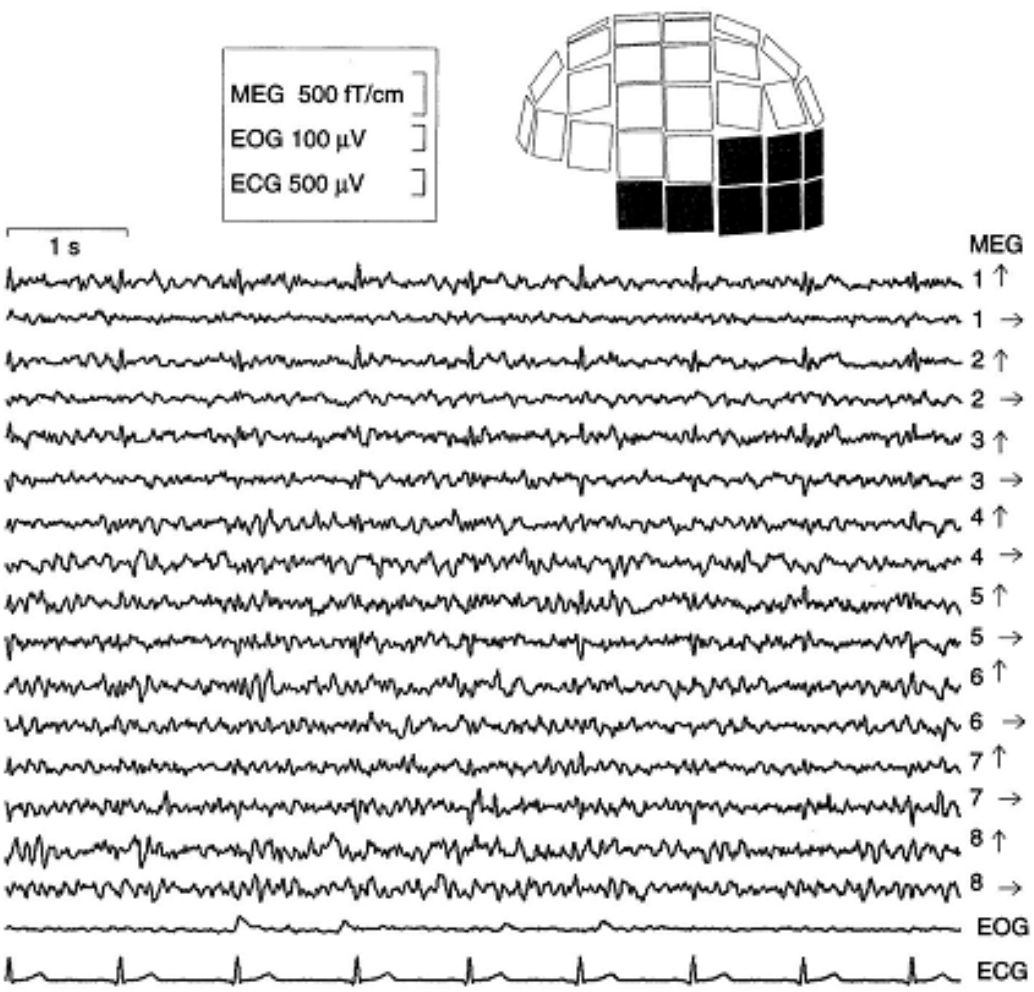

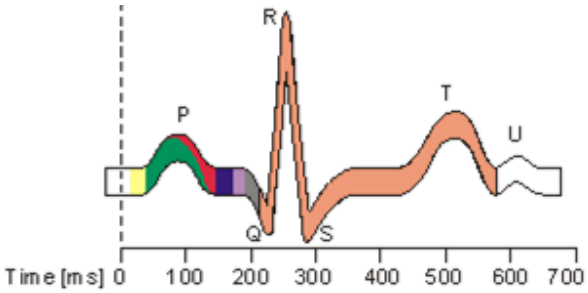

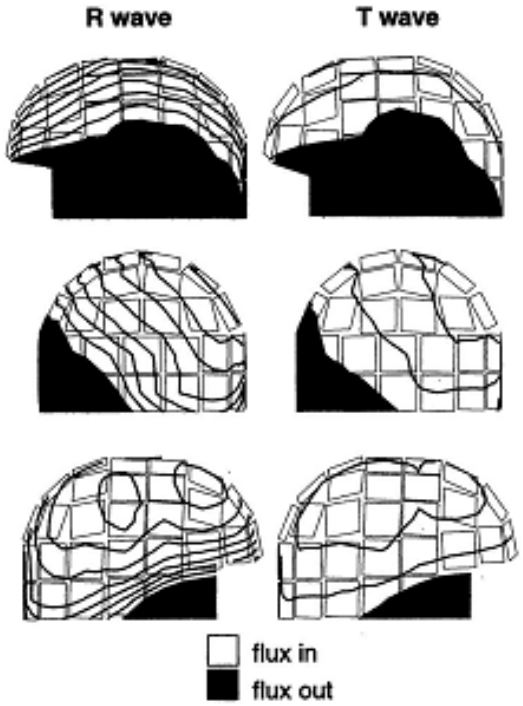

Jousmaki, Hari (1996)

signal (activity relevant to presented stimuli) + noise (ongoing brain activity)

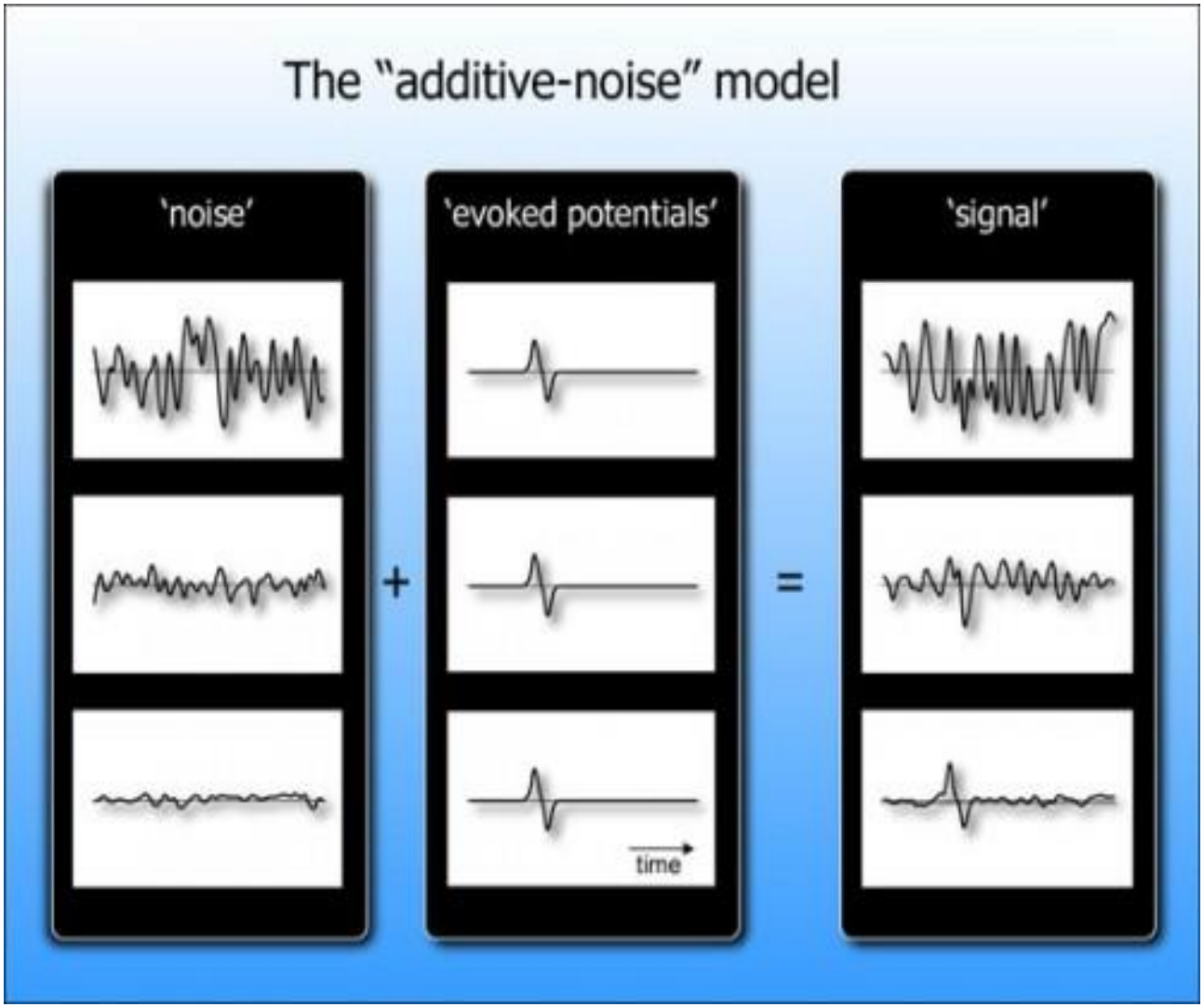

rationale =
averaging out the
"background noise"

from http://amouraux.webnode.com/

evoked response (ERP / ERF) vs. induced response

induced rhythm vs. locked response

Induced response evoked response

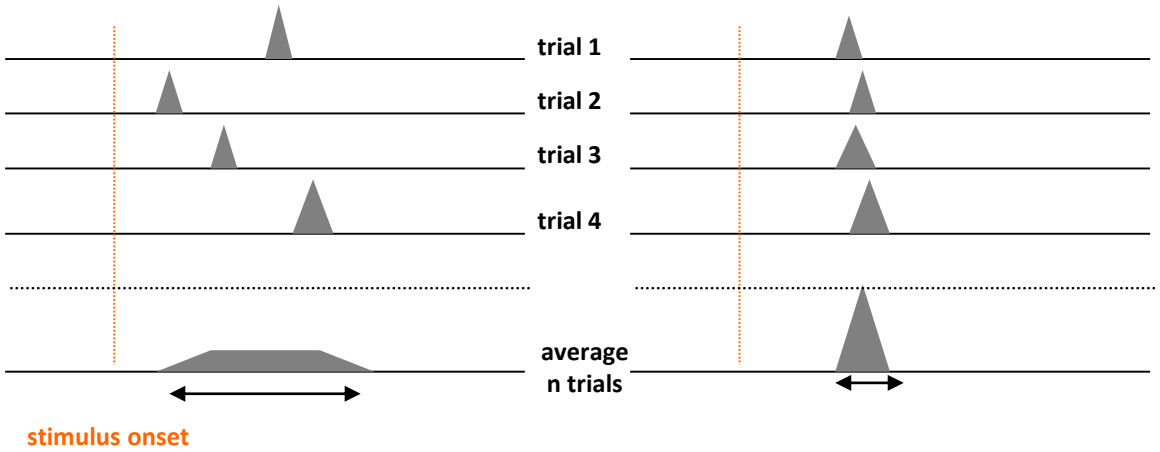

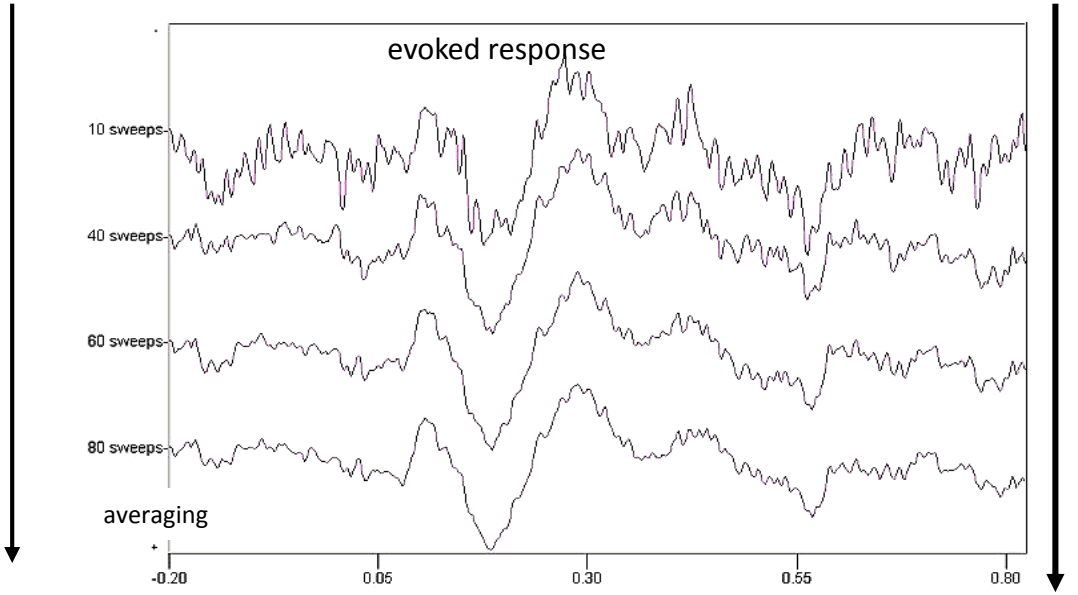

time-domain averaging - phase-locked activity

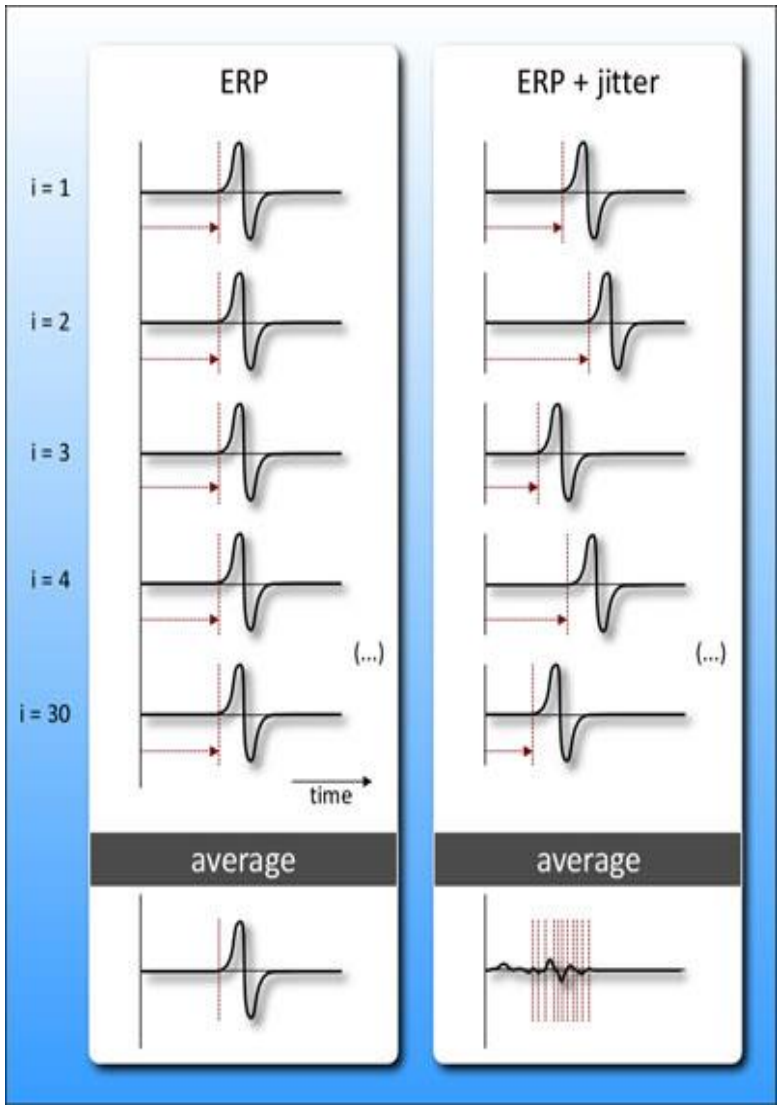

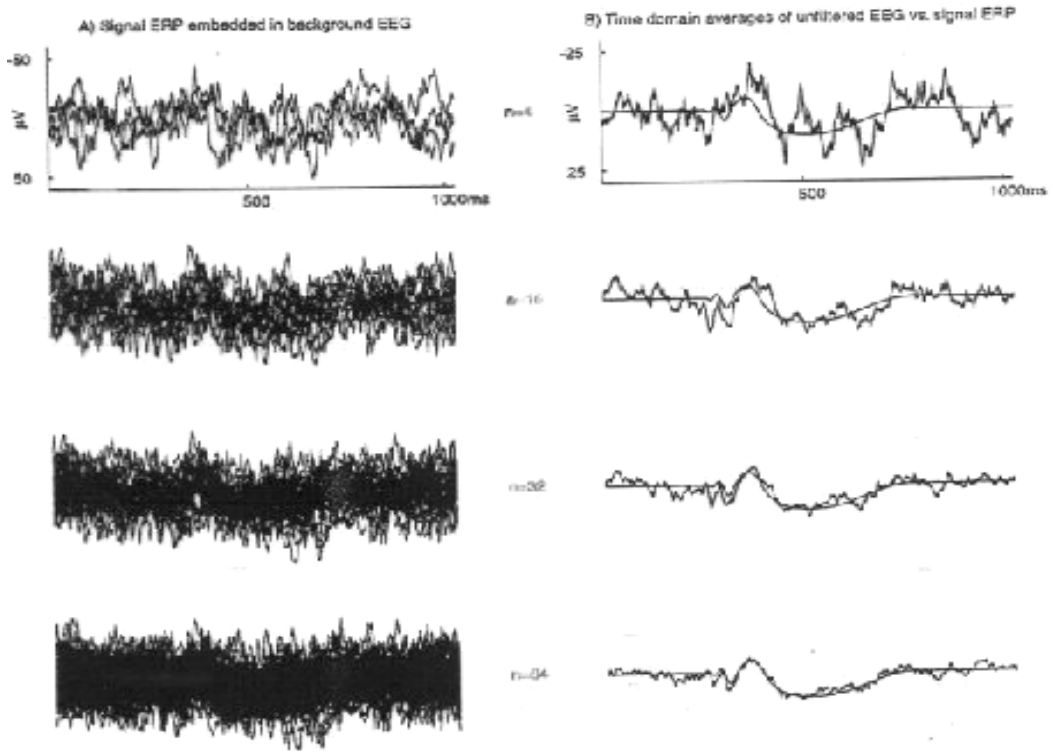

Fig. 18. Time domain averaging. (A) shows 4, 16, 32, and 64 epochs of an ERP-like signal embedded in simulated background EEG. In the ideal case, improvements in the signal to noise ratio vary with the square root of the number of epochs/trials, *n*, being averaged. (B) illustrates the difference between the time domain average and the embedded signal for different numbers of trials.

from http://amouraux.webnode.com/

ongoing oscillations

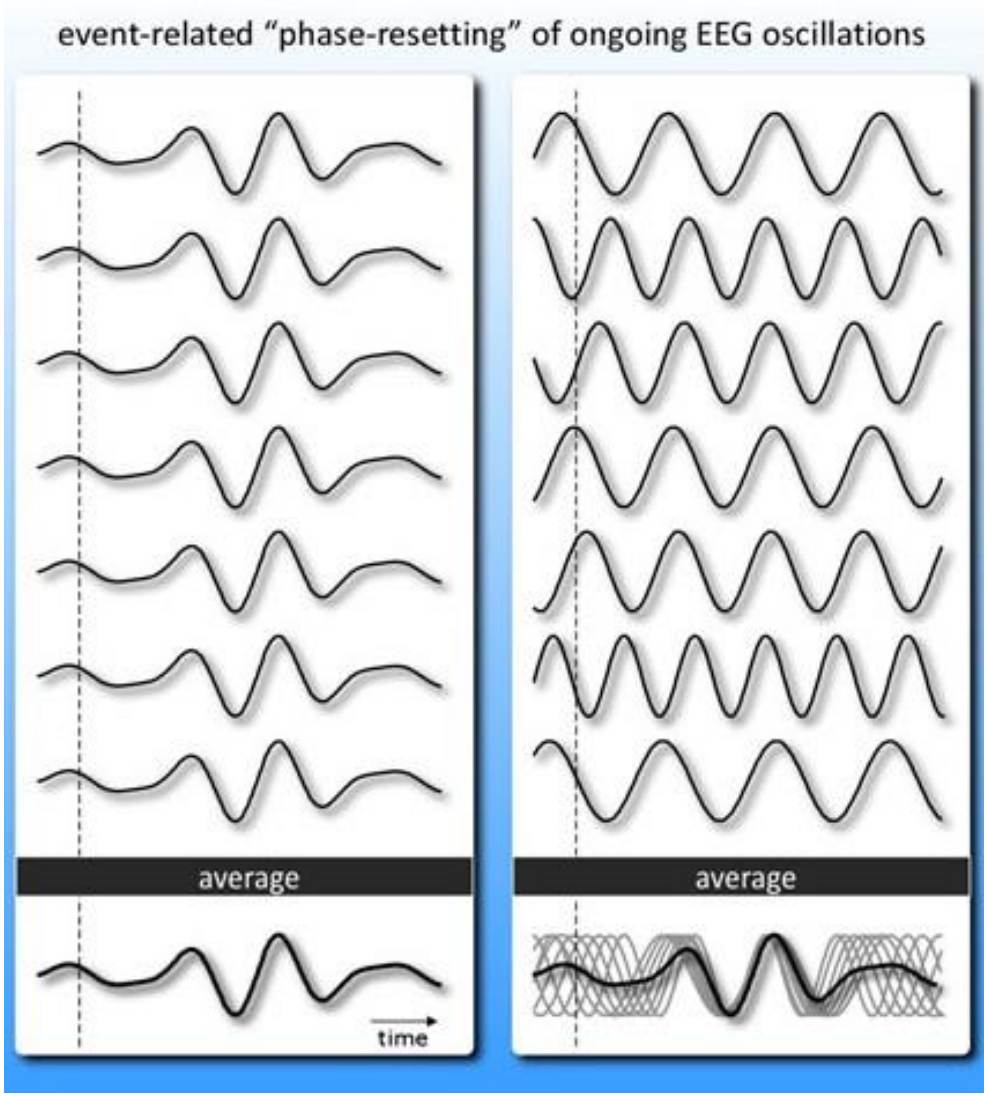

from http://amouraux.webnode.com/

ERS/ERD

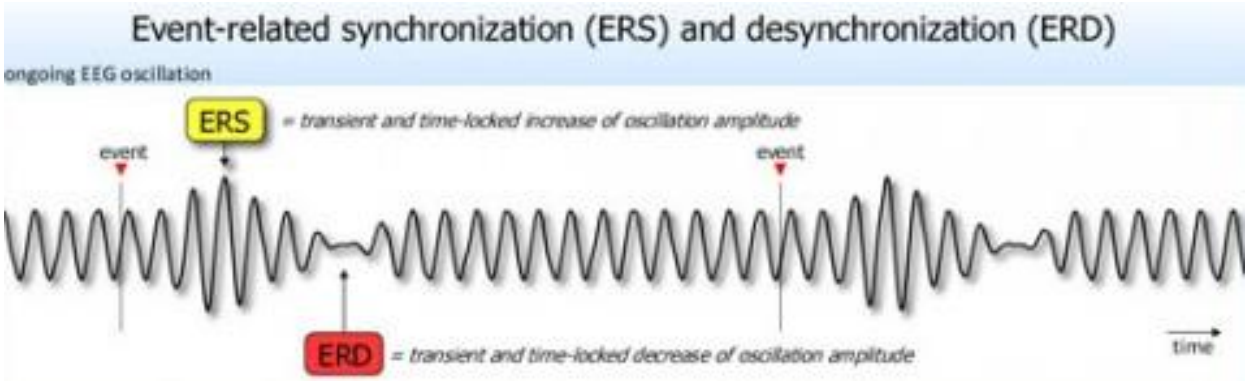

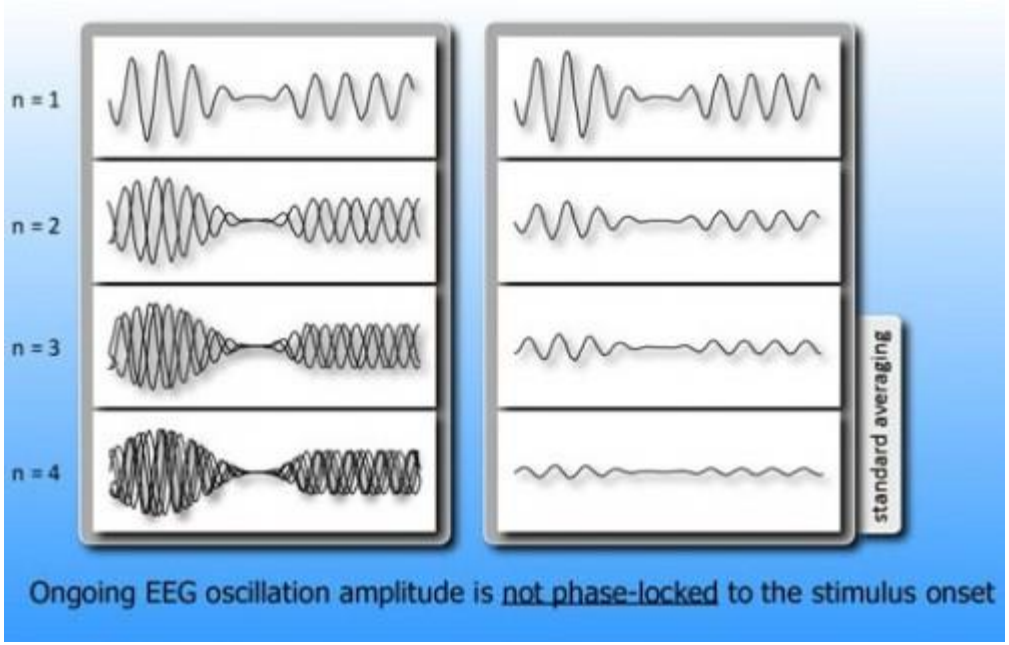

External events can induce transient enhancements or attenuations of ongoing brain oscillations

Event-Related Synchronization (ERS)
Event-Related Synchronization (ERD)

from http://amouraux.webnode.com/

interim summary

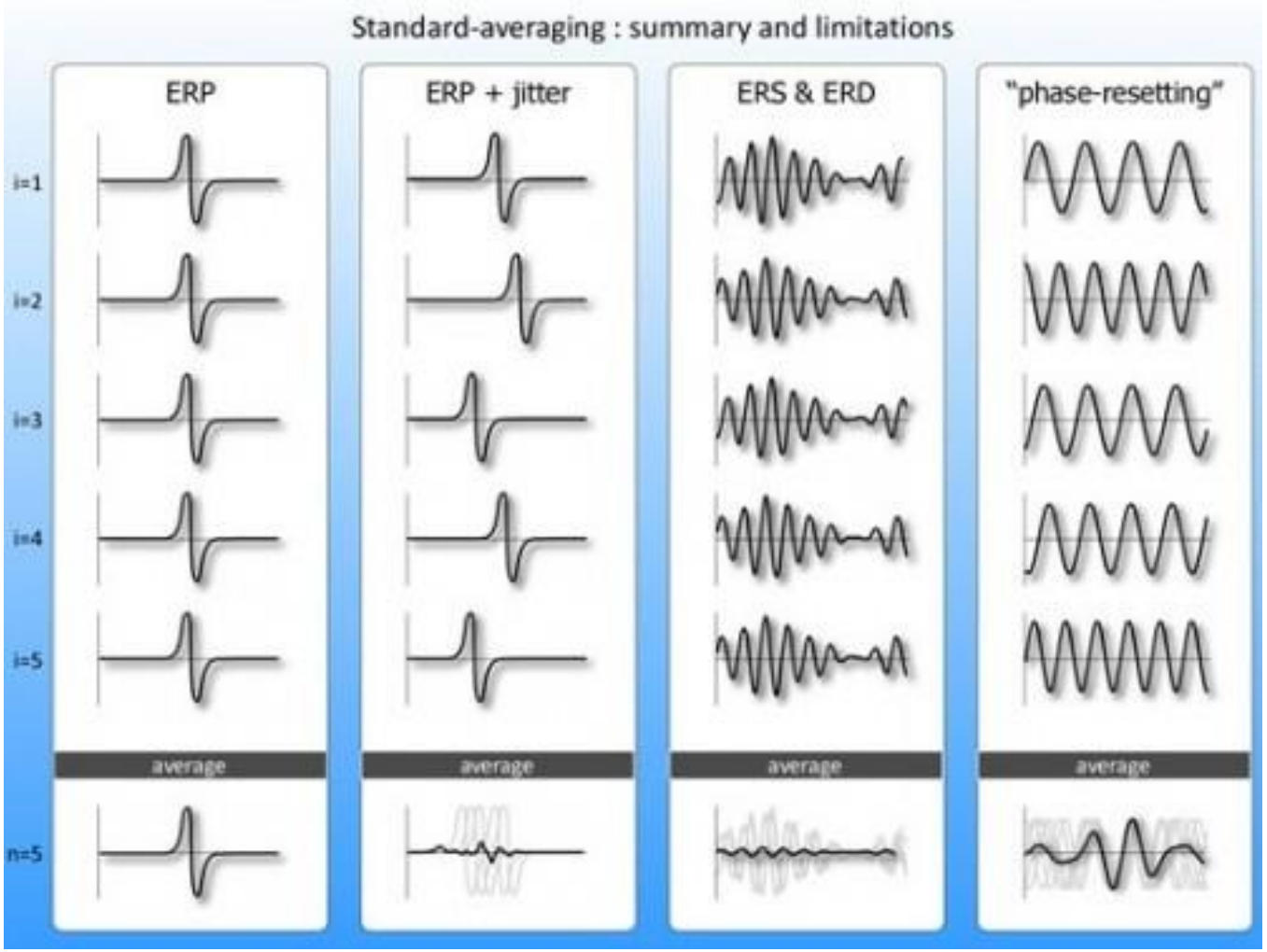

time-frequency approaches for non-phased locked signals

Frequency transform of recorded signals via
Fourier, Wavelet, filter…

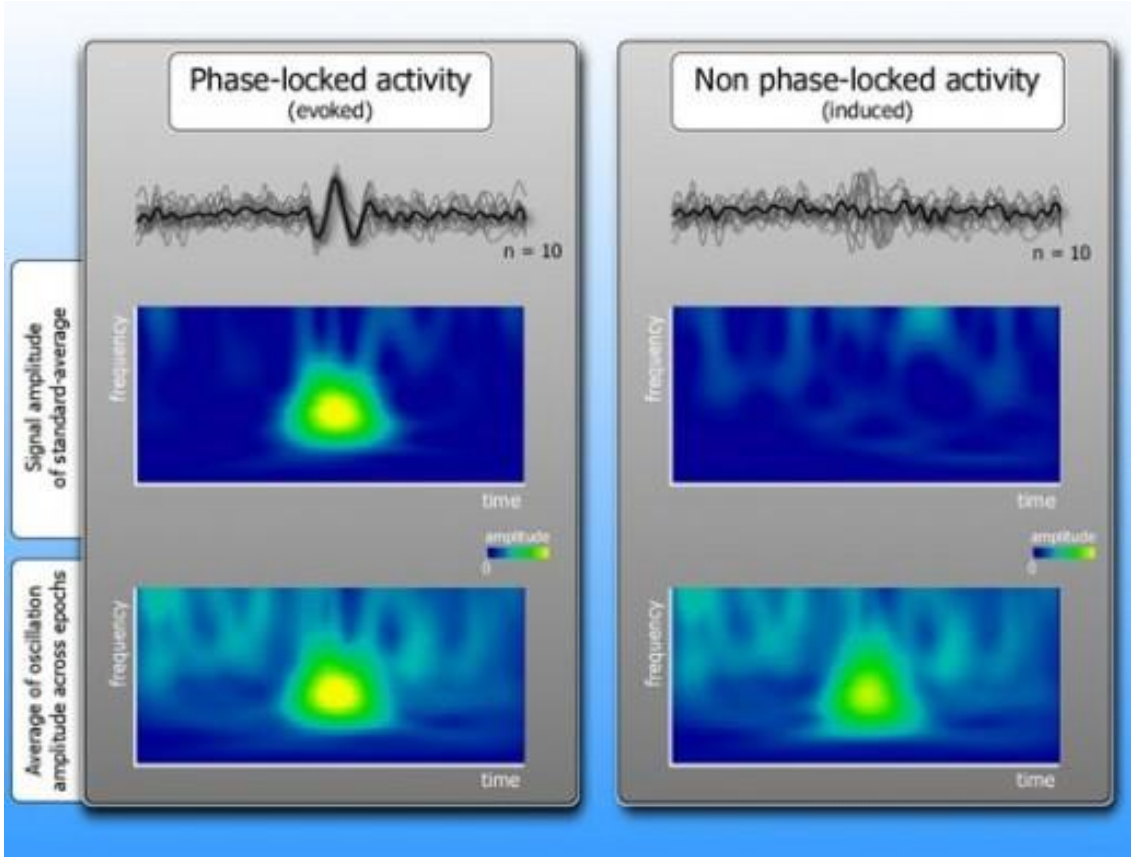

from http://amouraux.webnode.com/

source reconstruction

conductor models

- The geometry of the conducting medium affects the volume current distribution $\mathbf{J}_v(\mathbf{r})$ and thus the magnetic and electric fields

- **Sphere** is a good approximation of the intracranial volume
  - computationally easy and fast
  - radial inhomogeneities do not matter for MEG (but they do for EEG!)
  - ***inaccurate at inferior temporal and frontal areas, deep structures***

- **Realistic boundary-element models (BEM)**
  - a triangle mesh based on subject's anatomy
  - derived from segmented MRIs
  - computationally more demanding

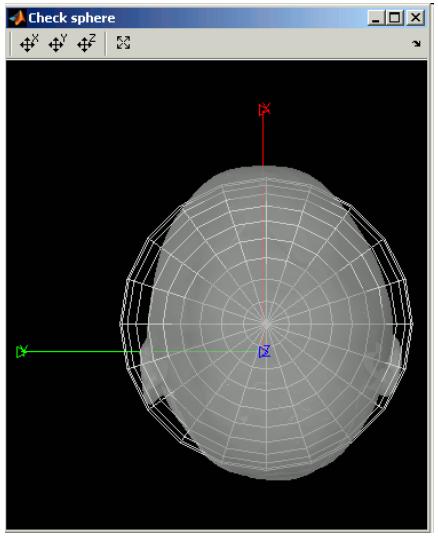

single sphere

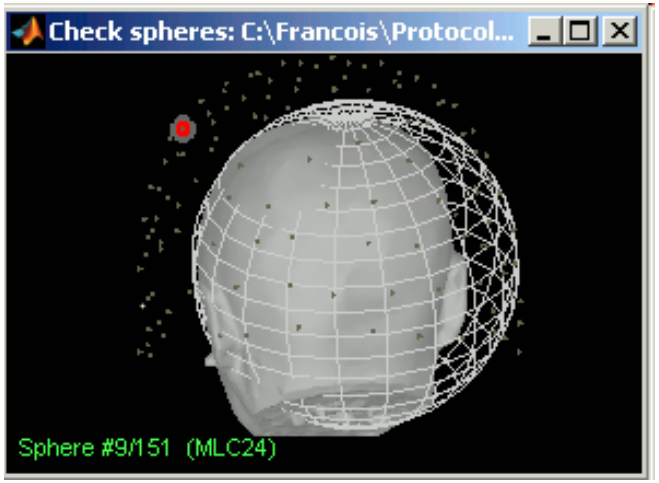

multiple spheres

source modeling

- forward problem : given the current distribution **J**(**r**), the corresponding electric and magnetic signals can be calculated uniquely

- inverse problem : mapping from electric and magnetic measurements to the current distribution **J**(**r**) in a conductor is **not** unique

  (e.g. assuming a spherical conductor, radial currents can be added without changing MEG and current loops can be added without changing EEG)

- Additional constraints required to estimate the primary currents $\mathbf{J}_p(\mathbf{r})$ = sources ≈ active areas

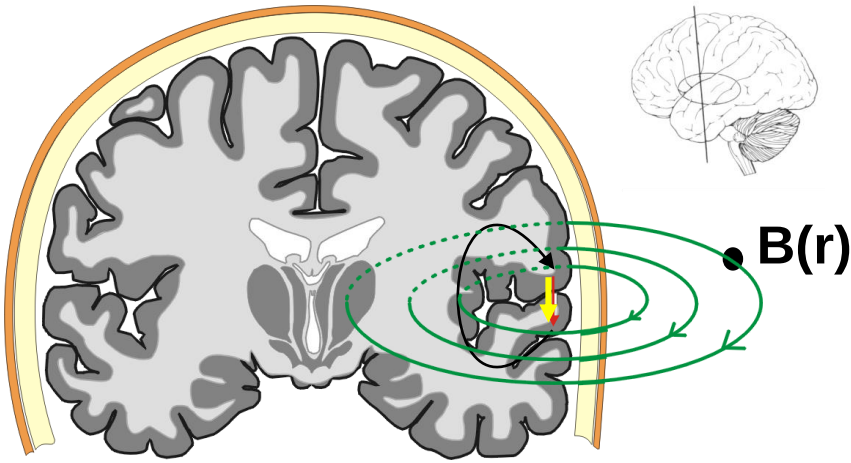

courtesy of Lauri Parkkonen

Equivalent Current Dipole (ECD)

- infinitesimally short current "line"
- has orientation and strength
- models the activity of ~ cm^2 of cortex
- fitted to the measured data in the least-squares sense
- located in grey matter
- oriented perpendicular to the cortical sheet
- the location is biased if the active area is large (extended source)
- the orientation may change over time (*rotating dipoles*), in association with minor (often undetectable) changes in location

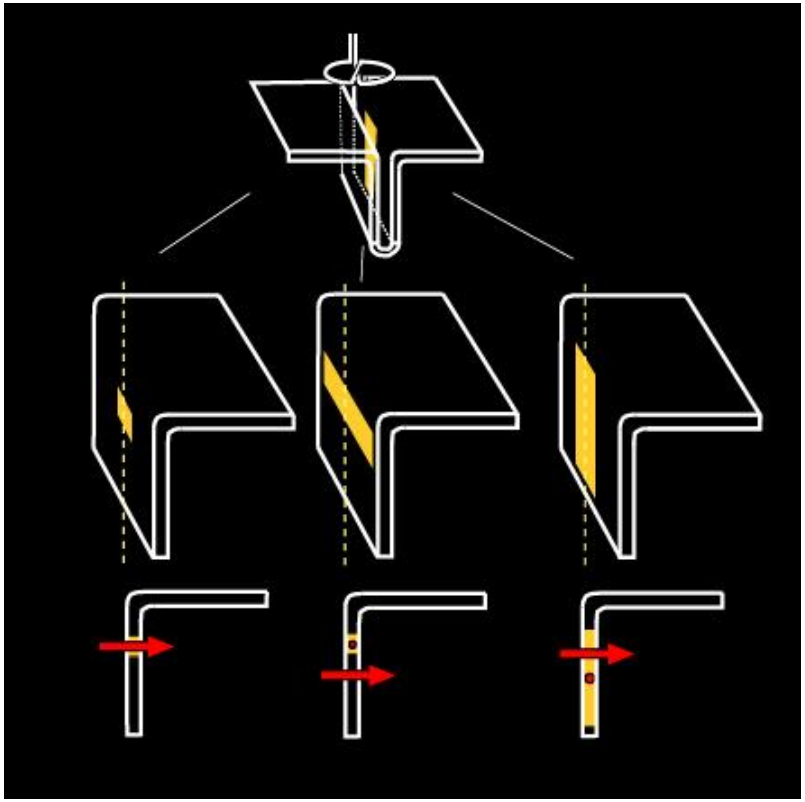

Hari (1991)

Single Dipole modeling

Dipole parameters

location (x,y,z coordinates)

⇔ a non-linear inverse problem (“difficult”)

amplitude/strength/moment (in nAm) and orientation (angle)

⇔ a linear inverse problem (“easy”)

Single dipole model

assuming that just **one source explains all the signals**

location estimate usually based on a **single time point**

amplitude (and orientation) can be estimated across a time span:

the dipole tries to explain the measurements by varying its strength (and orientation if it is allowed to change)

performs poorly with two or more simultaneously active regions

Multidipole model

accounts for multiple sources in separate regions, either simultaneous or sequential

can be a collection of single dipoles at different locations;

amplitude fit : a multidipole model is used to find the time courses of those dipoles, *i.e.* the variation of their magnitudes as a function of time

position fit : the locations of two or more simultaneously active dipoles can be found at once

improved localization accuracy as the contributions of all sources to the signals are taken into account

Dipole Modeling

To recover the true time courses, all major sources should be modelled even if some of them are not of interest. Otherwise **spatial leakage** contaminates the amplitudes.

Two nearby ECDs with parallel orientations are likely to **interact**, i.e. exhibit correlated and unreasonably large amplitudes.

> MEG's spatial resolving power of simultaneous sources is limited.

Position fit works only if all participating sources are active during the fit interval. Single dipole location fits are the usual ingredient to a multidipole model.

dipole modeling example

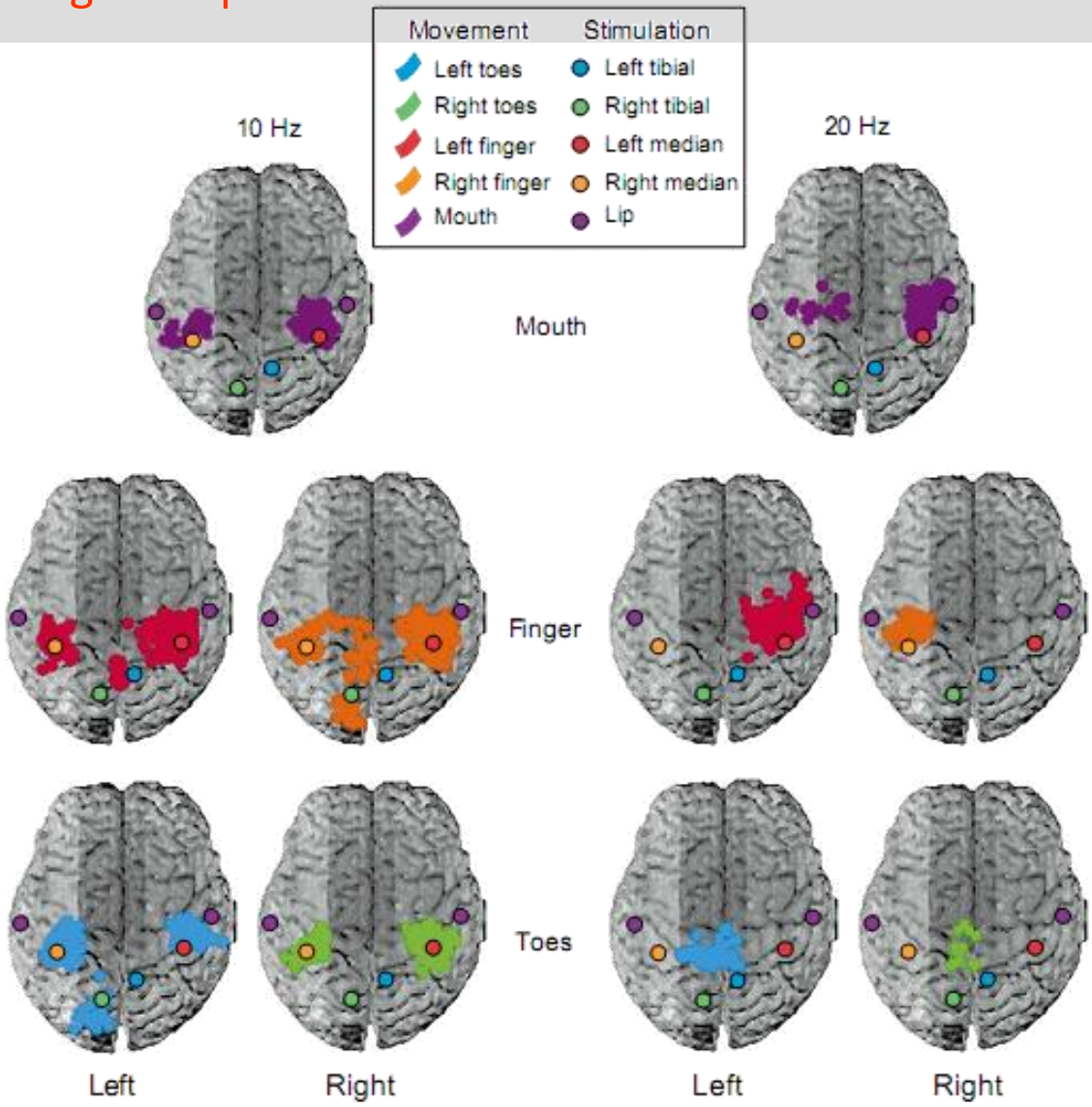

Fig. 4. ***Somatotopic order of sources of the somatomotor 20 Hz mu rhythm.*** *Source clusters for the reactive 10 Hz and 20 Hz rhythms in one subject, determined during mouth, finger and toe movements, superposed on a surface rendition of the subject's magnetic resonance images. The circles show functional landmarks obtained by stimulating electrically the same body parts and by identifying the sources of the elicited fields.* Modified from Ref. 44.

Hari, Salmelin (1997)

Minimum Norm Estimate

- Gives $\mathbf{J_p(r)}$ by minimizing the sum of $||\mathbf{J}||^2$ given the measurements **b (L2-norm)**

  gaussian priors

  without additional constraints, all the current is on the surface of the conductor
- **Computationally easy**
- **Gives a widespread/diffuse current distribution**

- Noise normalization, i.e., dividing the estimate with its standard error at each location, yields a statistical parametric map (SPM) that is typically more focal than the estimate itself [*Dale et al. Neuron 26, 2000*]

- Currents can be constrained to flow only in grey matter and to favor orientations perpendicular to the cortical sheet

- Time-variation is often shown as a movie

MNE

- Constrain sources to cortical mantle
- Compute forward solution with BEM model
- Full noise covariance matrix from raw data
- Display on inflated cortex (sulci based)
- Stats

(can combine MEEG and soom fMRI guided “fire”)

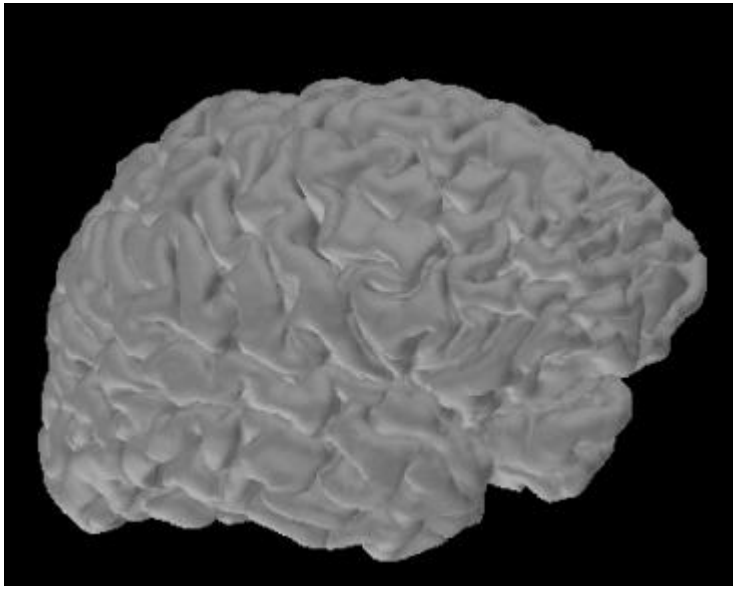

tesselation: source location and orientation

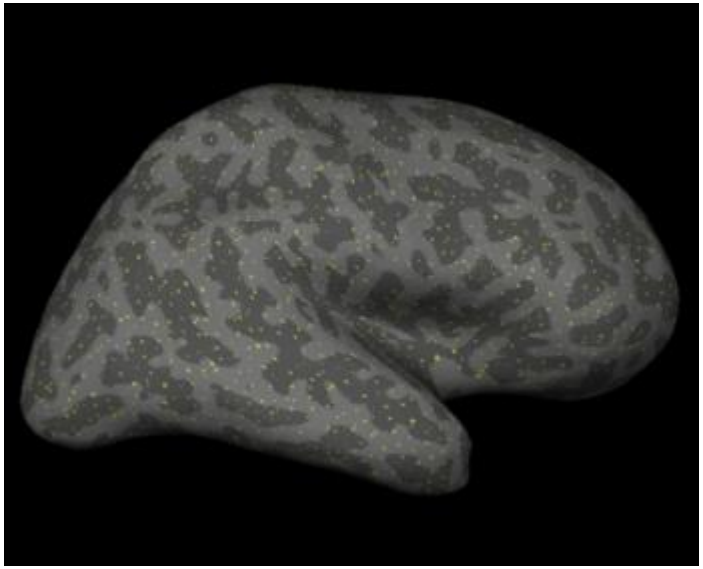

decimation: 6000 to 10000 source locations

auditory cortex response

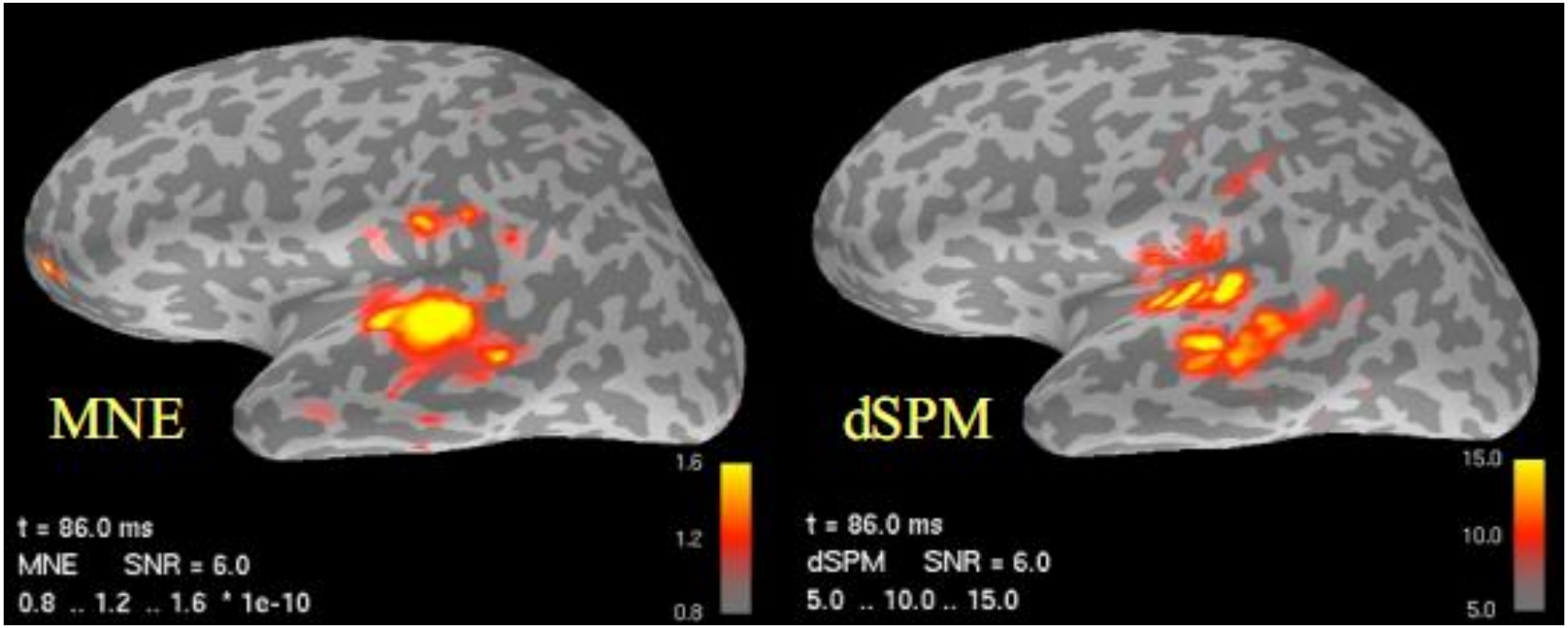

dSPM example

fMRI →

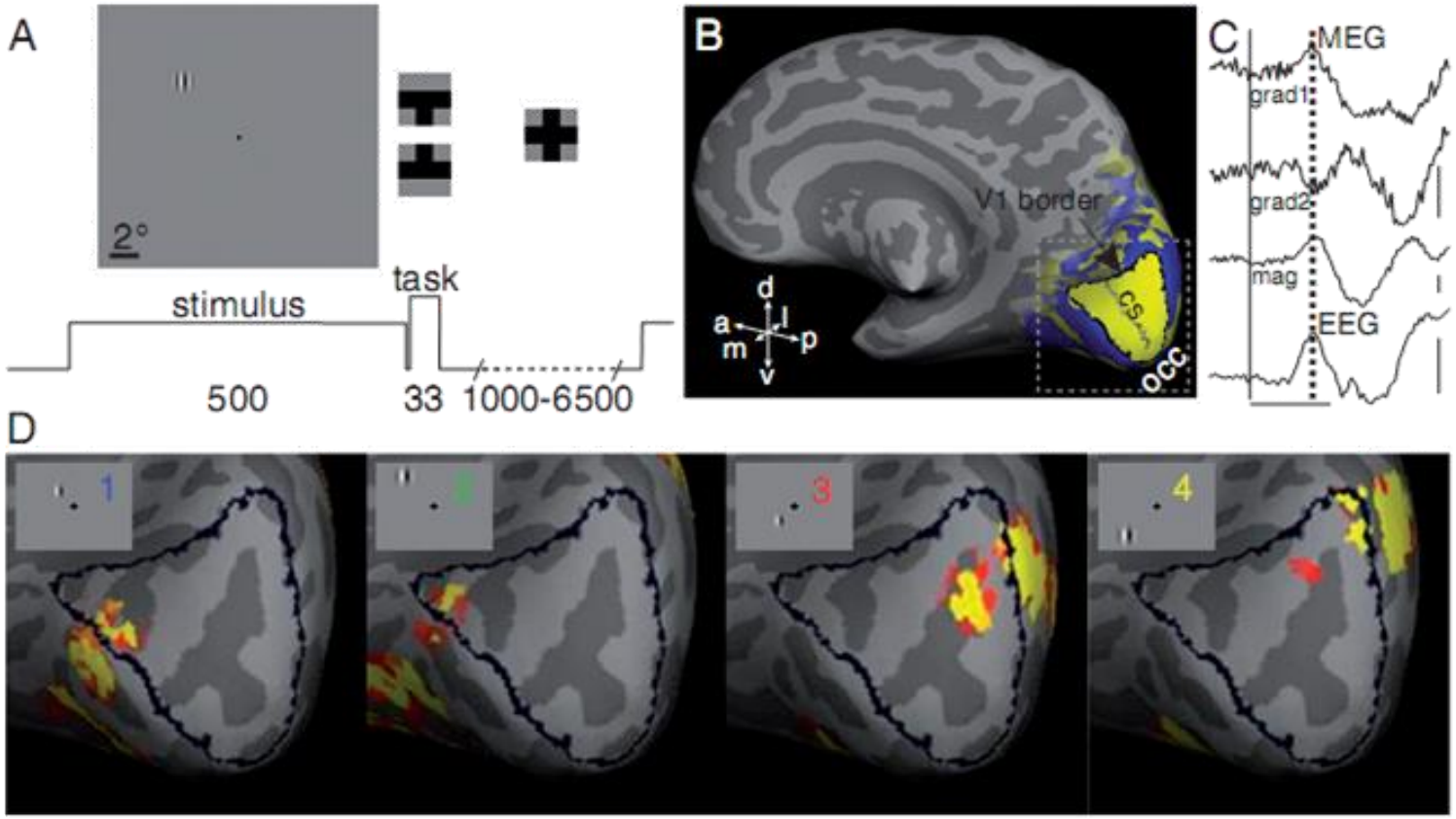

Fig. 1. V1 responses to focal visual stimuli: fMRI, MEG, EEG. (A) Stimulation paradigm. A Gabor patch was flashed for 500 ms in one of 4 locations (upper-left 5° eccentricity stimulus shown here), immediately followed by 33 ms of the fixation cross task. The subject indicated by a button press whether the upper or lower half of the vertical arm of the cross disappeared. The interstimulus interval varied between 1 and 6.5 s, during which only the fixation cross was present. The isoluminant gray background extended farther into the periphery than shown here. (B) V1 labeling using retinotopic mapping in subject 1. Field sign is either mirror image (yellow) or non-mirror image (blue). The mirror image representation abutting the calcarine sulcus is V1, delineated in black. Note that the anterior segment of the border is due to the peripheral limit of the visual stimulation. Gray dashed box indicates zoom-in region for D. White arrows indicate 3D directions: a—anterior, p—posterior, d—dorsal, v—ventral, m—medial, l—lateral. cs: fundus of the calcarine sulcus; occ: occipital pole. Dark gray: sulci; light gray: gyri. (C) Evoked MEG/EEG responses in occipital sensors, for the same subject as in panel B. All the analysis in this study was performed at the early peak, indicated by the dashed line (76 ms in this subject). Two upper panels: example traces from the two MEG planar gradiometer sets; third panel: MEG magnetometer; fourth panel: EEG electrode. Solid line: stimulus onset. Horizontal scale bar: 100 ms; vertical scale bars (from top): 20 fT/cm; 20 fT, 2 μV. (D) fMRI responses to the 4 stimulus conditions, for the same subject as in panels B and C. A focal response patch is evoked in V1 (and in each adjacent retinotopic visual area). The response pattern follows predictions from retinotopic mapping. The black line indicates the V1 border, as in panel B. Schematic representations of the stimuli, fixation cross and Gabor patch (not drawn to scale) are shown in the top left corner of each response panel.

dSPM

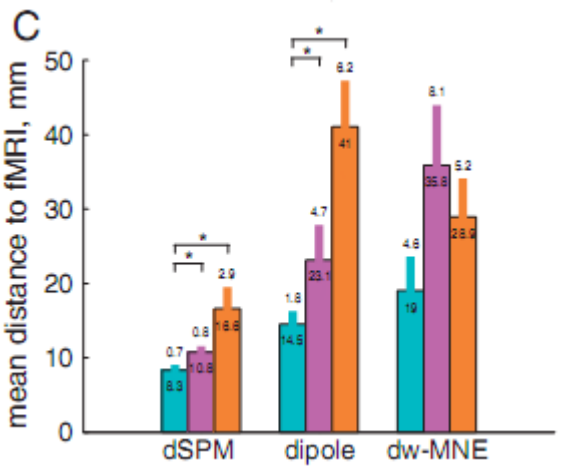

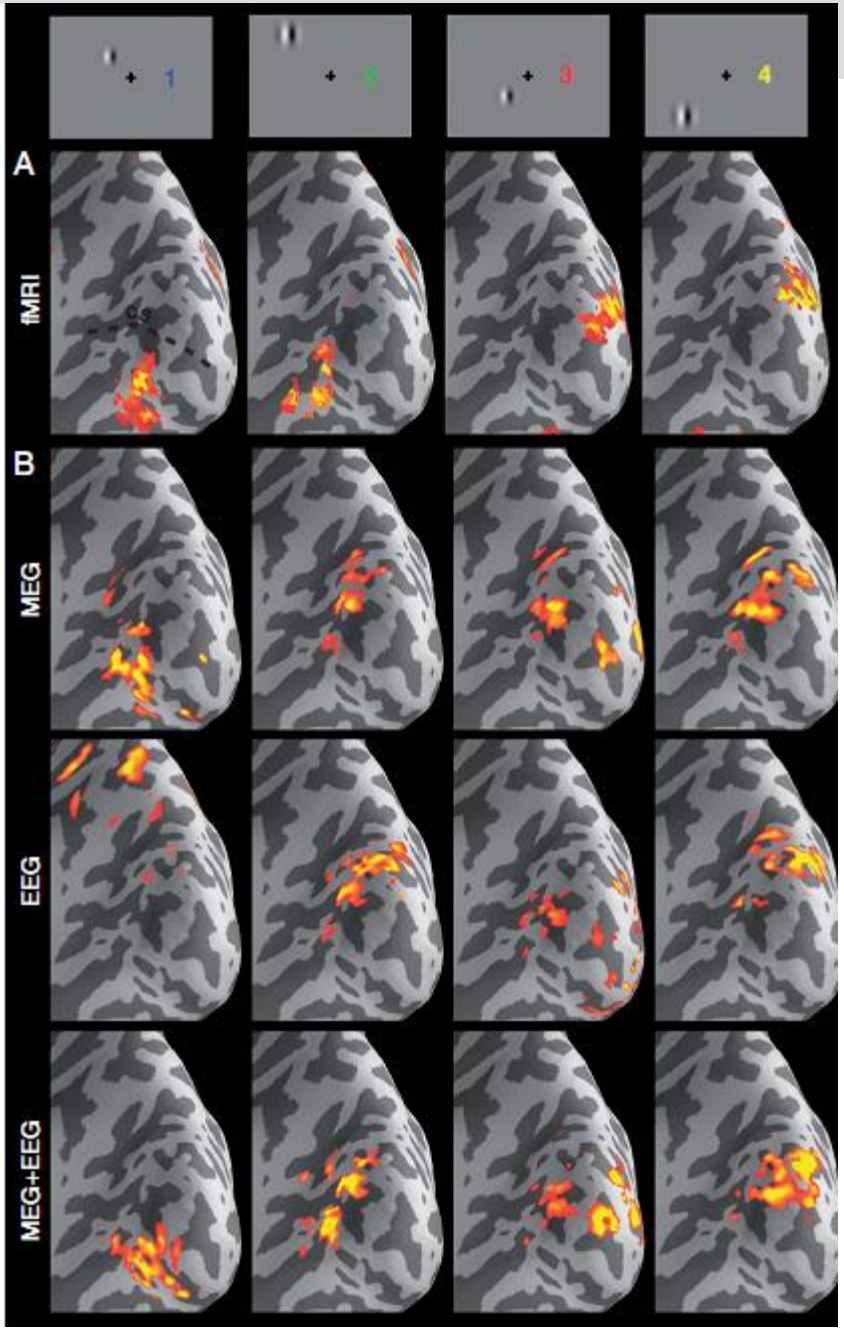

Virginie van Wassenhove 2010

Beamforming

~ adaptive (data dependent) or non-adaptive (data-independent) spatial filters

estimate the signal from a defined (small) volume

scan of the intracranial volume => 3D reconstruction of the sources

issues:

- bias the reconstructed source in the absence or presence of noise
- cannot recover correlated sources
- do not solve the inverse problem

beamforming example

auditory plasticity study : combining approaches

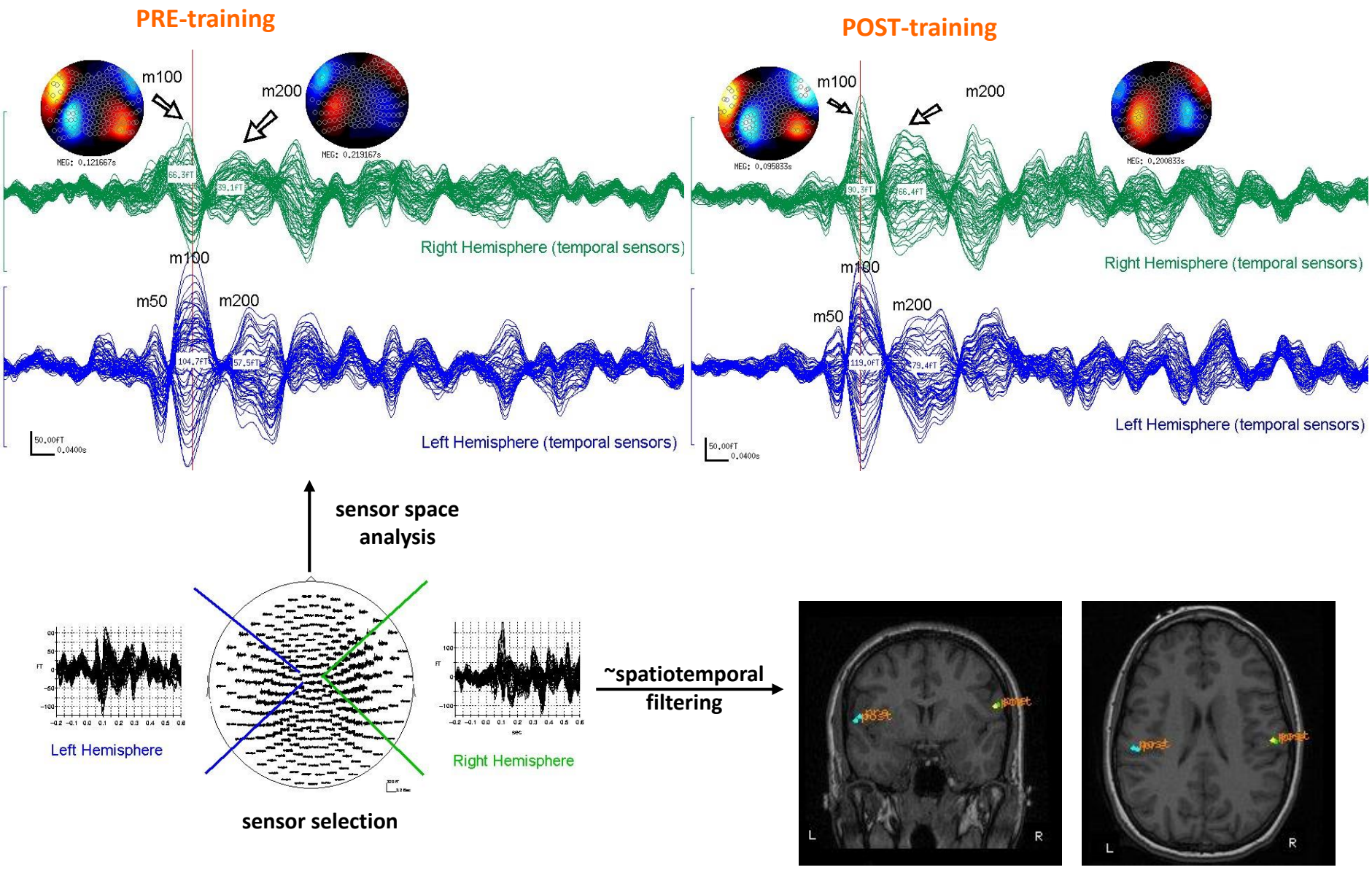

van Wassenhove & Nagarajan (2007)

source reconstruction :: time-frequency beamforming

1 time-frequency map single-trial

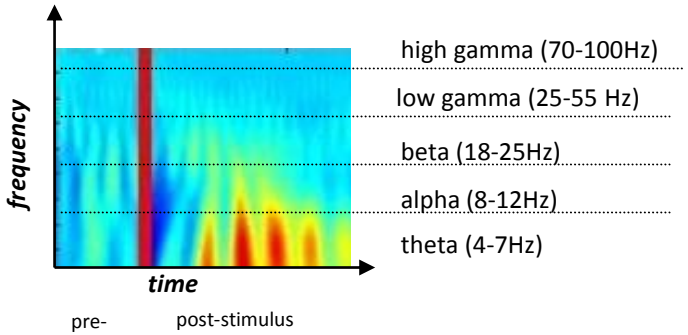

⇔ adaptive spatial filtering

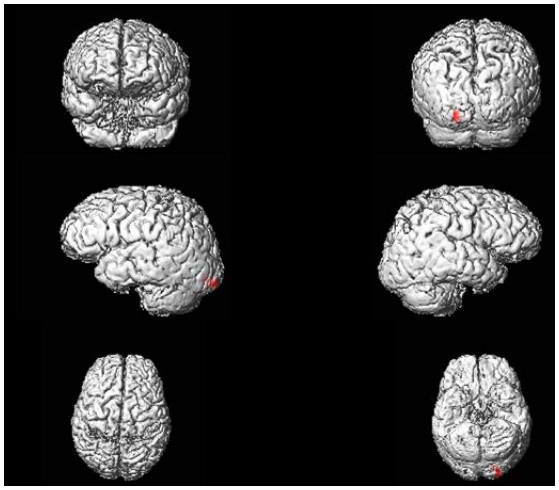

2 source-localization of MEG signal

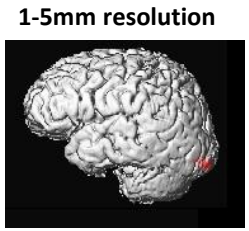

3 within condition contrast
pseudo F-ratio computed as contrast between pre- and post-stimulus period

4 statistical contrast across conditions
pseudo F-ratio computed as contrast between condition 1 and condition 2

5 Nutmeg F-ratio
(direct statistical significance)
MNI coordinates and functional anatomical mapping

auditory cortex plasticity

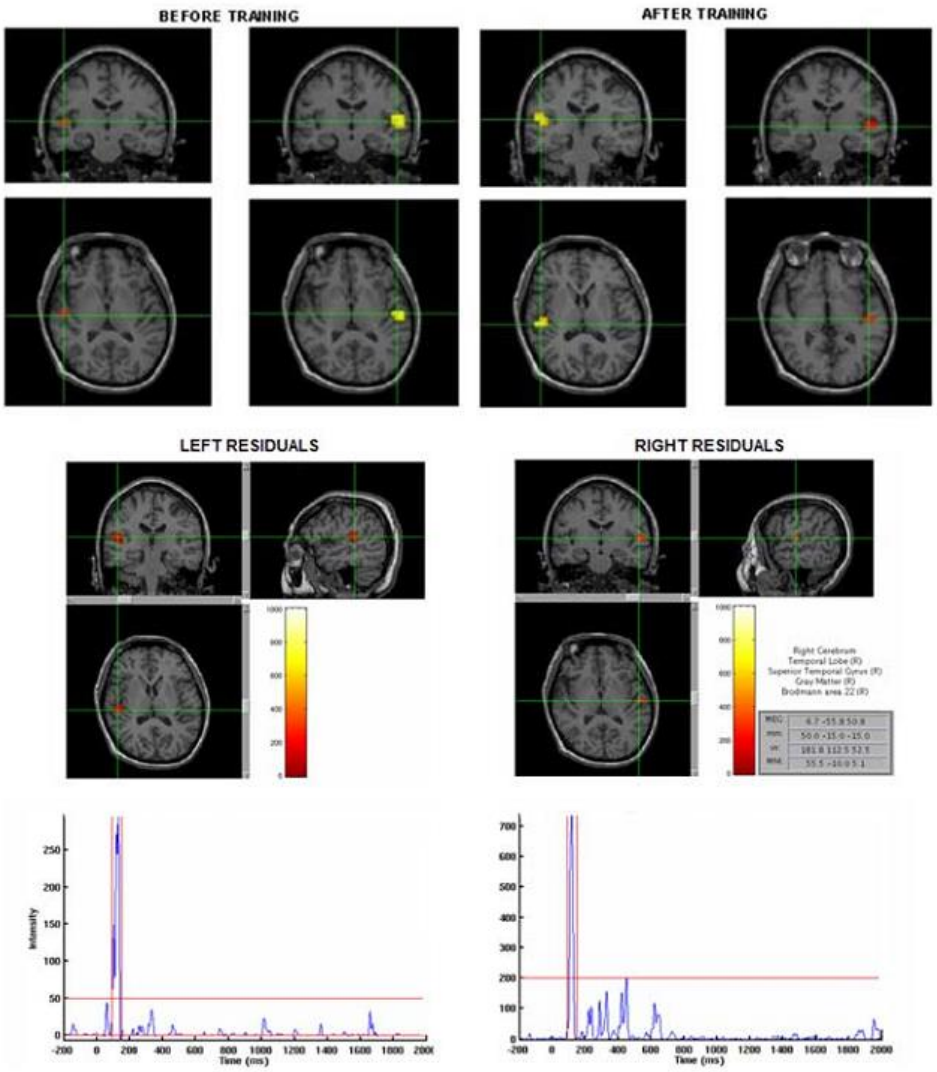

+

After > Before training

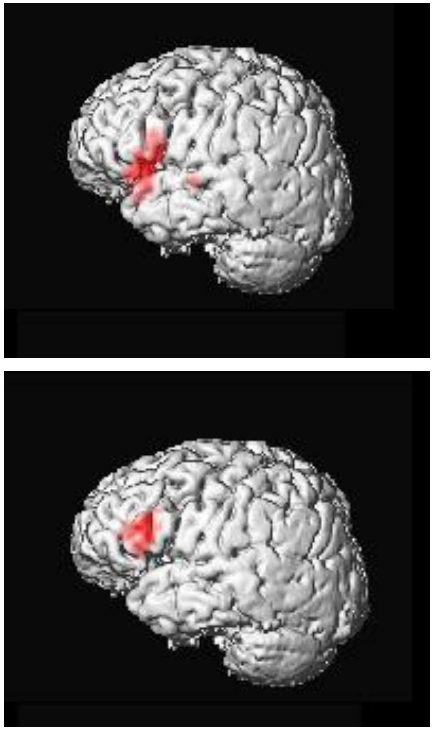

tf beamforming methods : *Dalal et al (2004)*

MEG in practice

MEG clinical – epileptic seizures

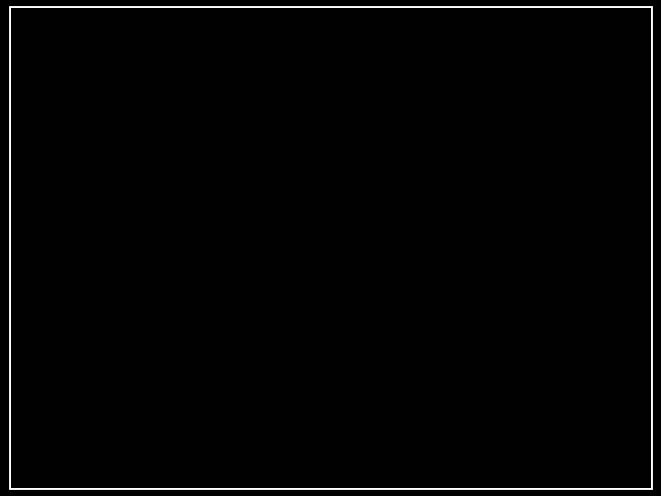

Altered temporal correlations in parietal alpha and prefrontal theta oscillations in early-stage Alzheimer disease

Teresa Montez[a,b,1], Simon-Shlomo Poil[c,1], Bethany F. Jones[b], Ilonka Manshanden[b], Jeroen P. A. Verbunt[b,d], Bob W. van Dijk[b,d], Arjen B. Brussaard[c], Arjen van Ooyen[c], Cornelis J. Stam[b], Philip Scheltens[e], and Klaus Linkenkaer-Hansen[c,2]

1614–1619 | PNAS | February 3, 2009 | vol. 106 | no. 5

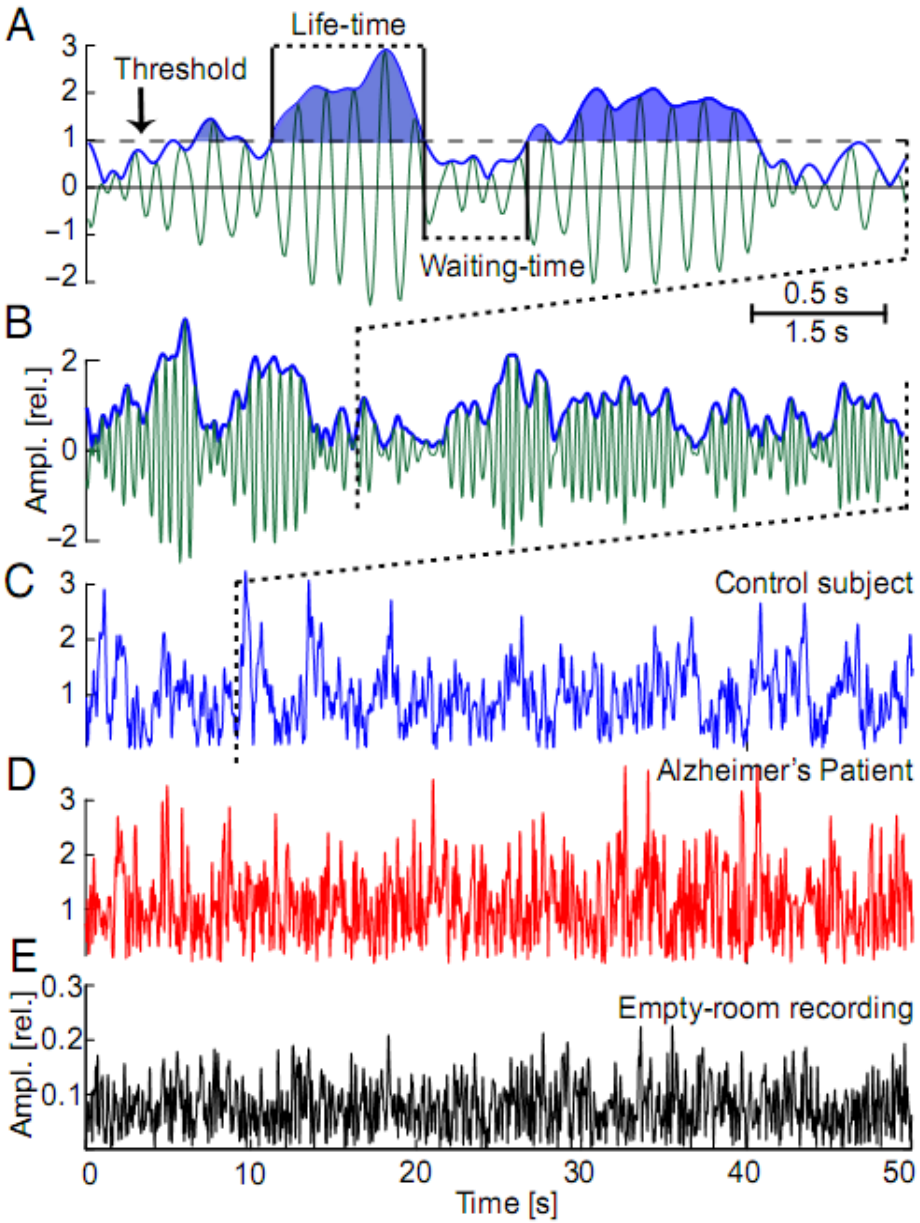

Tested early Alzheimers (AD) vs controls

Hypo: amplitude modulation of local oscillatory activity indicative of AD (here specific alpha and theta bands)

Both life-time (>25% above median level of sensor) and waiting-time (within 25% of median level) lasted longer compared to normals.

Increased temporal correlation (coefficient of Detrended Fluctuation Analysis)

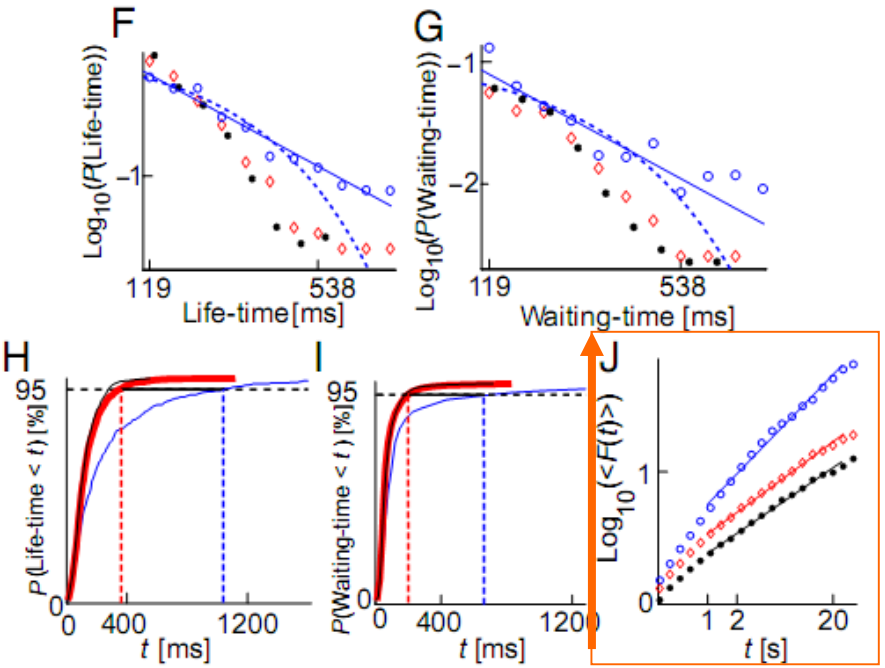

Magnetoencephalographic evaluation of resting-state functional connectivity in Alzheimer's disease

NeuroImage 32 (2006) 1335 – 1344

C.J. Stam,[a,*] B.F. Jones,[b,f] I. Manshanden,[a] A.M. van Cappellen van Walsum,[c] T. Montez,[d] J.P.A. Verbunt,[a,e] J.C. de Munck,[e] B.W. van Dijk,[a,e] H.W. Berendse,[a] and P. Scheltens [b]

Synchronization likelihood index in different frequency bands
(linear + non-linear mixture of 2 time series patterns matching)

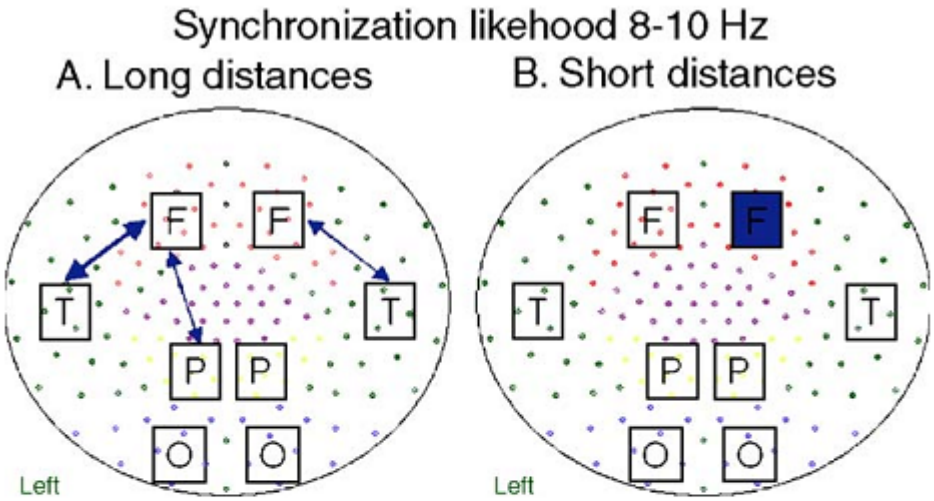

Fig. 3. Schematic illustration of SL (SL) results for the alpha1 band. A. Long distances. Decrease of bilateral fronto-temporal and left fronto-parietal SL in Alzheimer patients. B. Short distances. Local decrease of SL in right frontal region. Lines correspond to significant changes of average SL between two regions and squares to significant changes of local SL (thin line/light square: $P < 0.05$; thick line/dark square: $P < 0.01$; blue: Alzheimer lower than controls; red: Alzheimer higher than controls; significance is based upon two-tailed t tests and intended for illustration; formal testing was based upon a repeated-measures ANOVA).

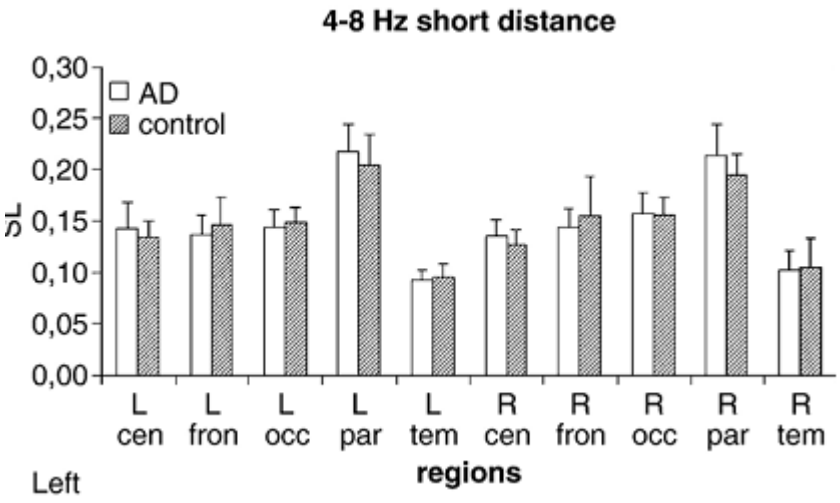

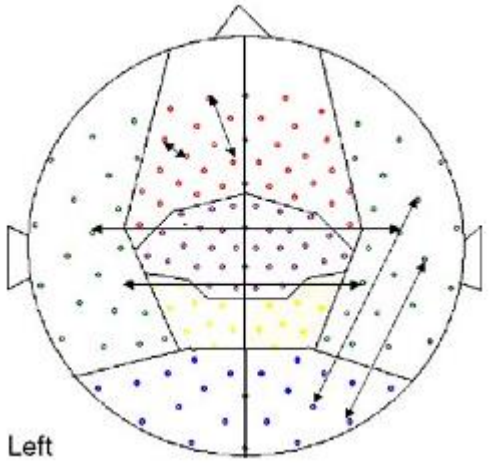

Magnetoencephalographic evaluation of resting-state functional connectivity in Alzheimer's disease

NeuroImage 32 (2006) 1335 – 1344

C.J. Stam,[a,*] B.F. Jones,[b,f] I. Manshanden,[a] A.M. van Cappellen van Walsum,[c] T. Montez,[d] J.P.A. Verbunt,[a,e] J.C. de Munck,[e] B.W. van Dijk,[a,e] H.W. Berendse,[a] and P. Scheltens [b]

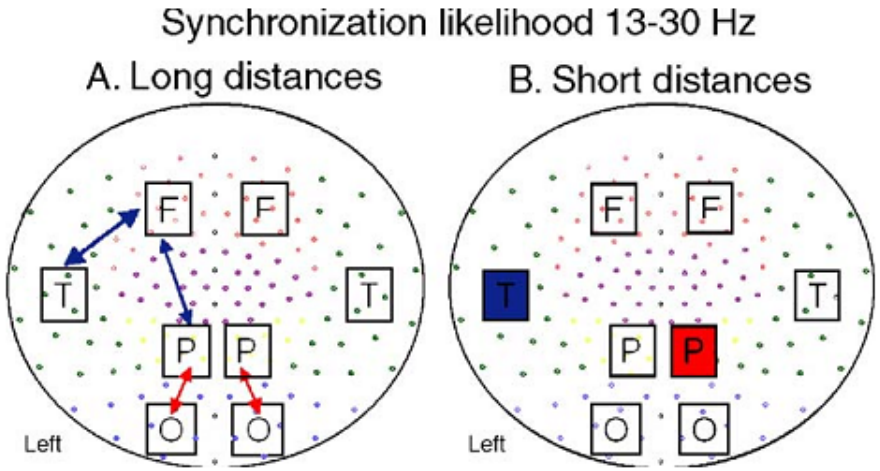

Fig. 4. Schematic illustration of SL (SL) results for the beta band. A. Long distances. Decrease of left fronto-temporal and fronto-parietal SL and increase in bilateral occipito-parietal SL in Alzheimer patients. B. Short distances. Local increase of SL in right parietal region and local decrease of SL in left temporal region. Lines correspond to significant changes of average SL between two regions and squares to significant changes of local SL (thin line/light square: $P < 0.05$; thick line/dark square: $P < 0.01$; blue: Alzheimer lower than controls; red: Alzheimer higher than controls; significance is based upon two-tailed t tests and intended for illustration; formal testing was based upon a repeated-measures ANOVA).

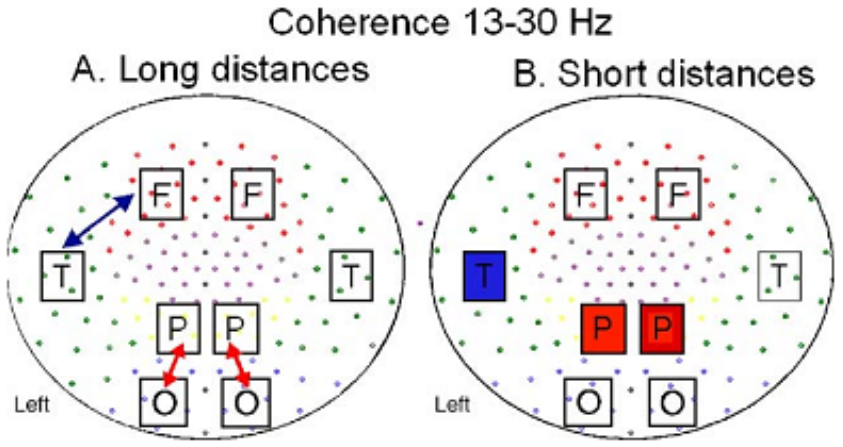

Fig. 7. Schematic illustration of coherence results for the beta band. A. Long distances. Decrease of left fronto-temporal coherence and increase in bilateral occipito-parietal coherence in Alzheimer patients. B. Short distances. Local increase of coherence in right and left parietal regions and local decrease of SL in left temporal region. Lines correspond to significant changes of average coherence between two regions and squares to significant changes of local coherence (thin line/light square: $P < 0.05$; thick line/dark square: $P < 0.01$; blue: Alzheimer lower than controls; red: Alzheimer higher than controls; significance is based upon two-tailed t tests and intended for illustration; formal testing was based upon a repeated-measures ANOVA).

Synchronization likelihood index in different frequency bands

(linear + non-linear mixture of 2 time series patterns matching)

Coherence index in different frequency bands

(cross-spectrum divided by product of the 2 power spectra

MEG cognitive

Six Families of Cognitive ERPs

	Processes:
Sensory/Perceptual (2-200 msec)	
Auditory P20-50, N100 Visual P100, N180 Visual N200 (faces) Mismatch Negativity	Early attentional selection Sensory memory Specialized perceptual modules Plasticity of sensory systems
Discrimination/Recognition (150-500 msec)	
N200's (modality & task-specific) Selection Negativity P300's	Late attentional selection Feature discrimination Pattern recognition Classification & decision Orienting to novelty
Memory-related (200-600 msec)	
Late positivities Late negativities	Storage & retrieval mechanisms Implicit vs. explicit memory
Language-related (200-600 msec)	
N400 Syntactic positive shift Lexical processing negativity Left anterior negativity	Lexical, grammatical, & semantic processing Sentence parsing Semantic memory
Readiness Potentials (preparatory)	
LRP Motor potentials CNV	Motor preparation Mental chronometry Continuous/Discrete models
Error-related Potentials (150-400 msec)	
ERN	Error detection & correction

Hillyard

Virginie van Wassenhove 2010

Sams et a (1991)

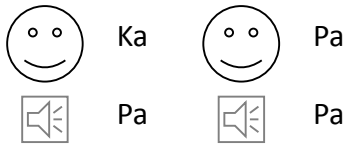

std std std std std DEV std std

time

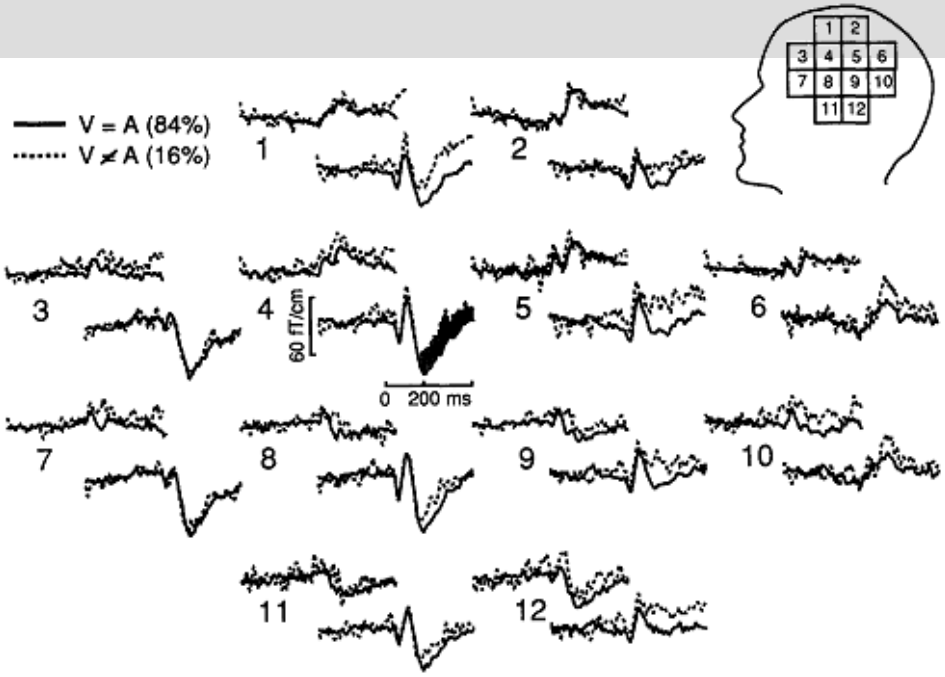

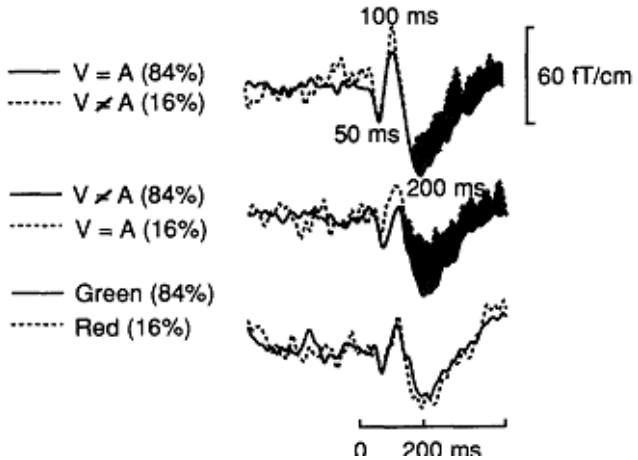

MMN paradigm

Neural suppression

MMN

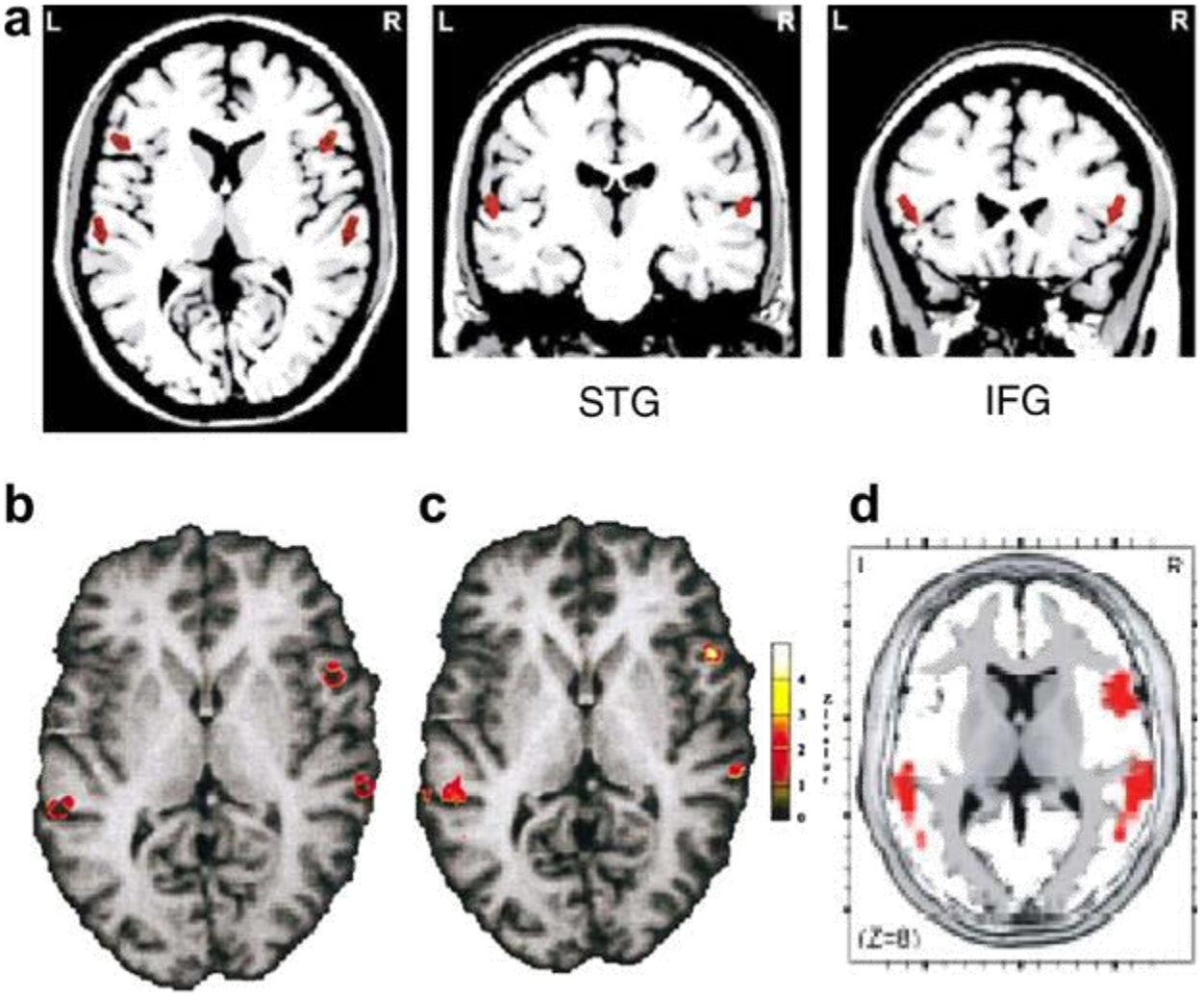

Fig. 3. MMN underlying sources revealed by EEG and conjoint EEG and fMRI measures. (a) Dipoles indicated by red arrows at bilateral **STG** and **IFG** (adapted from Doeller et al., 2003). (b) Dipole locations at bilateral **STG** and right **IFG** and (c) significant fMRI activation for deviants (adapted from Opitz et al., 2002). (d) Most significant independent component (computed by ICA-LORETA analysis, adapted from Marco-Pallarés et al., 2005). This figure shows consistency for MMN sources across different modalities.

temporal sequencing in perceiving, imitating and producing gestures

Viewing Lip Forms: Cortical Dynamics

Nobuyuki Nishitani[1,2,4] and Riitta Hari[1,3]

Neuron, Vol. 36, 1211–1220, December 19, 2002

1 participant, 5 sensors

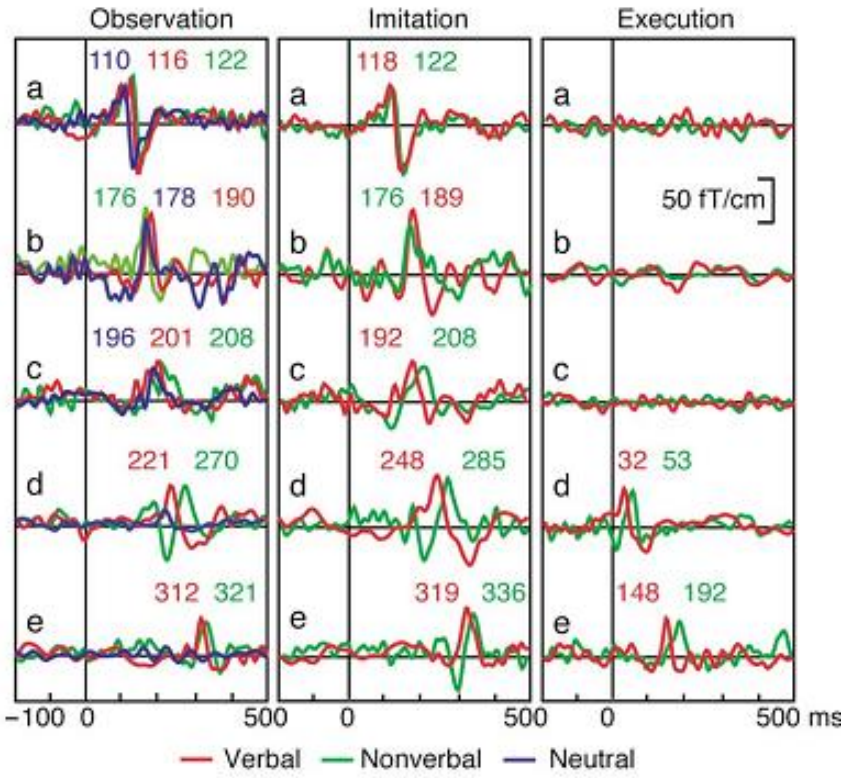

stim

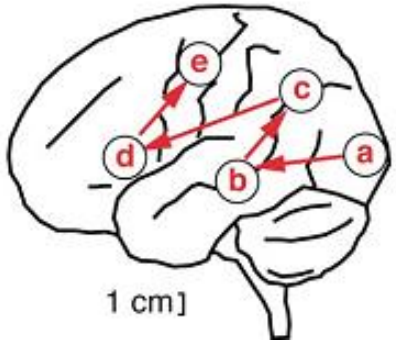

Example 2 –

Viewing Lip Forms: Cortical Dynamics

Nobuyuki Nishitani[1,2,4] and Riitta Hari[1,3] Neuron, Vol. 36, 1211–1220, December 19, 2002

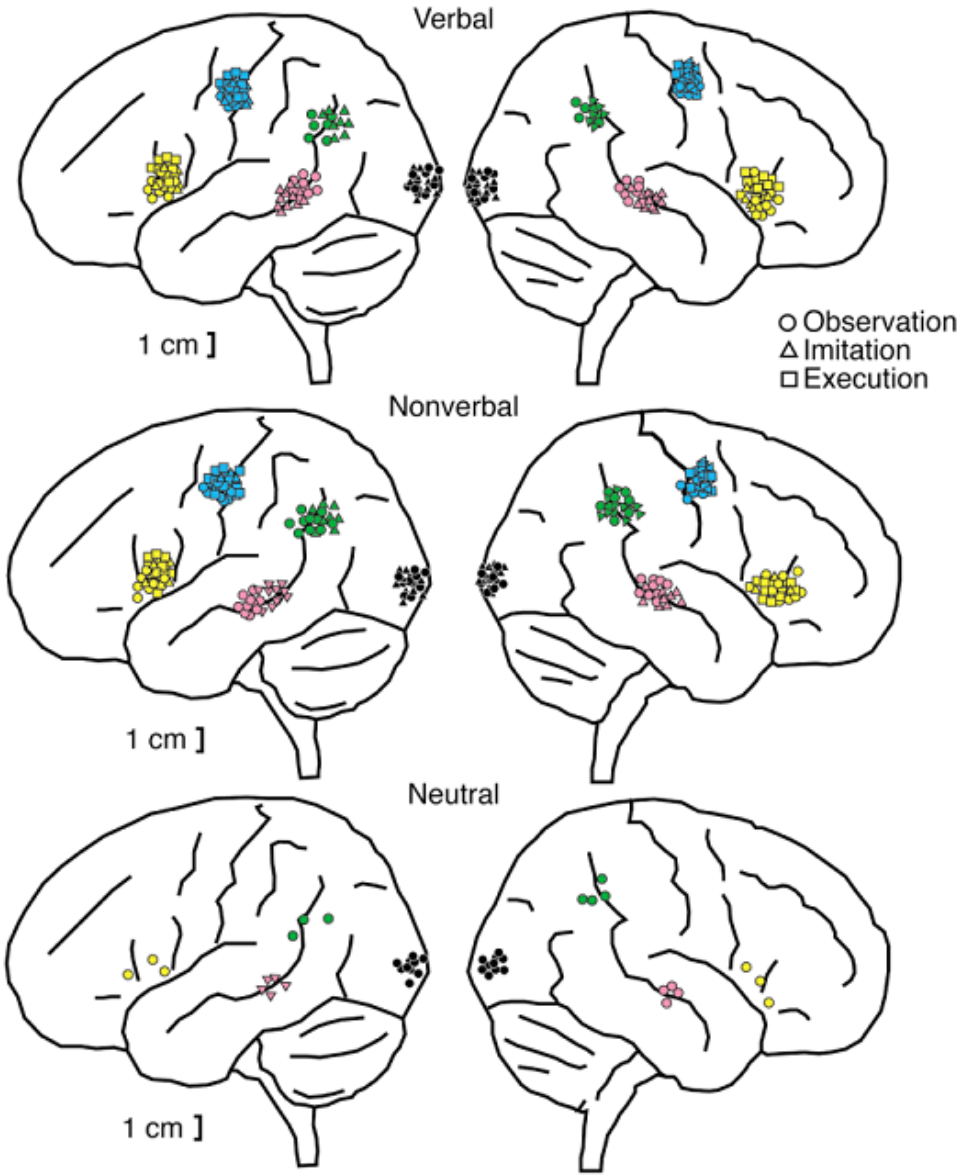

- Individual's MRI
- Spherical headmodel
- Equivalent Current Dipole (ECD)

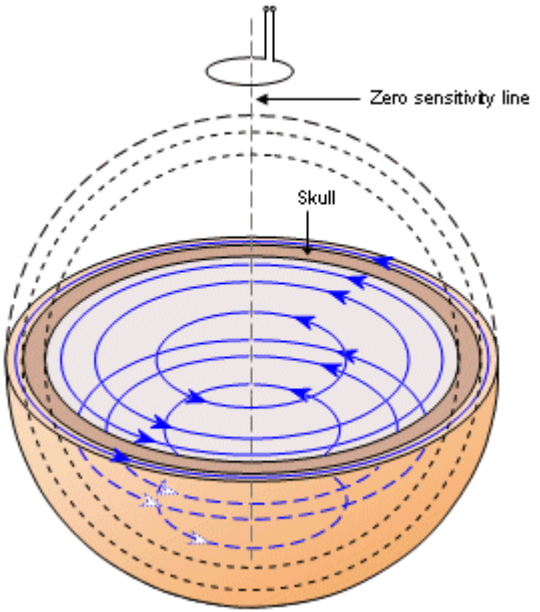

Example 2 –

Viewing Lip Forms: Cortical Dynamics

Nobuyuki Nishitani[1,2,4] and Riitta Hari[1,3] Neuron, Vol. 36, 1211–1220, December 19, 2002

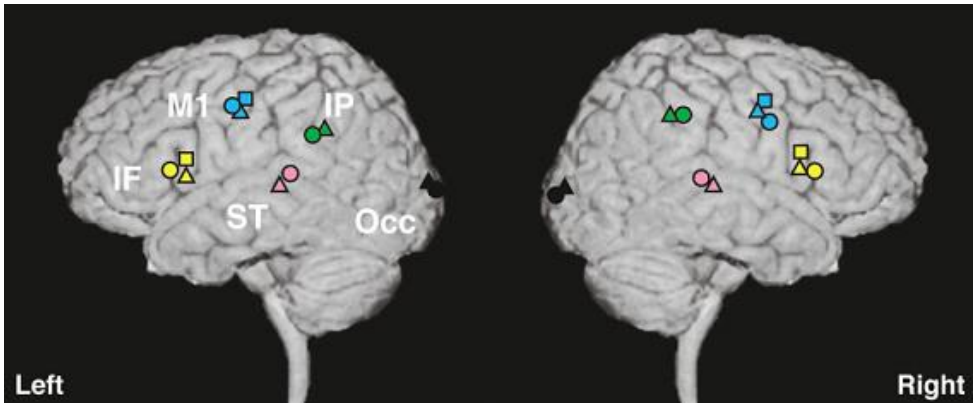

evolving over time

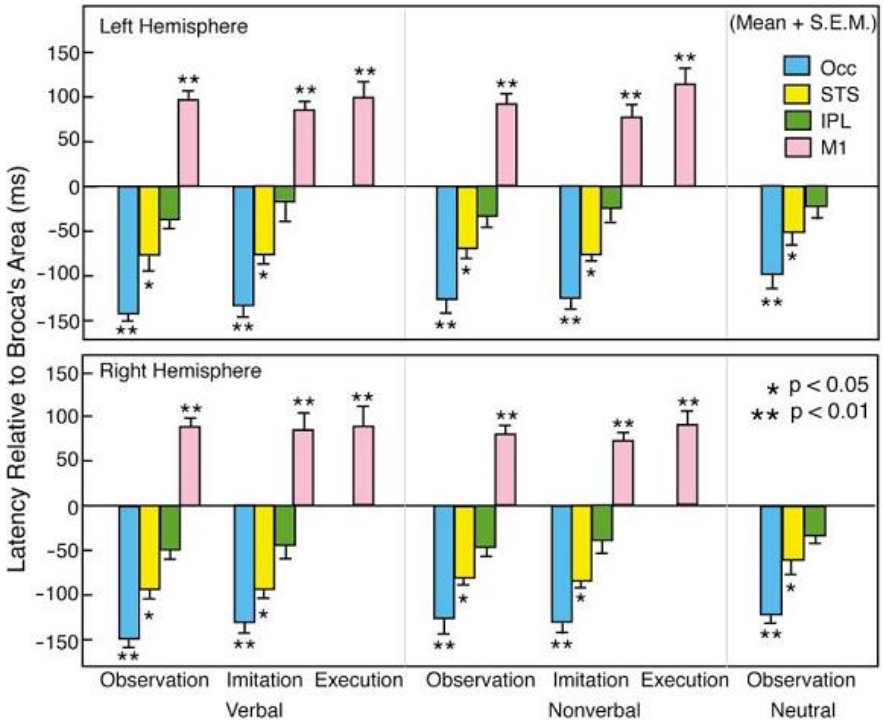

senhove 2010

Perception's shadow: long-distance synchronization of human brain activity

Eugenio Rodriguez, Nathalie George, Jean-Philippe Lachaux, Jacques Martinerie, Bernard Renault & Francisco J. Varela

NATURE | VOL 397 | 4 FEBRUARY 1999

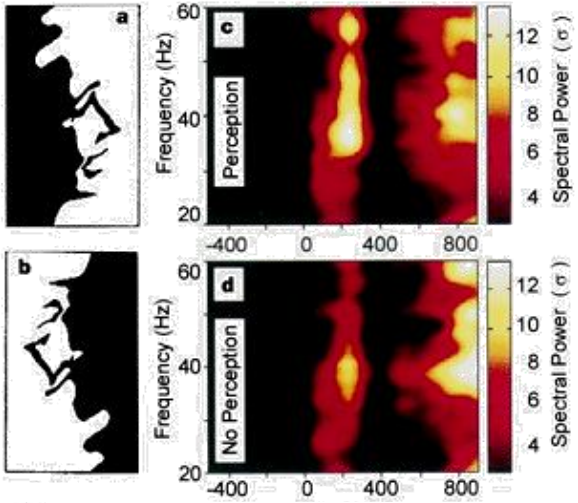

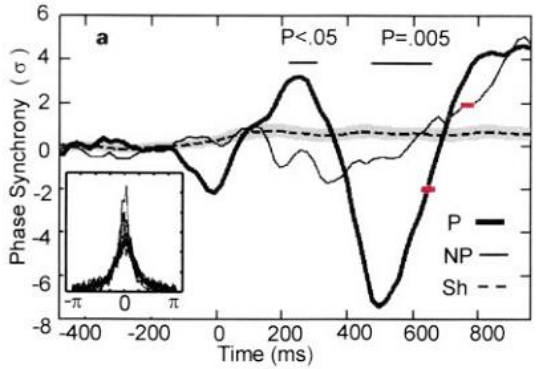

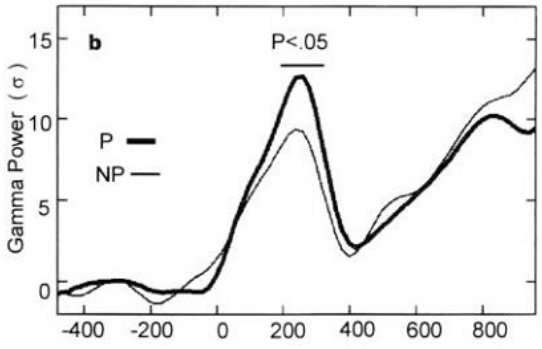

EEG gamma phase-synchrony

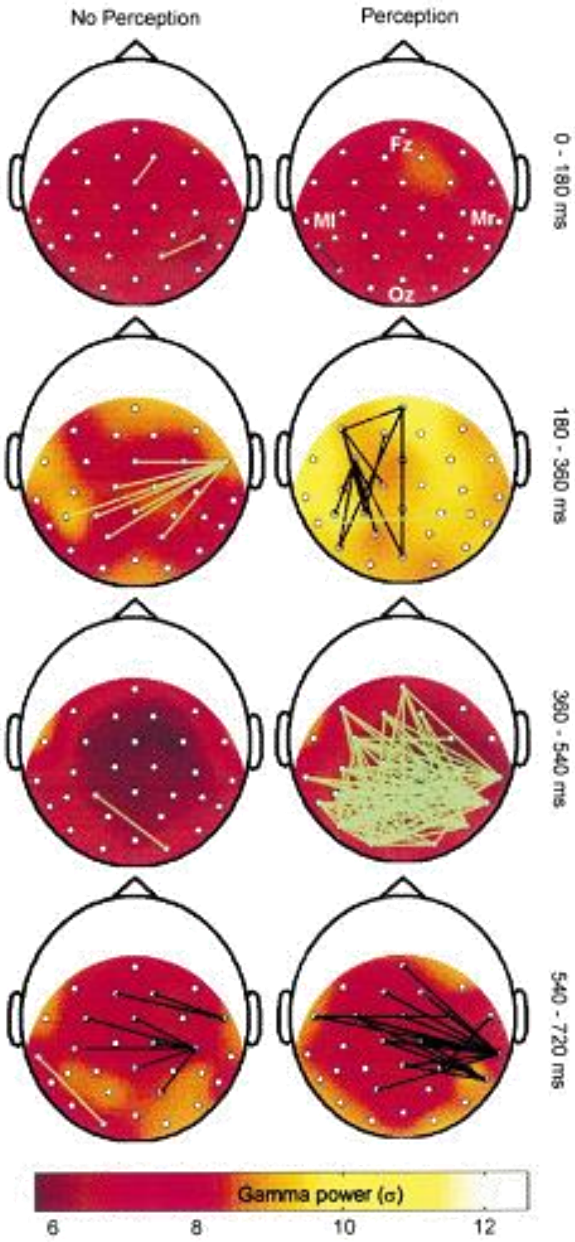

Virginie van Wassenhove 2010

MMN DCM

assumption =
ERPs/ERFs generated by temporal dynamics of few neural sources

temporal dynamics are fitted into equations (based on neural mass model)

each source project to particular sensor (forward model/lead field)

Solve model via Bayesian model inversion

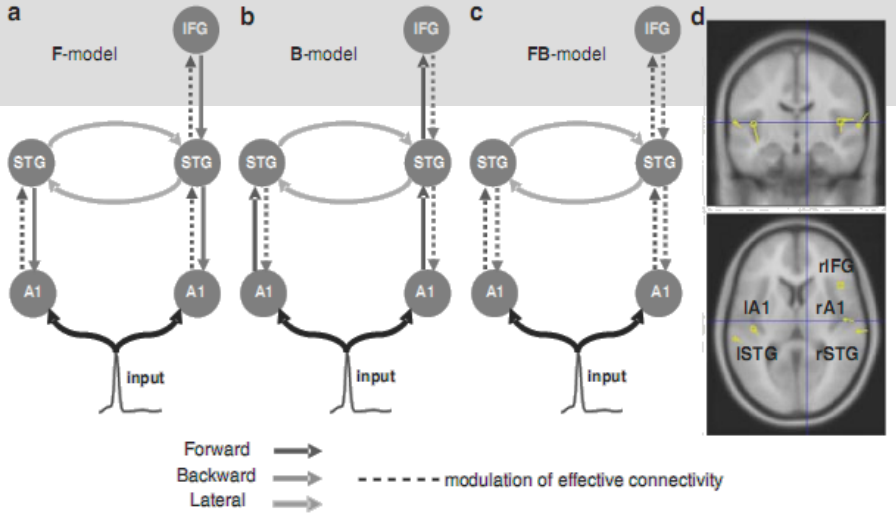

Fig. 2 Model specification. The sources comprising the network are connected with forward (dark grey), backward (grey) or lateral (light grey) connections as shown. A1: primary auditory cortex, STG: superior temporal gyrus, IFG: inferior temporal gyrus. Three different models were tested within the same architecture (**a**–**c**), allowing for learning-related changes in forward F, backward B and forward and backward FB connections, respectively. The broken lines indicate the connections we allowed to change. (**d**) Sources of activity, modelled as dipoles (estimated posterior moments and locations), are superimposed in an MRI of a standard brain in MNI space

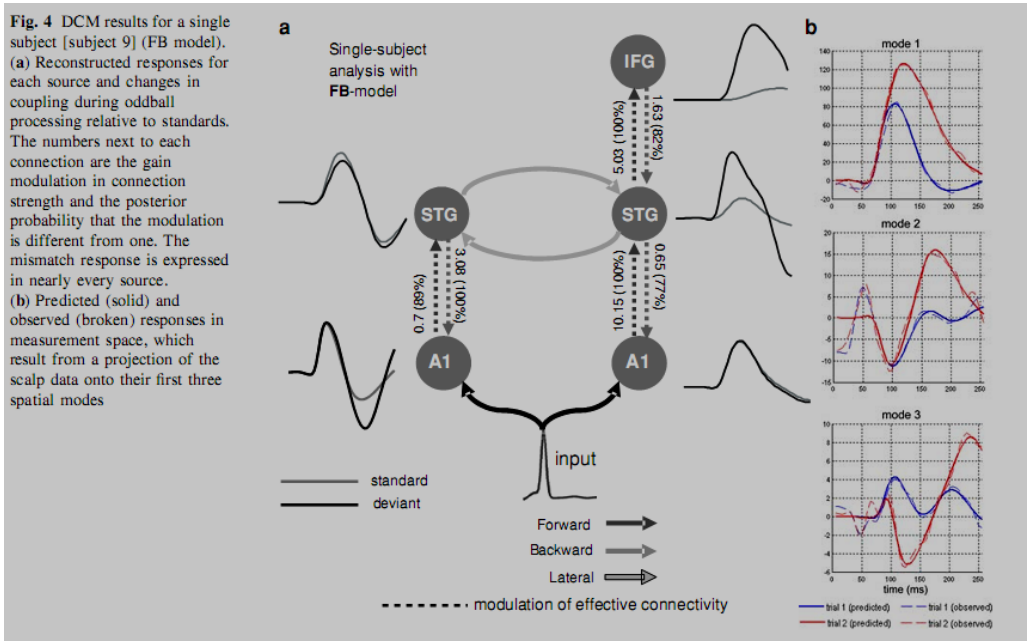

Fig. 4 DCM results for a single subject [subject 9] (FB model). (**a**) Reconstructed responses for each source and changes in coupling during oddball processing relative to standards. The numbers next to each connection are the gain modulation in connection strength and the posterior probability that the modulation is different from one. The mismatch response is expressed in nearly every source. (**b**) Predicted (solid) and observed (broken) responses in measurement space, which result from a projection of the scalp data onto their first three spatial modes

Thanks and more info …

Many thanks to Lauri Parkkonen for providing some of the material presented here
Some illustrations taken from here http://amouraux.webnode.com/

- Lots of resources on MEG soon to be here: http://megcommunity.org/

Preprocessing step - MaxShield principles

Signal Source Separation — Taulu et al (2004, 2005, 2006)

b_{in} : brain signals originating *inside* the sensor arrays (space S_{in})

b_{out} : external disturbances arisig *outside* the sensor array (space S_{out})

n : noise and artifacts generated by the sensors and the sources of interference located very close to the sensors (space S_T)

One hypothetical spherical shell inside of the sensor array encloses the subject's brain, and another one encloses all MEG sensors.

The radii of the shells are determined by the smallest and the largest distances from the origin of the sensor locations, respectively.

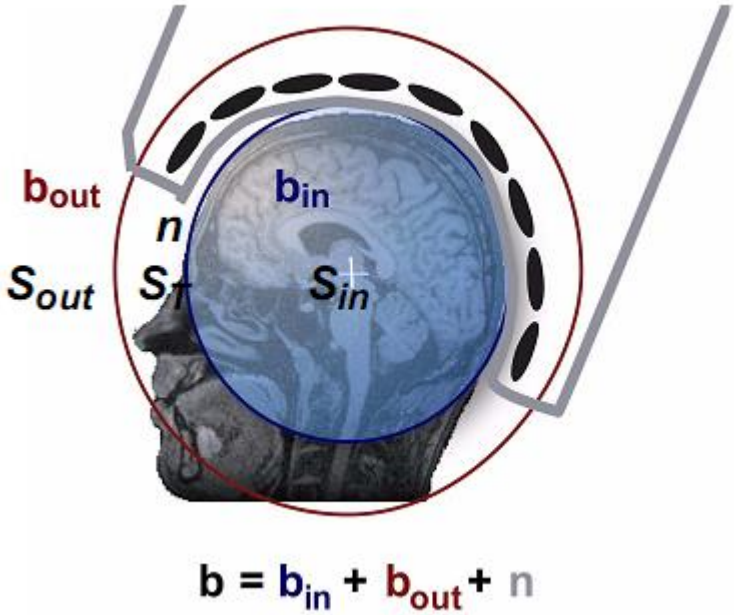

Geometry in Maxwell Filtering

Signal Source Separation

- **Maxwell filtering =~ spatial filtering** based on spatial patterns of b_{in} and b_{out} independently of time; external interferences (S_{out})
- **Spatio-temporal extension of Maxwell filtering** additionally uses temporal dynamics and suppresses internal interferences (S_T)
- MEG signals are transformed into **virtual channels** = harmonic function amplitudes that are independent of the device.

2 subspaces

signal source of interest (S_{in}) | External disturbances (S_{out})

$$\boldsymbol{B}(\boldsymbol{r}) = -\mu_o \sum_{n=0}^{\infty} \sum_{m=-n}^{n} \alpha_{nm} \frac{\nu_{nm}(\theta, \varphi)}{r^{n+2}} - \mu_o \sum_{n=0}^{\infty} \sum_{m=-n}^{n} \beta_{nm} r^{n-1} \omega_{nm}(\theta, \varphi)$$

α , β = amplitude coefficients

v, w = basis functions

Y_{nm} = ordinary spherical harmonic functions

i = imaginery unit

$$\nu_{nm}(\theta, \varphi) = -(n+1) Y_{nm} \boldsymbol{e}_r + \frac{\partial Y_{nm}}{\partial \theta} \boldsymbol{e}_\theta + \frac{im Y_{nm}}{\sin\theta} \boldsymbol{e}_\varphi$$

$$\omega_{nm}(\theta, \varphi) = n Y_{nm} \boldsymbol{e}_r + \frac{\partial Y_{nm}}{\partial \theta} \boldsymbol{e}_\theta + \frac{im Y_{nm}}{\sin\theta} \boldsymbol{e}_\varphi$$

Signal Source Separation – Harmonic Amplitudes

MEG signals expressed as

$$b = Sx = \begin{bmatrix} S_{in} & S_{out} \end{bmatrix} \begin{bmatrix} x_{in} \\ x_{out} \end{bmatrix}$$

where,

$$S_{in} = \begin{bmatrix} \nu_{1,-1} & \cdots & \nu_{N,N} \end{bmatrix} \qquad x_{in} = \begin{bmatrix} \alpha_{1,-1} & \cdots & \alpha_{N,N} \end{bmatrix}^T$$

$$S_{out} = \begin{bmatrix} \omega_{1,-1} & \cdots & \omega_{M,M} \end{bmatrix} \qquad x_{out} = \begin{bmatrix} \beta_{1,-1} & \cdots & \beta_{M,M} \end{bmatrix}^T$$

$$x = \begin{bmatrix} x_{in} \\ x_{out} \end{bmatrix} = S^{\dagger} b$$

$$S^{\dagger} = (S^T S)^{-1} S^T$$